Ph.D. Dissertation

Applied Innovative Engineering and Chemical Approaches for Flue Gas Emission Reductions

Owais A. Al-aqtash

Supervisor

Dr. András Sápi

Associate professor

DOCTORAL SCHOOL OF ENVIRONMENTAL SCIENCE

Department of Applied and Environmental Chemistry

Faculty of Science and Informatics

University of Szeged

Szeged

2025

Table of contents

List of abbreviations

ICE – Internal combustion engine

SI Engine – Spark ignition engine

CI Engine – Compression ignition engine

CC – Catalytic converter

rpm – Revolutions per minute

$V_{Exhaust}$ – Exhaust volume flow rate

$T_{Exhaust}$ – Temperature of exhaust gas in kelvin

V_{Intake} – Intake volume flow rate

V_{stroke} – Swept volume of the engine

$\mu_{volumetric}$ – Volumetric efficiency of the engine

NRMM – Non-road mobile machinery

DPF – Diesel particulate filter

TWC – Three-way catalyst

SCR – Selective catalytic reduction

SNCR – Selective non-catalytic reduction

EGR – Exhaust gas recirculation

FEM – Finite element method

XRD – X-ray diffraction

TEM – Transmission electron microscopy

XRF – X-ray fluorescence

BET – Brunauer-Emmett-Teller method for determining specific surface area (physical adsorption)

TGA – Thermogravimetric analysis

Introduction

Air pollution represents one of the most pressing environmental challenges of the modern era, with profound and well-documented consequences for human health, ecological stability, and global climate. While regulatory and research efforts have historically concentrated on mitigating emissions from on-road vehicles, this focus has left a critical and substantial source of pollution largely unaddressed: Non-Road Mobile Machinery (NRMM). This diverse category includes heavy-duty equipment used in construction, agriculture, and industry, such as excavators, tractors, and generators.

The impact of this regulatory discrepancy is significant. While on-road vehicle emissions standards have become progressively stricter, NRMM has faced less scrutiny, leading to a disproportionate and growing contribution to total particulate matter (PM) and nitrogen oxide (NOx) emissions in many regions. The unique and varied operating conditions of NRMM create significant challenges for emission control, as conventional testing protocols, developed primarily for road vehicles, often fail to capture their real-world emission profiles. This gap between laboratory data and actual emissions underscores a critical need for new, innovative approaches to both assess and control NRMM pollution.

This dissertation directly addresses this need by developing and validating an innovative, high-efficiency flue gas conversion system tailored for combustion engines, particularly within NRMM applications. The research introduces a dual-innovation strategy that combines a novel catalyst design with an optimized catalytic converter chamber, demonstrating a synergistic approach to achieving near-zero emissions.

First, the geometric features and the composition of the ceramic support have a huge effect on the conversion of flue gas as published in our first article of this project [1]; By exploring alternatives to traditional honeycomb structures, we developed adaptable catalyst shapes suitable for various applications, this novel approach enables modular, application-specific solutions for both irregular and conventional catalytic converters [2–4] and the conclusion indicated that pelletized and spherical gamma aluminum oxide supports loaded with 0.2wt% Pd achieved an impressive 95^{+}% reduction of NO_x and CO as their amorphous nature and the order of magnitude larger BET surface area synergized with the conversion process and further promoted the activity.

Second, we developed a pioneering reaction chamber design that dramatically influences conversion efficiency. Our innovative approach to optimizing gas flow dynamics resulted in up to fivefold improvement in emission reduction, demonstrating the critical importance of environmental conditions within the converter.

Third, we explored a cost-effective alternative to traditional noble metal catalysts by investigating various promoters (Cu, Ni, and Co) at different concentrations (1%, 2%, and 5%) combined with minimal Pd loading. This novel approach was validated using Real Driving Emission testing at multiple operating conditions (1.0 kW and 0.5 kW), demonstrating superior performance compared to conventional pure Pd catalysts [5].

The culmination of this research led to a breakthrough design combining optimized geometry with minimal noble metal usage: a six-way reactor containing 70 grams of catalyst with 5wt% Co and only 0.1wt% Pd on pelletized gamma-Al_2O_3 support, achieving an unprecedented 98% stable flue gas conversion. This comprehensive research program advanced three fundamental aspects of flue gas conversion technology: innovative support geometry and composition design, revolutionary reaction chamber configuration, and optimal metal-promoter synergy for enhanced catalytic activity. Each component delivered exceptional results, with subsequent validation experiments confirming the effectiveness of our integrated approach to emission control technology; *The results showed that through innovative engineering and chemical approaches the treated flue gas emission caused by internal combustion engines were near-zero.*

1. Literature Background

1.1 Engine emissions and legislation:

The combustion of gasoline in internal combustion engines produces exhaust flue gases composed of four primary pollutants: carbon monoxide (CO), nitrogen oxides (NOx), unburnt hydrocarbons (HC), and particulate matter (PM). Each component contributes significantly to air pollution and poses distinct risks. CO is toxic to human health; NOx is a precursor to smog and acid rain; and HCs react with sunlight to form ground-level ozone. Particulate matter, composed of soot and smoke, not only causes respiratory damage when inhaled but also contributes to atmospheric warming by absorbing and scattering sunlight. The variety of diseases these emissions contribute to include stroke, chronic obstructive pulmonary, trachea, bronchus, lung cancer, increased asthma, and lower respiratory infections [6–9]. In addition to the previously mentioned primary exhaust gas components, the combustion process produces a variety of contaminants, both regulated and unregulated, however, the legislation primarily focuses on CO, NO_x, HC, and PM. The extensive use of ICE can be observed mainly in the transportation sector which includes many types of vehicles ranging from heavy-duty to light-duty, another vast use of ICE can be found in NRMM which is usually overshadowed by its counterpart in on-road vehicles, however, NRMM does include a significant number of machines that make up a huge part of global emissions, NRMM encompass various industries and sectors, each contributing to the overall emissions. Construction machinery, such as excavators, bulldozers, and cranes, play a vital role in infrastructure development but also release substantial pollutants into the atmosphere. Agricultural equipment, including tractors, harvesters, and sprayers, is another significant source of emissions, especially in farming regions. Additionally, industrial machinery like forklifts, generators, and compressors contribute to the emissions from the manufacturing and energy sectors, Table 1 provides some of the widespread machines that are utilized in various fields and are referred to as NRMM. According to the European Commission reports in 2017 NRMM was responsible for about 15% and 5% of NO_x and PM overall emissions respectively [10], nevertheless the pollution caused by NRMM was noticed as early as 1997 which prompted the need for emission limits legislation, The restrictions for nonroad machines were first established in two stages: Stage I in 1999, and Stage II from 2001 to 2004, depending on engine power output, the stages of legislation kept evolving to reach five stages in total, stage V was proposed in 2014 and finalized in 2016, in which several

important changes were introduced to cover all engine capacities ranging from below 19 kW to above 560 kW, finally the standards were made to be effective from 2019 for engines with capacities lower than 56 kW and over 130 kW, where the standards for engines with power output in between of the former values were made to be effective only in 2020, see Table 2.

Table 1. *Examples of NRMM fields and their related machines*

Field	Example machinery
Construction	Excavators Loaders Bulldozers Forklifts Cranes
Railway	Locomotives Railcars
Mines	Underground trucks Mining loaders Excavators
Agriculture	Harvesters Cultivators Tractors ATVs
Gardening	Lawnmowers Chain saws Hedge trimmers
Miscellaneous	Generators

The importance of discussing all the different sources of emissions produced by ICE instead of only focusing on the popular contributors, comes from their underrated input to the overall emission as collectively they present a significant portion of the different components of flue gases,

see Figure 1 and 2. Manufacturers of engines must demonstrate compliance with emission requirements through various tests of their exhaust systems to get their product approved, In the case of NRMM they are not particularly overlooked by legislators as governments have been introducing stricter standards regularly to control their harmful emissions as shown in Table 2 [11], however, it certainly not getting the same attention from research and development sectors. For quite a while the preferred solution for meeting emission requirements was by increasing the mass of the catalytic converter which increases the cost as catalytic converters rely on expensive noble metals, but the technology itself remains the same, part of this dissertation is dedicated to investigating new concepts of operation and how it compares to the ongoing methods later on that to be discussed deeply in chapter two.

Table 2. *Non-road engines stage V standards*

Net power	**CO**	**HC**	**NO_x**	**PM**
kW	g/kWh			
P < 8	8	7.5		0.4
8 ≤ P < 19	6.6	7.5		0.4
19 ≤ P < 37	5	4.7		0.015
37 ≤ P < 56	5	4.7		0.015
56 ≤ P < 130	5	0.19	0.4	0.015
130 ≤ P ≤ 560	3.5	0.19	0.4	0.015
P > 560	3.5	0.19	3.5	0.045

Figure 1 below represents the proportions of CO_2, CO, HC, NO_x, and PM emitted by NRMM compared to road vehicles in six different European countries including the Netherlands, Switzerland, Germany, Finland, Sweden, and Denmark, data are taken from the references [10,12–15]. Sometimes it could be a difficult task to obtain an accurate reading of NRMM emissions in different parts of the world because of the lack of collected data related to this field and the purpose of Figure 1 is to show an approximate result of their representation in six European countries combined.

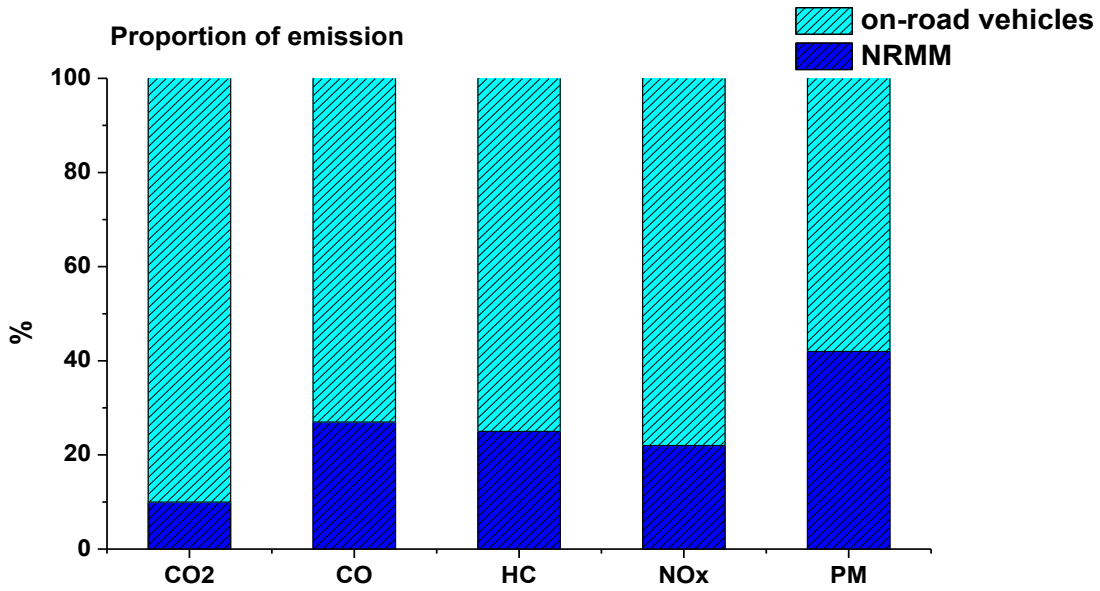

Figure 1. *NRMM proportion of emissions compared to road vehicle in six different European countries combined*

Besides that, figure 2 shows how much CO_2 is emitted by them in Giga tons and the portion of diesel-operated vehicles of the total amount annually [16,17].

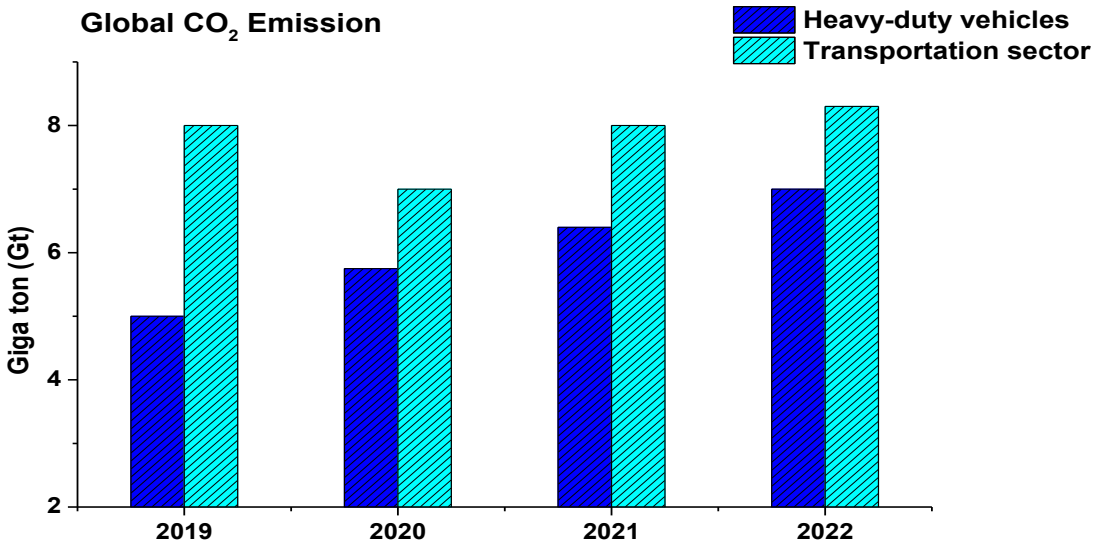

Figure 2. *Global CO_2 emission of the transportation sector, and the portion of diesel vehicle of the total amount*

1.2 Overview of Engine Basics:

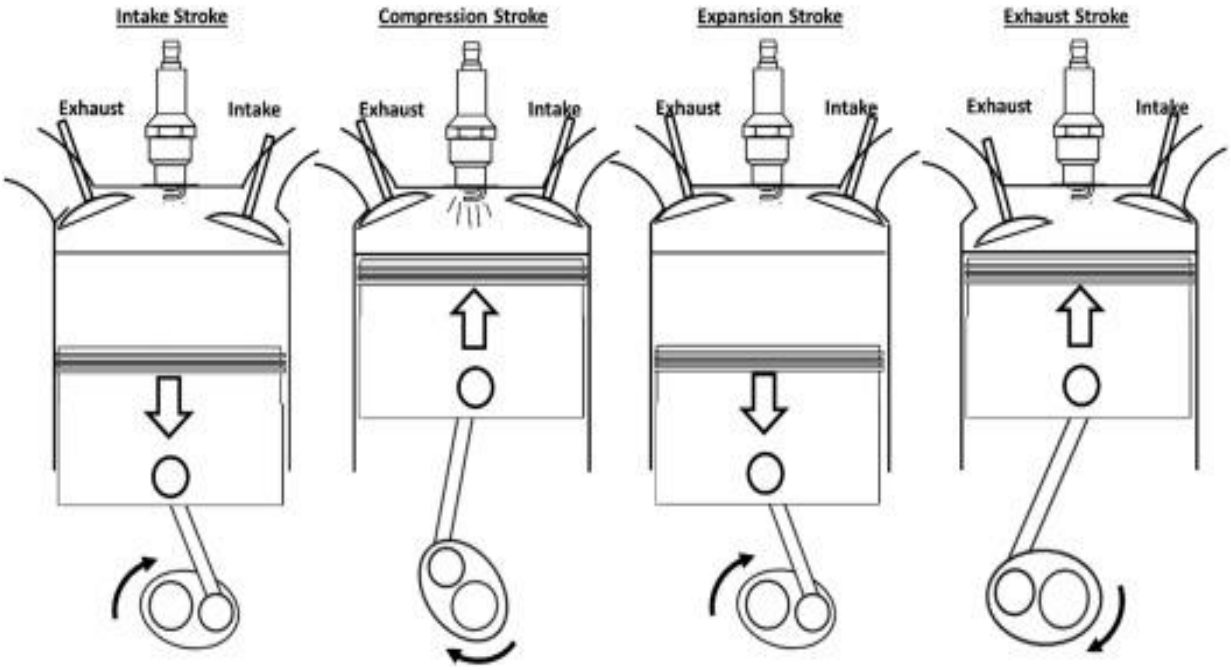

Figure 3. *The four strokes of combustion engines*

Spark Ignition engines (SI Engine), is a term that refers to combustion engines that use spark plugs to ignite the air-fuel mixture inside the engine cylinder, the working cycle of these engines is commonly consisting of four strokes, where at the first stroke the fuel mixture of air and fuel is sucked into the cylinder, the second stroke compresses the fuel mixture, at the third stoke a spark plug ignites the mixture and expand the piston to give power, and at the fourth and final stroke, the byproduct of the combustion are pushed into the exhaust stream.

The other type of engines is called Compression Ignition Engine (CI engine), it differs from SI engines by the process of combustion where the heat of compression is enough to ignite the air-fuel mixture, otherwise, the four-stroke cycle for the two remains the same.

As this dissertation focuses on the treatment of the flue gas emissions of these ICEs it was imperative to understand the behavior and the fundamentals of their operating parameters. The simplest definition of ICE is a device that converts heat into a mechanical movement, this is generally the main purpose of an ICE where this transaction happens in a confined space called a combustion chamber. As for the heat needed to generate the mechanical energy it is acquired

through the combustion of chemical fuel happening at the third stroke (Figure 3. c), afterward the crank-piston system converts the linear movement of the piston into rotary movement in the crankshaft. Now that we've established that, we'll turn our attention to the byproduct of fuel combustion produced at the third stroke and pushed out through the exhaust stream at the fourth stroke (Figure 3. c, d). Analyzing the exhaust flow from an engineering and chemical standpoint will provide us with the necessary factors that influence exhaust flue gases.

1.2.1 Engineering point of view

Starting with the fundamentals of exhaust stream from an engineering point of view, where the parameters mainly revolve around the exhaust flow. The volume of the flue gas generated by the engine depends on various factors such as the size and type of engine, fuel efficiency, and operating conditions. The simplest way to represent that is through the following equation:

$$V_{Exhaust} = \frac{T_{Exhaust}}{300} * V_{Intake} \quad \text{Eq. 1}$$

In applying that to a four-stroke cycle we will get the intake volume represented by the following equation:

$$V_{Intake} = \left(V_{stroke} * \frac{N}{2}\right) * \mu_{volumetric} \quad \text{Eq. 2}$$

N refers to the rpm of the crankshaft. From these equations, we can point out that the various operating conditions of the engine such as speed, load, and temperature are the factors that affect exhaust flow parameters, which begs the question if an engine is operating on stable readings of operating parameters does that mean the exhaust flow should be constant in its mechanical parameters?

To answer this question, we need to introduce the second set of parameters that affect the flow of exhaust flue gas emissions besides the operating conditions of the engine which is the flow path of the exhaust, this path in a car engine is an important aspect of its overall performance. After combustion, the exhaust gases travel through the exhaust manifold, a pipe that collects and channels the gases away from the engine. From there, the gases enter the catalytic converter, where harmful pollutants are converted into less harmful substances. Depending on the resistance the flow endured through its journey resulting from the pressure drop that occurred because of back pressure, the engine is inevitably going to continuously change its operating parameters

automatically to compensate for the lost power. So, the answer to the question above is that the engine in its nature is a device that adapts to the working environment rather than creating one. Thus, as the engine produces power, it continuously adjusts its operating parameters to compensate for resistance in the exhaust flow pathway, meaning the volume of flue gas flow is always changing.

This issue can be tackled in many different ways for instance we can take the average of the flow amounts over a prolonged period to set a constant base-line that can be used as a reference point; however, this method is time-consuming and not very accurate as we can't say for sure that the engine faced the same type of resistance every time and it also requires a base-line for every operating condition of the engine which is endless. This leads us to the second solution in which we do real-time monitoring of the flow at two different points, the first one is at the outlet of the exhaust, and the second is after the flow path. This type of comparison is the most accurate way to determine the actual flow rate. By measuring the flow at the outlet of the exhaust and then again after the flow path, we can calculate the difference in flow and identify any discrepancies or obstructions. This method provides real-time data that allows for immediate adjustments or interventions, ensuring optimal flow and performance.

So far, we established the two dominant factors that affect the flow of our exhaust products rendered in the engine operating conditions and the path-way of the exhaust flow, some other factors can affect the flow of the exhaust such as exhaust gas recirculation and altitude, and atmospheric pressure change however these conditions do not apply to our experimental process so they will not be taken into consideration.

1.2.2 Chemical point of view

Analyzing the exhaust flow from a chemical point of view is a tool that is used to determine the products of the fuel combustion inside the reaction chambers of the engine. For example, in a car engine, analyzing the exhaust flow can help identify the presence of harmful pollutants. Additionally, this analysis can also reveal the composition of the exhaust gases. This step is vital to our project as we need to identify the types and quantities of combustion products to set an optimal treatment for them.

Now, we must specify the elements that contribute to the components of flue gas emissions starting by the Fuel type. The flue gas emissions produced from the combustion of gasoline inside the reaction chambers of the engine consist of various gases such as carbon monoxide (CO), unburnt hydrocarbons (HC), nitrogen oxides (NO_x), and particulate matter, the formation of these products is initially influenced by the type of fuel used to run the engine, so different type of gasoline produce different amounts of byproducts [18]. The European Union (EU) regulates gasoline quality through the Fuel Quality Directive (FQD) and the European standard EN 228. These laws provide specifications and requirements for gasoline to ensure its quality and environmental performance; the specifications are meant to regulate the following:

- Octane Number: Gasoline must fulfill certain minimum octane number specifications. The octane number is a measure of a fuel's resistance to knocking or pinging in internal combustion engines.
- Sulfur Content: The FQD restricts the sulfur content of gasoline to prevent sulfur dioxide (SO_2) emissions and protect vehicle emissions control systems. The limitations are usually given as parts per million (ppm).
- Benzene level: To restrict emissions of this recognized carcinogen, gasoline's benzene level is limited. Reducing benzene levels helps to improve air quality.
- Oxygen Content: The oxygen content of gasoline can be adjusted to improve combustion efficiency. However, oxygenate additions, such as MTBE (methyl tert-butyl ether), have been restricted due to environmental concerns.
- Distillation Characteristics: Gasoline must have specific distillation characteristics, which determine the temperature ranges at which different fuel components evaporate. This helps to ensure appropriate engine performance and emission management.
- Vapor Pressure: Regulations may set restrictions on gasoline vapor pressure, which is vital for reducing evaporative emissions, especially during warmer months.
- Aromatics Content: Limits on the aromatic hydrocarbon content of gasoline may be imposed to control emissions and improve air quality.

Every set of regulations that governs the fuel has the purpose of reducing the quantities of harmful emissions mainly CO, NO_x, PM, and HC, it's important to note that these limits can vary according to the type of vehicle and fuel. below are the Euro standards for CO and NO_x for light-duty vehicles as it is the closest to the engine used in this project:

Table 3. *The Euro standards for CO and NO_x for light-duty vehicles.* [19]

	Year	**CO limit (g/km)**	**NO_x Limit (g/km)**
Euro 1	1992	2.72	0.97
Euro 2	1996	2.2	0.5
Euro 3	2001	2.3	0.15
Euro 4	2005	1	0.08
Euro 5	2011	1	0.06
Euro 6	2015	1	0.06

These values represent the maximum allowable emissions for newly type-approved vehicles under each Euro standard. It's also important to note that real-world on-road emissions may be different than the laboratory tests, and the Euro 6 standard in particular, introduced Real Driving Emissions (RDE) testing to address discrepancies between laboratory tests and on-road performance.

The fuel type being the first criterion that affects the exhaust flue gas from the chemical point of view, it was, therefore, important to keep using the same type of fuel during one set of experiments to ensure the consistency of the results. Using different types of fuel would introduce variables that could potentially affect the chemical composition of the exhaust flue gas. This consistency in fuel type allowed for accurate comparisons and analysis of the data obtained. Additionally, by using the same fuel type, any changes observed in the composition of the exhaust flue gas could be attributed solely to the experimental conditions and not to variations in fuel properties.

The second important factor that affects the exhaust flue gas parameters from the chemical standpoint is the air-fuel ratio in the combustion chamber of the engine. The air-fuel ratio refers to the ratio of air to fuel that is being burned in the combustion process. The ideal air-fuel ratio for complete combustion is known as the stoichiometric point which is the air-fuel ratio at which there is precisely enough air to burn all of the fuel completely. In other words, it is the chemically

balanced ratio that ensures the most efficient combustion with no excess fuel or oxygen. If the air-fuel ratio is too lean, meaning there is an excess of air, incomplete combustion occurs, resulting in higher levels of nitrogen oxide emissions. On the other hand, if the air-fuel ratio is too rich, meaning there is an excess of fuel, incomplete combustion occurs as well, leading to higher levels of carbon monoxide and hydrocarbon emission. For gasoline engines, the stoichiometric point is typically around 14.7:1 by mass, meaning that for every 14.7 parts of air, there is 1 part of fuel. But, it's also important to note that the air-fuel ratio during combustion in an ICE may vary under different operating conditions. The stoichiometric point serves as a reference point, and engine control systems adjust the mixture based on factors such as engine load, speed, and temperature, which brings us back to the engineering point of view to complete the circle. From this notion, we find out that the mechanical and chemical standpoints in this matter are linked, where the mechanical standpoint focuses on the physical aspects of the combustion process, such as air intake and fuel injection systems. In contrast, the chemical standpoint investigates the reactions and kinetics involved in the combustion process.

The chemical reactions:

There are two main stages at which chemical reactions take place, first inside the ICE and second inside the CC, considering the SI engine with EGR and gasoline as a fuel the main reaction will revolve around the decomposition of hydrocarbon as follows [20]:

$$C_8H_{18} + 8H_2O \longrightarrow 8CO + 17H_2 \quad (1)$$

$$C_8H_{18} + 16H_2O \longrightarrow 8CO_2 + 25H_2 \quad (2)$$

$$CO + H_2O \longrightarrow CO_2 + H_2 \quad (3)$$

$$C_8H_{18} + 8CO_2 \longrightarrow 16CO + 9H_2 \quad (4)$$

$$C_8H_{18} + 4O_2 \longrightarrow 8CO + 9H_2 \quad (5)$$

$$C_8H_{18} + \frac{25}{2} O_2 \longrightarrow 8CO_2 + 9H_2O \quad (6)$$

Reactions 1 and 2 are steam reforming reactions where hydrocarbons react with steam at high temperatures (700 – 1000) °C, normally steam reforming has CO as a product, however, hydrocarbon can also be steam reformed into CO_2 and H_2 directly as in reaction 2, water gas shift reaction

can be seen in reaction 3 as reaction 4 exhibits a dry reforming reaction, and lastly, reaction 5 and 6 are partial and complete oxidation reactions of hydrocarbon respectively.

$$CO + 3H_2 \longleftrightarrow CH_4 + H_2 \quad (7)$$

$$2CO + 2H_2 \longleftrightarrow CH_4 + CO_2 \quad (8)$$

$$CO_2 + 4H_2 \longleftrightarrow CH_4 + 2H_2O \quad (9)$$

$$C_8H_{18} \longleftrightarrow CH_4 + C_7H_{14} \quad (10)$$

$$C_8H_{18} + H_2 \longleftrightarrow CH_4 + C_7H_{16} \quad (11)$$

The reforming reactions are always associated with the formation of methane products, reactions 7 and 8 show methanation from CO while reaction 9 shows methanation from CO_2, or directly from decomposing hydrocarbons as in reactions 10 and 11.

From reactions 1 to 11, we can say that the main components entering the catalytic converter are CO, CO_2, H_2, H_2O, and hydrocarbons, however, in addition to the previous component's NO_x is also formed at increased combustion temperature due to the tendency of N_2 to react with O_2, now the components entering the CC are known, the typical chemical reaction will be as follows [21]:

$$CO + ½\ O_2 \longrightarrow CO_2 \quad (12)$$

$$H2 + ½\ O_2 \longrightarrow H_2O \quad (13)$$

$$C_3H_6 + 9/2\ O_2 \longrightarrow 3CO_2 + 3H_2O \quad (14)$$

$$CO + 2\ NO \longrightarrow CO_2 + N_2O \quad (15)$$

$$H_2 + 2\ NO \longrightarrow H_2O + 2\ N_2O \quad (16)$$

$$5/2\ H_2 + NO \longrightarrow NH_3 + H_2O \quad (17)$$

$$2NO + 2CO \longrightarrow N_2 + 2CO_2 \quad (18)$$

$$2NO + C_xH_y \longrightarrow N_2 + xCO_2 + (y/2)H_2O \quad (19)$$

The reactions 12 to 19 are possible due to the presence of catalysis where active noble metals are typically used as a wash coat on the ceramic support surface, for instance, Palladium is widely used for its high catalytic activity and the ability to promote various gas phase reactions [22–24], however, for the reduction of NO_x it's more efficient to use Pd along with Pt for its high activity toward NO reduction [25,26], where Pd acts like a promoter for Pt in the NO conversion process, as it reduces the hydrothermal sintering of Pt [27]. Finally, in this project, we are implementing a new chemical composition that combines cheap and expensive metals which will be discussed later in detail.

1.3 Flue-gas reduction:

Reaching the level of emissions discussed in the legislation part, vehicle manufacturers resorted to several different methods. Engine development is one of these methods and it falls under the Before-Treatment of emissions, this particular type of treatment is popular and has received continuous development since it was introduced as it doesn't only decrease the flue-gas emission but also improves the engine performance. Some of the engine optimization methods that helped keep an improved emission limit include: Turbocharging [28,29], fuel injection timing [30–33], exhaust gas recirculation (EGR) [33–37], and the use of several methods to limit emissions is called engine control [38,39]. As previously observed, the demand for additional methods to reduce flue gas emissions increased as environmental standards increased, which is why the catalytic exhaust converter system was created. However, contrary to engine modification catalytic converter technology hasn't received continuous fundamental development; rather, progress has largely involved scaling up the mass and volume. Catalytic converters are usually constructed on a ceramic honeycomb monolithic substrate that has multiple parallel channels flowing in the axial direction. The support material has no catalytic activity, while the catalytic material is coated on the monolith walls [40–42], the focus of this work is to implement a new approach to catalytic converter technology taking into consideration their shortcomings.

The criteria we used to categorize our sample performance during these projects was its ability to reduce Carbon Monoxide (CO) and Nitrogen Oxides (NO_x) in flue gas emissions, for that the focus of literature going forward will be on the oxidation of CO and the reduction of NO_x.

1.4 CO oxidation and NO_x reduction

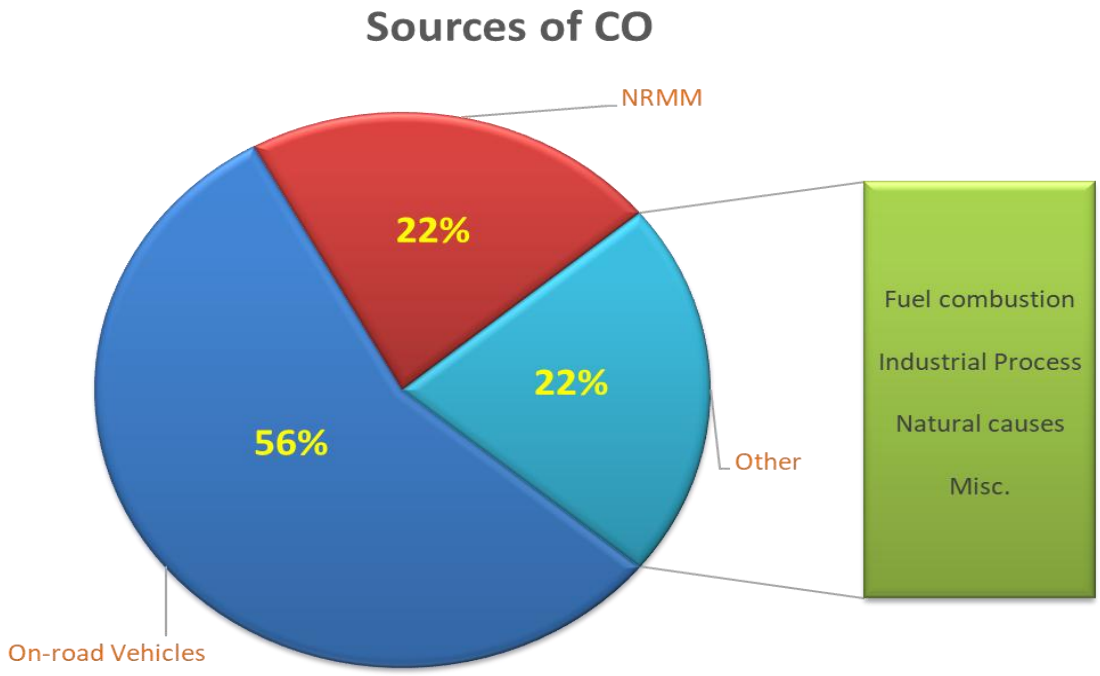

***Figure 4**. The portion of global CO emission per sector.*

The global concentrations of CO range between 0.06 and 0.14 mg/m^3, and the sectors that utilize ICE make up about 78% of the global CO emission portion [43–45], moreover, the CO makes up 0.7vol% of the exhaust concentration typically, but this value is subject to change depending on air-fuel ratio [46].

As stated earlier, CO has a huge impact on the environment and is regarded as a serious threat to health, for that the annual number of CO oxidation articles has been increasing since the 1970s, where multiple scientific fields generated these articles such as heterogeneous catalysis and surface chemistry, table 4 below summarizes some of the recent findings.

***Table 4.** Comparison of various Pd catalysts studied in the literature for CO oxidation.*

Loading	Flow condition	Start of Conv. (°C)	Light-off ($T_{100\%}$, °C)	Ref.
0.1wt% Pd	1CO:20O_2	150	200	[47]

0.3wt% Pd	1CO:20O_2	145	180	[47]
0.5wt% Pd	1CO:20O_2	143	175	[47]
0.8wt% Pd	1CO:20O_2	142	175	[47]
0.5wt% Pd	1CO:20O_2	130	165	[47]
0.5wt% Pd	-	-	170	[48]
5.0wt% Pd	-	-	170	[49]
0.8wt%Pd	-	-	170	[50]
1.0wt% Pd	-	-	170	[51]
0.5wt% Pd	-	-	190	[52]
3wt% Pd	1CO:2O_2	175	200	[53]
5wt% Pd	1CO:2O_2	160	200	[54]
8wt% Pd	1CO:2O_2	170	190	[54]
10wt% Pd	1CO:2O_2	150	190	[54]

Table 4 presents a summary of representative palladium-based catalysts for CO oxidation from the recent literature. The data indicate that for various Pd loadings on different supports, complete CO conversion (T_{100}%, or light-off) is typically achieved in the range of 165–200 °C. It is notable that performance is not solely dependent on metal loading; for instance, the 10wt% Pd catalyst reported by shows a light-off temperature of 190 °C, which is comparable to catalysts with significantly lower palladium content. This variability highlights that factors such as the support material, synthesis method, and pretreatment conditions play a crucial role in determining catalytic activity.

A critical analysis of these literature values underscores the advanced performance of the catalysts developed in this work. As will be detailed in the Results and Discussion section (Figure 17), our self-prepared catalysts, particularly those on amorphous γ-Al_2O_3 supports (spheres and pellets), achieve complete CO conversion at significantly lower temperatures. Even with a minimal loading of only 0.1wt% Pd, our catalysts demonstrated light-off temperatures as low as 150-175 °C. This represents a substantial improvement over many of the systems listed in Table 4, which often require higher temperatures despite utilizing much higher palladium loadings (e.g., 0.5wt% to 10wt%). This superior low-temperature activity establishes a clear benchmark for our work and

highlights the effectiveness of our unique support geometry and synthesis methodology in creating a more efficient catalyst.

NO_x in flue gas mainly exists as nitric oxide (NO) and nitrogen dioxide (NO2), with NO constituting 90-95% and NO2 making up 5-10% of the total NO_x emissions [55], NO_x reduction is less straight forward and has multiple approaches to reduce its content depending on the application, following is a list of some of these methods and their efficiency:

The most popular method is Selective Catalytic Reduction (SCR) / Selective non-Catalytic reduction (SNCR): This technology utilizes ammonia (NH_3) or Urea as a reductant to convert NO_x into nitrogen (N_2) and water (H_2O). SCR is noted for its high efficiency (up to 90%) and stability, where SNCR has less efficiency and usually operates at application with higher temperature [56–58]. Other, commercial catalytic converters use a mixture of noble metals, such as (Pt, Pd and Rh) [25,59,60], and because Pt is mostly active for NO reduction, Pd functions as a promoter for Pt in the NO conversion process, reducing the hydrothermal sintering of Pt [27].

Absorption and adsorption methods: Absorption methods involve capturing NO_x in liquid solutions, with a focus on the mechanisms at play in alkaline solutions. The efficiency of this process is heavily influenced by gas-liquid equilibrium and solution PH. In contrast, adsorption techniques utilize solid materials such as activated carbons, zeolites, and Metal-organic frameworks (MOFs) to capture NO_x. The effectiveness of adsorption is affected by various factors, including the presence of other gases and humidity levels. Both methods are analyzed for their potential in reducing NO_x emissions from industrial processes [61,62].

Oxidation methods for NO_x removal focus on increasing the valence of nitrogen in NO_x compounds, primarily by converting NO to NO_2, which is more easily removed due to its higher water solubility. These methods employ various oxidants, including gaseous (O_2, O_3, Cl_2) and liquid (H_2O_2, peroxydisulfate) reagents, with the choice of oxidant affecting process efficiency. Catalysts are often used to enhance oxidation reactions, with ongoing research aimed at developing more resilient catalysts that can withstand challenging flue gas conditions such as water vapor and SO_2 presence [63].

Laboratory-Scale Methods: Recent laboratory-scale innovations in NO_x removal include Non-Thermal Plasma (NTP) technology, which generates reactive species for NO_x oxidation at ambient

temperatures, and combination techniques that merge oxidation and reduction processes using methods like dielectric barrier discharge plasma with reducing agents. Current research focuses on optimizing these methods for practical applications, improving radical generation efficiency in NTP systems, and exploring their scalability for industrial use. These innovative approaches show promise for developing more cost-effective and high-performance NO_x removal solutions, representing significant advancements in flue gas purification technology [64,65].

1.5 Ceramic support

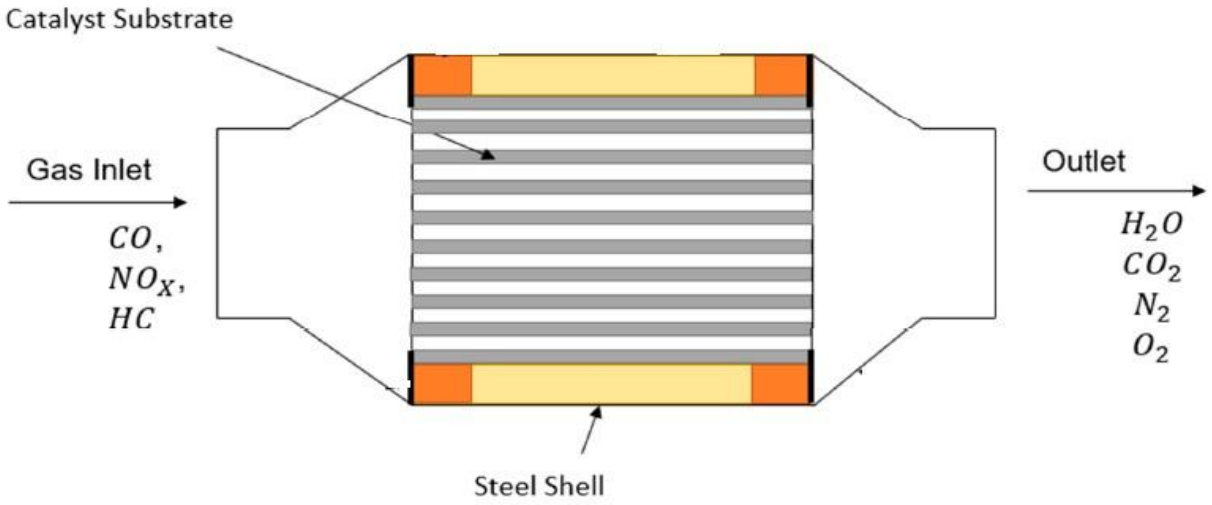

Figure 5. *Representation of a typical catalytic converter structure. Adapted from [65].*

A honeycomb ceramic structure typically coated in Al_2O_3 is utilized as catalyst support by using the principles of heterogeneous catalysis and rate of reaction. The choice of Al_2O_3 as a support is because it enhances the catalytic activity, providing a robust platform for the catalytic conversion process. Additionally, Al_2O_3 is often employed as a support material for catalysts due to its high surface area, thermal stability, and resistance to sintering [66–68]. Where the typical choice for the honeycomb structure is because it provides good contact between the flowing exhaust gases and the catalyst surface [69]; A mixture comprising various noble metals, including palladium, rhodium, and platinum, is afterward applied to the structure [70].

Figure 6 shows a representation of the internal structure of the honeycomb design, which mainly consists of multiple channels where the exhaust gases pass through, and usually, they are

categorized according to their cell density which refers to the number of channels per square inch (CPSI) and it ranges between 400 and 900 CPSI [71].

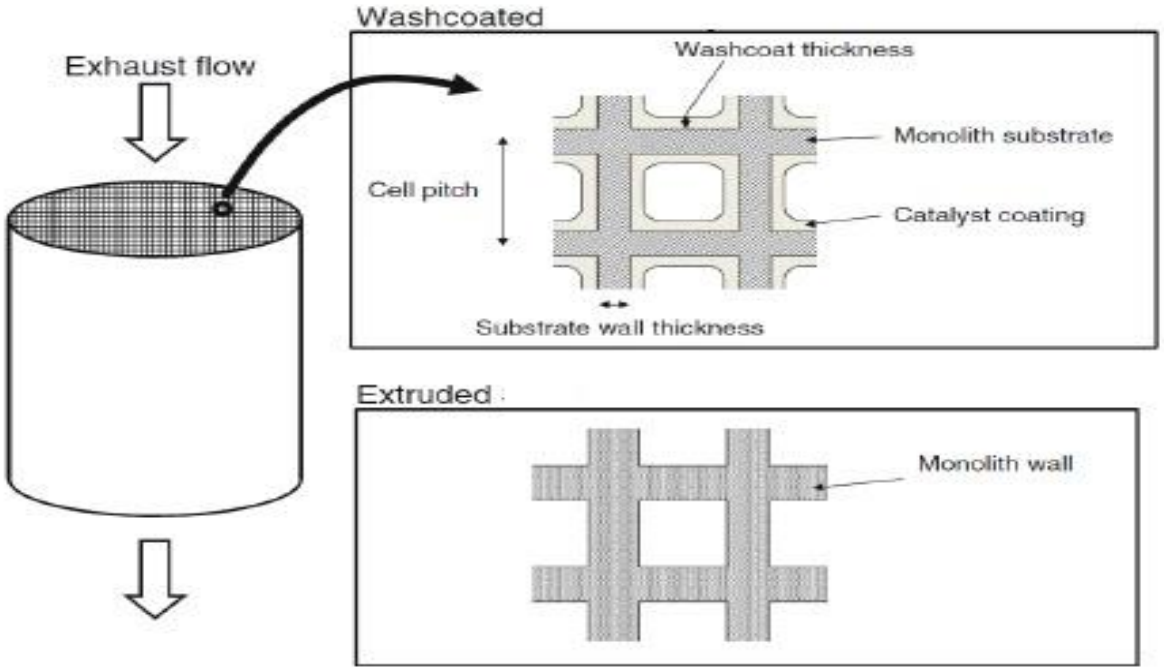

***Figure 6**. The internal representation of the honeycomb structure inside the catalytic converters. Adapted from [68].*

However, despite the advantages of honeycomb structure it still has some disadvantages, perhaps the most prominent disadvantage is the affinity of the channels to melt and block the flow causing increased back-pressure, and over time the number of blocked channels will increase which will result in reduced engine efficiency and reduced conversion of flue gas emissions [72]. For that, in this project, we opted to follow a different approach rendered in the use of individual support units with different shapes and Al_2O_3 as the primary material.

Extruded ceramic supports, on the other hand, have important applications as catalysts in various industries, including their use in non-road mobile machinery (NRMM). Ceramic materials, particularly in pelletized form, are often used as supports for catalysts as they provide a high surface area for the dispersion of active catalytic substances such as metals platinum, palladium, and rhodium. Their thermal stability, chemical resistance, and structural strength are the main key benefits of using this type of support [73,74]. Moreover, improved fuel efficiency can be achieved by utilizing this type of support, this claim was investigated in our second article, in which the

results showed a 20% decrease in fuel consumption, by optimizing combustion and reducing harmful emissions, catalytic systems using ceramic supports can improve the overall fuel efficiency of NRMM [75,76].

In conclusion, the benefits of using individual support units rather than a Honeycomb structure are the ability to avoid path blockage, the easy restoration of the catalyst, their convenience to use inside the irregular-shaped reaction chamber, and their easy-to-design structure [2–4,77].

1.6 Catalytic converters

1.6.1 Bimetallic catalytic converters

While CO is highly regulated in flue gas emissions emitted by ICE, Catalytic converters play a crucial role in reducing their harmful emissions, the performance of these devices largely depends on the efficiency of the catalysts utilized inside them.

The use of transition metals as promoters for noble metal catalysts has been a subject of significant interest in recent years. Literature demonstrated that adding nickel to palladium catalysts could significantly enhance methane oxidation, showing a synergistic effect that improved catalytic activity and stability. This work highlighted the potential of bimetallic systems in catalysis [78–81]. In separate studies, Cobalt also has been extensively studied as a promoter for platinum-based catalysts in CO oxidation, they found that cobalt not only improved catalytic activity but also enhanced the catalyst's resistance to sulfur poisoning, a common issue in automotive catalytic converters [82–84]. Copper has also shown promise as a promoter. Research revealed that copper-promoted palladium catalysts exhibited superior performance in the reduction of NO_x, CO, and C_xH_y another critical function of automotive catalytic converters [85–88]. Moreover, the following references [89–93] explain the convenience of bimetallic use in catalysts for automotive applications. They emphasized the potential of transition metal promoters to enhance performance and reduce the overall noble metal content in catalytic converters, improving both efficiency and cost.

1.6.2 Catalytic converter design

Reaction chamber design plays a crucial role in determining the efficiency, yield, and overall success of chemical reactions. The design affects various aspects of the reaction process, such as

mixing and mass transfer as chamber geometry influences fluid dynamics, affecting how reactants mix which in turn ensures uniform concentration and temperature distribution [94,95], heat transfer as surface area-to-volume ratio impacts heating and cooling rates, also materials with high thermal conductivity improve temperature control [96]. Moreover, custom-designed catalytic converters can be scaled up and scaled down as geometric similarity helps maintain reaction conditions across scales, besides the energy efficiency, we found during our testing that some reaction chamber designs reduced fuel consumption.

To conclude careful consideration of reaction chamber design can significantly enhance reaction performance, improve product quality, increase safety, and optimize resource utilization in chemical processes.

1.6.3 Shortcomings of catalytic converters supports

Catalytic converters have been quite effective at lowering emissions from vehicles, but some issues remain unresolved, particularly concerning the ceramic supports utilized in these systems.

Catalytic converters operate at high temperatures, often exceeding 800 °C during normal operation. Such extreme thermal conditions can lead to thermal expansion and contraction, causing mechanical stress. Over time, this stress can result in cracking or fragmentation of the ceramic substrate. Moreover, over time, the ceramic support material may sinter, reducing its surface area, which is crucial for catalytic activity. This leads to reduced efficiency of the catalytic converter in controlling emissions.

Another focus point of our research was the durability of the ceramic support, NRMM operates in highly demanding environments such as construction sites, agriculture, and mining where dust, debris, and rough terrain are common. This can cause physical wear and tear on catalytic systems, including the ceramic substrate. Premature wear of the catalytic support material reduces the lifespan of the converter, leading to more frequent replacements and increased operational costs [97,98].

Now that we have the fundamentals established, we can dive deeper into the motivation for this work and the legislation that surrounds it.

2. Aim and Motivation

Internal combustion engine exhaust emissions are subject to increasingly stringent regulations. As a result, precious-metal-based catalytic converters, which typically treat exhaust through diesel particulate filters and three-way catalysts, are in dire need of innovative improvement.

And although selective catalytic reduction catalysts are a well-studied subject in the literature it mainly adopts the same typical approach of implementing a honey-comb structure loaded with a high mass of expensive materials and only scaling up the process if the regulations get stricter which is costly and testing its limits for what a conventional after-treatment system can do.

Beyond that, the after-treatment processes will lack the ability to meet the upcoming standards on their own while keeping an improved fuel efficiency as a crucial criterion. Thus, the main focus point of this research is to address the difficulties of converting flue gas emissions of ICEs and to provide a new approach for treating those emissions through a system that consists of an improved catalyst and a custom-designed reaction chamber to house it, where together they can function in tandem increasing the overall efficiency.

Despite significant advancements in catalytic converter technology, a crucial research gap persists in the comprehensive analysis of catalyst performance under real driving conditions across various engine parameters. Specifically, the integrated study of different support types, custom-designed reaction chambers, and promoter metal utilization has not been thoroughly explored in a single, comparative investigation. Our research aims to address this gap through a three-pronged approach: First, we will enhance the working catalyst by examining diverse support materials and shapes, as well as optimizing noble-metal loading percentages. Second, we'll assess promoters to determine ideal loading combinations, an often-overlooked factor in holistic catalyst design. Finally, we'll improve reaction chamber efficiency by implementing optimal heat diffusion and steady-state flow along the chamber length, utilizing simulation software and finite element methods. This comprehensive strategy not only targets individual components but also their synergistic effects, potentially revolutionizing catalytic converter performance in real-world applications. By bridging the divide between theoretical models and practical implementation, our study seeks to provide a more complete understanding of catalyst behavior in optimized reaction environments under authentic operating conditions.

Therefore, handling the challenges mentioned above in this research will be through the following hypotheses

1) Does the shape of the support affect the efficiency of converting flue gas emissions and what are the optimum loadings and their percentages?

2) What are the support properties responsible for the increase/decrease in flue gas conversion performance?

3) Does the shape of the reaction chamber improve the efficiency of the catalytic converters?

4) How does the reaction chamber design promote the performance of the catalyst inside?

5) What are the ideal promoters that can synergize with noble metals for flue gas conversion?

6) How do the loading combinations of different metals over ceramic support affect the overall performance of the catalyst?

3. Experimental Methods and Materials

This chapter is concerned with the synthesis of catalysts and their ceramic supports used in the three projects mentioned earlier as well as the characterization methods and materials involved.

3.1 Materials

Preparation of 0.1 wt.% Pd and 0.2 wt.% Pd / Al_2O_3 catalysts

- Palladium (II) acetate (Pd $(OCOCH_3)_2$; ≥ 97%, Sigma Aldrich)
- Raw materials for support: Alumina (Al_2O_3, ≥ 95%, SILKEM Hungary ltd.); Talc ($Mg_3(Si_4O_{10}(OH)_2$) ≥ 85%, Imerys Refractory manufacturer Ltd. Hun.); Clay ($Al_2O_3SiO_2$ + $2H_2O$, clay minerals ≥ 85%, Keraclay Plc)
- Acetone (C_3H_6O, 99.5%, VWR)

All reagents were used without further purification, and all glassware was cleaned thoroughly with aqua regia, solutions were prepared using pure Acetone.

Fixed-bed characterization

- Carbon monoxide (CO, 99.5%, Messer)
- Compressed air (20.5% O_2, 79.5% N_2)
- Argon (Ar, 99.9%, Messer)
- Nitrogen (N_2, 99.9%, Messer)
- Helium (He, 99.9%, Messer)

All reagents were used without further purification. All catalyst samples were produced using wet impregnation, which resulted in a wash coat that covered the ceramic support. To start with, the impregnating solution is prepared by dissolving palladium (II) acetate in acetone solvent for 5 minutes using an ultrasonic sonication bath. The exact amount of dissolved palladium (II) salt was proportional to the mass of the ceramic support, resulting in a sample with 0.1 wt.% Pd and 0.2 wt.% Pd for 125 g of ceramic support. When the solution was ready for use, a dropper was used

to impregnate the ceramic support. Finally, it was dried in an 80 °C oven for 1 h, and the same process was repeated until all the solution was completely absorbed by the ceramic sample.

Using the necessary quantities of raw materials, a dense ceramic mass was created by adding water and homogenizing it multiple times to allow the clay components to unfold. After about a week of daily homogenization, when the moisture content of the ceramic mass reached 22–25%, we began producing the three types of cylindrical ceramic bodies using the vacuum press extrusion method. This sort of extruded sample dried for two weeks before being heat-treated twice at elevated temperatures (900-1250 °C). The ceramic bodies, including the cylinders without holes, one-hole, and four-hole ones, were all formed of a hard porcelain ceramic mass, with the following typical oxide composition: (64,21% SiO_2; 20,98% Al_2O_3; 2,08% Fe_2O_3; 1,85% TiO_2; 1,75% Na_2O; 1,69% K_2O; 0,90% CaO; 0,35% MgO; 6,19% LOI = Loss on Ignition).

As for the spherical-shaped and the Pellets catalysts, both are Gamma-Alumina, which means both of them were annealed below 900–1000 °C in their fabrication process with the following approximate chemical composition for spheres (46% SiO_2, 39% Al_2O_3, and 14% H_2O).

Catalytic converter reaction chamber

- Structural steel (S235JR, 0.17% C)
- Palladium (II) acetate (Pd $(OCOCH_3)_2$; ≥ 97%, Sigma Aldrich)
- Gamma-Aluminum Oxide (Al_2O_3 ≥ 93, Thermo Scientific Chemicals)

The steel used falls under EN10025 European Production standards, this non-alloy structural steel contains 0.17% Carbon, with a tensile strength between 400-500 n/mm^2. The electrical resistance is 0.14 Ω · mm2/m, and the thermal conductivity is 54 W/(m·K). The three reaction chambers were manufactured and called Reactor A, Reactor B, and Reactor C, each with a distinct design as follows: Reactor A is a simple cylindrical chamber where the flow inlet is located at the bottom of the chamber passing through the spherical-shaped catalyst in a vertical flow before exiting from the top of the chamber. Reactor B forces the flow to go through a tube before dispersion evenly along the length of the reactor. Reactor C replicates the process of reactor B but the flue gas gets dispersed into six evenly distributed cylinders

All catalyst samples were prepared using the wet impregnation method to form a wash-coat covering the ceramic support. For starters, the impregnating solution is made by dissolving palladium (II) acetate in Acetone using a stirrer at room temperature with 500 rpm for 2 hours. The exact amount of dissolved palladium (II) salt was proportionate to the mass of the ceramic support, yielding a sample with 0.1wt% Pd for 195 g of ceramic support referred to as Pd/ Al_2O_3 hereafter. When the solution was ready, a dropper was used to impregnate the ceramic support with it. After that, it was dried in an 80 °C oven for 1 h, and the same process was repeated until the ceramic support completely absorbed all the solution. The resulting catalyst was then treated first in an oxidation furnace with air at 400 °C for 4 hours, and second, in a reduction furnace with an H-Ar mixture at 750 °C for 12 hours, the temperature ramping was 5 °C/min for the first 2.5 hours, then 9.5 hours at 750 °C, and finally it cooled inside the furnace at room temperature.

Cu, Ni, and Co loaded Al_2O_3 catalyst (promoters project)

- Palladium (II) acetate (Pd $(OCOCH_3)_2$; ≥ 97%, Sigma Aldrich)
- Nickel (II) acetylacetonate ($C_{10}H_{14}NiO_4$; Ni ≥ 98%, Merck KGaA)
- Copper (II) acetate monohydrate ($C_4H_6CuO_4$. $1H_2O$; Cu ≥ 98%, VWR)
- Cobalt (II) acetate tetrahydrate ($C_4H_6CoO_4$. $4H_2O$; Co ≥ 99%, Fluka)
- Acetone (C_3H_6O, 99.5%, VWR)
- Ethanol (C_3H_6O, purity ≥ 98%, VWR)
- Distilled water

Gamma-Aluminum Oxide (Al_2O_3 ≥ 93) was manufactured by Thermo Fischer Scientific under the product name Aluminum oxide, catalyst support, high surface area, Thermo Scientific Chemicals with pellet form and 0.6 ml/g pore volume

Structural steel – S235JR The reaction chamber was built to EN10025 European Production standards. This non-alloy structural steel comprises 0.17% carbon and has a tensile strength of 400-500 n/mm2. The electrical resistance is 0.14 Ω · mm2/m, while the thermal conductivity is 54 W/(m·K). Figure 12 below shows the reaction chamber design.

The process of preparing this project's samples was similar to the previous projects where all catalyst samples were prepared using the wet impregnation method to form a wash-coat covering the ceramic support.

Starting with the Ni and Ni/Pd Samples, the impregnating solution is made by dissolving Ni (II) acetylacetonate in distilled water using a stirrer at 40 C with 500 rpm for 6 hours and when the solution was ready, a dropper was used to impregnate the ceramic support with it, once the solution was completely absorbed by the ceramic support, it was then treated in an oxidation furnace with air at 400 °C for 4 hours, afterward the sample was wet impregnated with 0.1wt% Pd, and finally, the resulting samples were treated first in an oxidation furnace with air at 400 °C for 4 hours, and second, in a reduction furnace with an H-Ar mixture at 750 °C for 12 hours.

The Cu, Cu/Pd, Co, and Co/Pd samples followed the same process of preparation except they were dissolved in their suitable solvent.

Finally, the resulting samples are mentioned in Table 10. In the result and discussion section.

3.2 CO oxidation Tests in a Fixed-bed reactor

Initially, we employed a fixed bed attached to a Hewlett Packard 5890 Series II gas chromatography (GC) system to measure the catalyst activity. During the measurements, a quartz tube with a wall thickness of 1 mm, an internal diameter of 8 mm, and a length of 200 mm was vertically inserted into a tube furnace. The tube contained a constant mass of 450–500 mg of solid catalyst samples, which were put in the middle of the tube. Prior to starting the experiment, the samples underwent oxidation and reduction. The sample was purged with pure O2 gas for 30 minutes at 300 °C during the oxidation process. Following oxidation, pure argon was used to purge the system for five minutes. The samples were reduced after argon purging and oxidative preparation. To get rid of undesired surface toxins, the sample was purified with pure H2 for 30 minutes at 300 °C during the reduction. After that, argon was used to cleanse the system for five minutes. After the catalyst samples were pretreated, our system was cooled down to 60 °C. A CO–O2–Ar reaction gas mixture was used to take measurements at seven different temperatures, ranging from 60 to 200 °C. In the O2-rich measurement condition, our reaction gas mixture flow rate was 4–10–46 mL/min, and in the CO-rich measurement condition, it was 10–4–46 mL/min.

Based on the various thermal conductivities of the components, the thermal conductivity detector (TCD) produced the signal.

Figure 7 shows some of the support designs that were investigated during this project, and the reason for not exploring different materials as the main structure of the support apart from Al_2O_3 is to decrease the variables affecting our measurements and to avoid melting of the support Al_2O_3 was the most convenient.

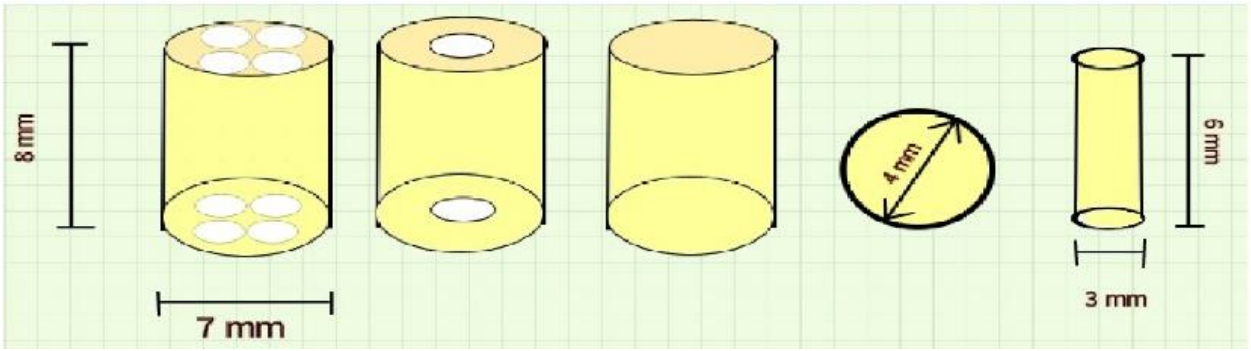

Figure 7*. Five different ceramic supports that were investigated during this project, where the main material is Al_2O_3.*

The first three support designs from the left called hereafter cylindrical shape were prepared as follows, using the necessary quantities of raw materials, a dense ceramic mass was created by adding water and homogenizing it multiple times to allow the clay components to unfold. After about a week of daily homogenization, when the moisture content of the ceramic mass reached 22–25%, we began producing the three types of cylindrical ceramic bodies using the vacuum press extrusion method. As for the spherical-shaped and the pellet-shaped catalysts are both made of Gamma-Alumina, which means they were both annealed below 900-1000 ^{o}C during the manufacturing process. Afterward, to create a wash-coat on the ceramic support, all catalyst samples were prepared using the wet impregnation method so that the resulting sample contained 0.1wt% Pd, and finally, the carried-out tests indicated that Pd supported Aluminum-oxide catalysts are promising for efficient CO oxidation and selective oxidation of flue gas components. Led by the spherical-shaped and pellet-shaped catalysts as they showed a superior performance. In conclusion, we established that the shape of the support has a huge impact on the flue gas conversion.

CO oxidation measurements were held to select the most appropriate catalyst to perform heterogeneous catalysis measurements inside the catalytic converter see figure 8 and 9.

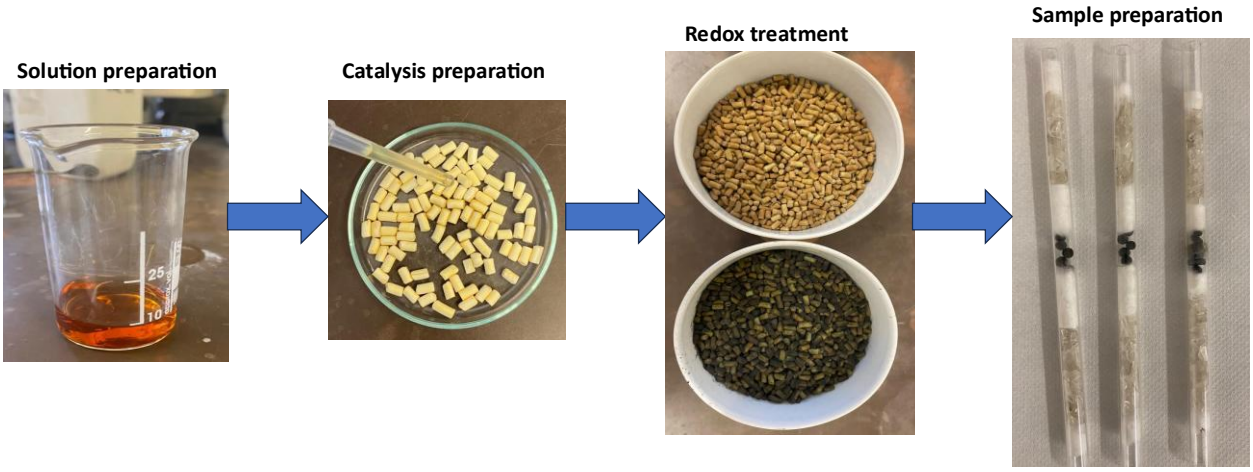

Figure 8. *The process of sample preparation for CO oxidation test.*

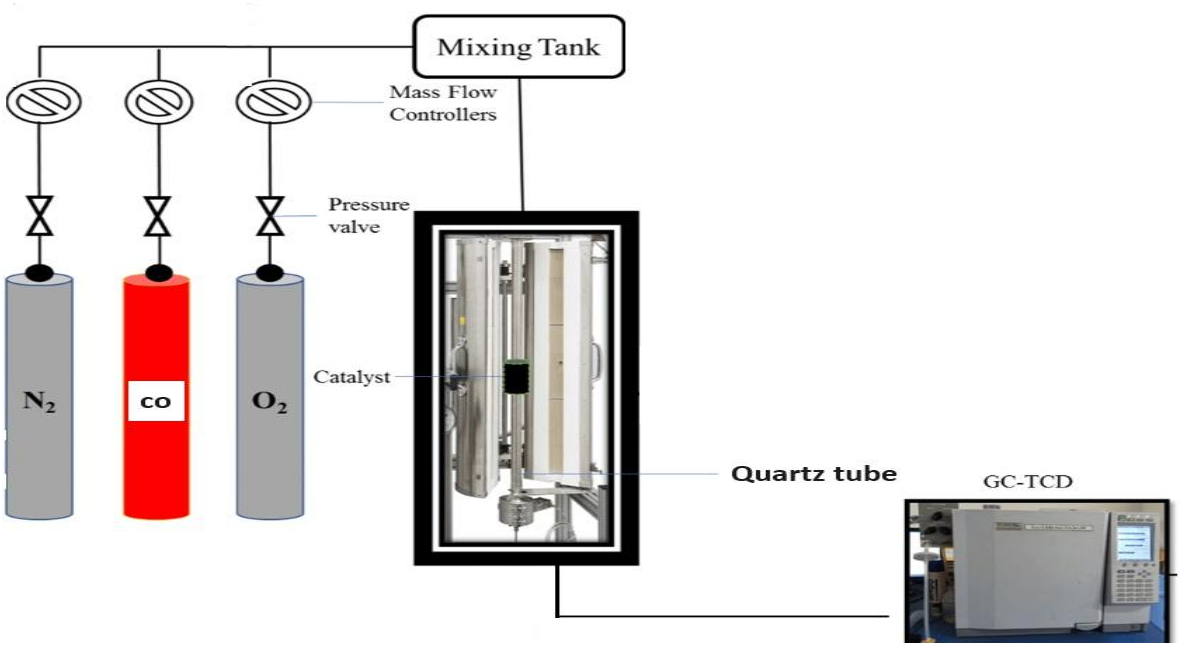

Figure 9. *Schematic representation of the fixed bed reactor setup for CO oxidation tests.*

3.3 Flue gas treatment in Real Driving Emission setup

A gas analyzer and a controlled flue-gas emission source make up the two primary systems of the system. The first has a moveable measurement table with a frame that prevents damage and a galvanized surface that is mobile.

An internal combustion engine is started through a 3-phase asynchronous electric motor, which serves as the load unit. The engine in use is a 4-stroke, single-cylinder, OHV petroleum engine with a net power of 8.7 KW, called the HONDA GX390.

The ENERGOPOWER (Telj-4) measurement software, which also regulates the functioning of big braking systems, can be used to set the static working point or to control the entire measuring cycle. The second is a set of Testo 350 gas analyzer probes that were placed both before and after the catalyst sample. Many flue gas components, including carbon monoxide (CO), carbon dioxide (CO_2), sulfur dioxide (SO_2), nitrogen oxides (NO_x), and pressure and temperature variations, can be measured by the Testo 350 emission analyzers.

Data from gas analyzers is gathered via easyEmission software once the analyzers are connected to a computer. Three distinct measuring points—1500 rpm, 2500 rpm, and 3500 rpm—were used for gathering the data, however, later in this project the measuring points were adjusted to – 1.0 kW and 0.5 kW power output – which typically occurs at the following operating conditions [2000 rpm / 4.5 – 5 N.m and 2000 rpm / 2 – 2.5 N.m] respectively, see table 6 for more information about the engine and the exhaust flow parameters.

The engine's exhaust output was connected to the catalytic converter chamber, which was made to accommodate our catalyst samples. See Figures 10 and 11.

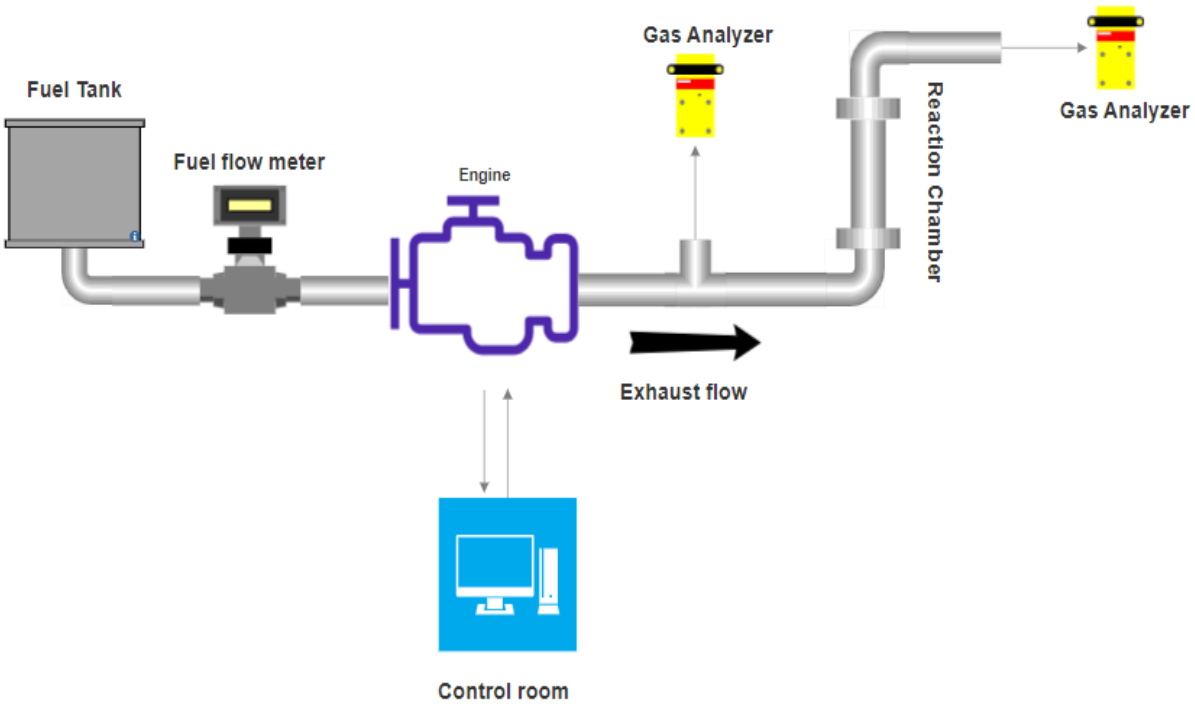

***Figure 10**. Schematic representation of the flue gas conversion setup and the monitoring system.*

The realistic system differs in dimension and size from the schematic representation as shown in Figure 11.

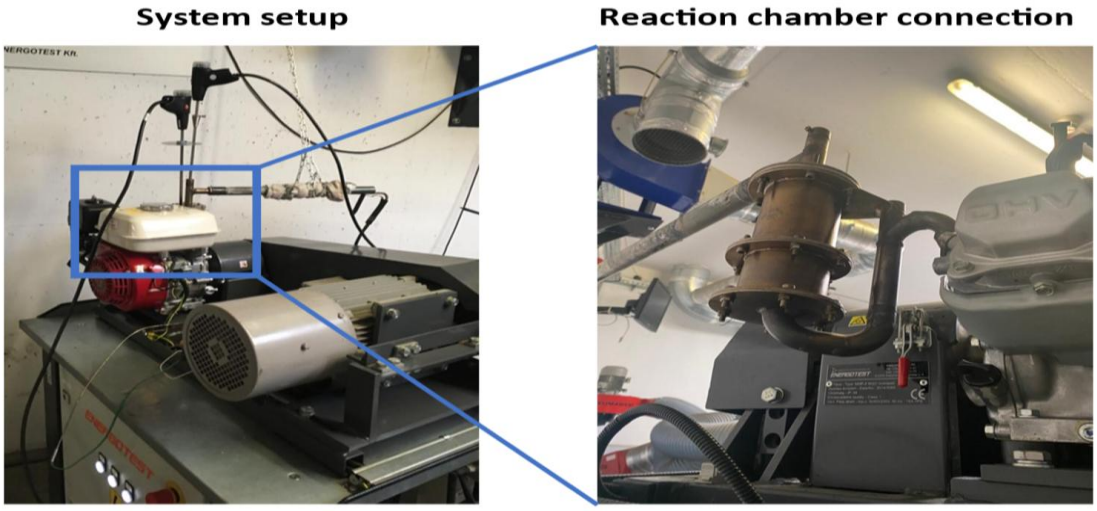

***Figure 11.** Real photo of the flue gas conversion system and a close-up of the manufactured reaction chamber connected to the exhaust flow of the engine*

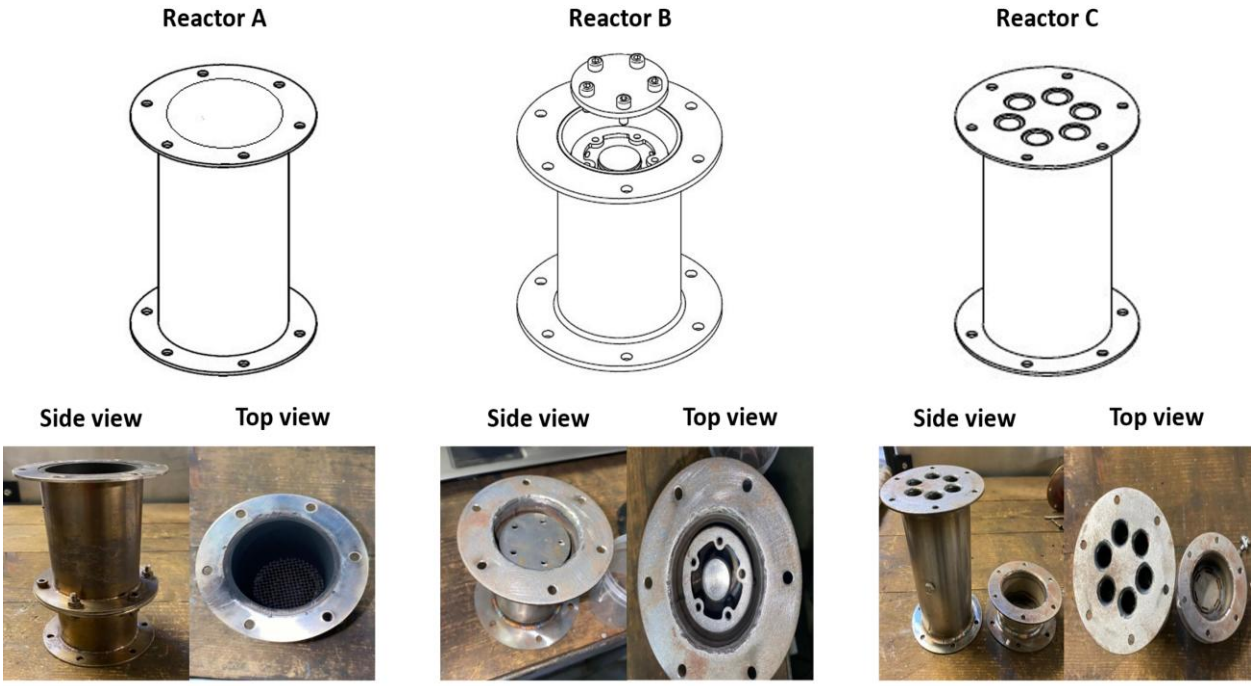

Figure 12. *Schematic representation of the three reactors' design, and real photos of their top and side view*

Moreover, the second project of my research studied the effect of reaction chamber design on flue-gas conversion, to which three different reaction chambers were manufactured and tested, the three reaction chambers were constructed to explore their impact on the efficiency and effectiveness of the flue-gas conversion process. The chambers were named Reactor A, Reactor B, and Reactor C, see Figure 12. Each had a unique design, as follows:

Reactor A: a simple cylindrical chamber with a flow entrance at the bottom, the direction of the flow is vertical passing the catalyst and exiting from the top.

Reactor B: cylindrical chamber where the flow goes through a tube before dispersion evenly along the length of the reactor, the exhaust flow enters from the bottom and exits from the top.

Reactor C: cylindrical chamber, the exhaust flow is vertical entering from the bottom, and the flue gas gets dispersed into six evenly distributed cylinders before exiting from the top.

Table 5. *Basic properties of the three reactors.*

	Reactor dia. (mm)	Effective dia. (mm)	Reactor Length (mm)
Reactor A	56	56	90
Reactor B	48.3	27	95
Reactor C	70	(16) *6	149

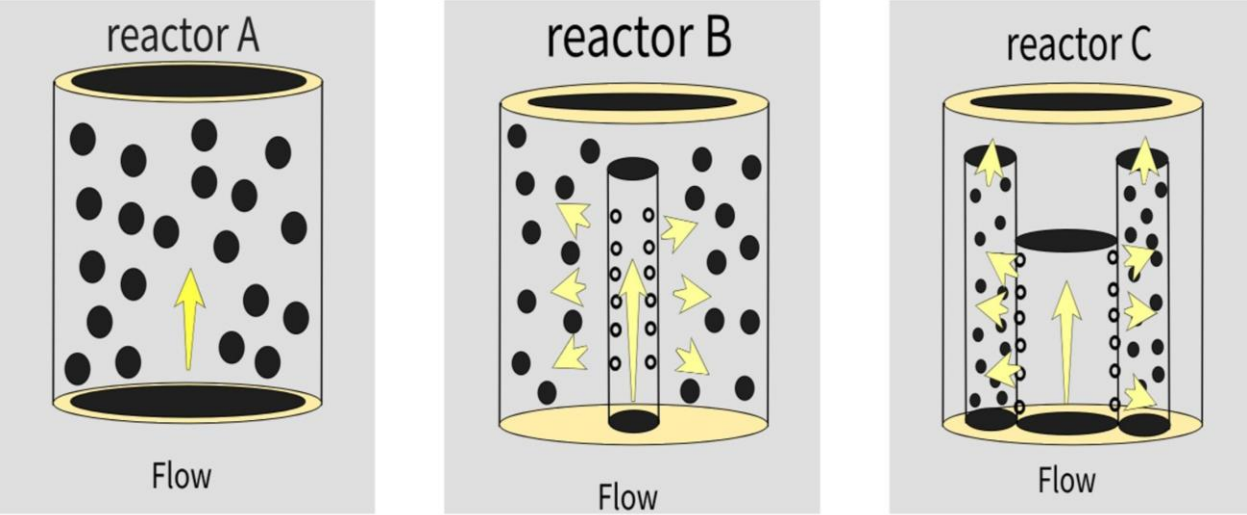

Figure 13. *Schematic representation of the exhaust gas flow through the three reactors*

Table 6. *The 0.5 kW and 1.0 kW operating conditions and their correspondent inlet flow and engine operating parameters*

	Inlet flow parameters			Engine operating parameters		
	Temp.(°C)	Flow(m^3/h)	Vel.(m/s)	rpm	Torque (N.m)	Power (kW)
0.5 kW condition	500	11000	3.7	2000	2 – 2.5	0.5
1.0 kW condition	585	18000	6.5	2000	4.5 – 5	1

3.4 Characterization methods

This section is divided into two primary parts, the first is the characterization of the catalysis samples, and the second is the characterization of the reaction chambers.

3.4.1 Surface characterization

X-ray diffraction (XRD)

X-ray diffraction is a powerful, non-destructive analytical technique used to determine the crystal structure, atomic and molecular structure of materials [99]. In this study, XRD measurements were conducted to determine the crystal structure and composition of the samples at various stages of the project process.

Methodology:

- **X-ray Source**: Co anode, chosen for its ability to provide increased resolution compared to more common Cu sources
- **Measurement Speed**: 1°/min, allowing for high-resolution data collection
- **Diffractometer**: Rigaku MiniFlex II, a versatile benchtop system
- **Sample Preparation**: Samples were finely ground into powder form using a mortar and pestle to ensure homogeneity and minimize preferred orientation effects

XRD analysis provides critical information about the crystalline phases present, their relative abundances, and any structural changes occurring during the project's various stages.

Transmission electron microscopy (TEM)

Transmission Electron Microscopy is an advanced microscopy technique that allows for the visualization of materials at the nanoscale, providing invaluable insights into their structure and morphology [100].

Applications in This Study:

- **Morphological Analysis**: TEM images were used to study the detailed morphology of the prepared samples.
- **Particle Size Estimation**: accurate estimation of average particle sizes is crucial for understanding the material's properties and performance.
- **Coke Formation Resistance**: TEM was instrumental in assessing the pellet sample's ability to resist coke formation. By monitoring the deposited or adsorbed carbon on the

support, we could evaluate the material's stability and potential longevity in relevant applications.

TEM's ability to provide both imaging and diffraction information makes it an indispensable tool for comprehensive materials characterization.

X-ray fluorescence (XRF)

X-ray Fluorescence is a non-destructive analytical technique used to determine the elemental composition of materials [101]. This method is particularly valuable for its ability to analyze a wide range of elements simultaneously.

Instrumentation and Methodology:

- **Analyzer**: Olympus Vanta VMR-CCX-G3-E XRF analyzer
- **Beam Configuration**: Beam 1: 10 keV - Beam 2: 40 keV
- **Analysis Protocol**: Each beam is applied for 30 seconds, total analysis time per sample: 1 minute, repeated 3 times per sample for statistical reliability, and results reported as an average of the three measurements

This dual-beam approach allows for the detection of both light and heavy elements, providing a comprehensive elemental profile of the samples.

Physical adsorption (BET)

The Brunauer-Emmett-Teller method is a widely used technique for determining the specific surface area of materials, which is crucial for understanding their adsorption properties and potential catalytic activity [102].

Experimental Setup:

- **Instrument**: NOVA 3000 multi-station nitrogen sorption analyzer
- **Analysis Gas**: Nitrogen
- **Degassing Temperature**: 200 °C
- **Analysis Temperature**: 88.3 K (liquid nitrogen temperature)

- **Duration**: Approximately 113 minutes per sample

The BET analysis provides insights into the material's porosity, and surface area, which are critical parameters for catalysis

Thermogravimetric analysis (TGA)

Thermogravimetric Analysis (TGA) is a thermal analysis method that measures changes in the mass of a sample as a function of temperature or time, providing crucial information about material composition, thermal stability, and decomposition characteristics [103].

Experimental Parameters:

- **Instrument**: TA Instruments TGA Q500
- **Atmosphere**: Air (oxidizing environment)
- **Heating Rate**: 10 °C/min
- **Maximum Temperature**: 900 °C

TGA data can reveal information about moisture content and volatile components, thermal decomposition temperatures, oxidation and reduction reactions, and composition of multi-component systems

This comprehensive suite of analytical techniques provides a multi-faceted approach to materials characterization, enabling a thorough understanding of the samples' structural, compositional, and thermal properties throughout the project lifecycle.

3.4.2 Fuel consumption Tests

The new BRONKHORST ES-FLOW ultrasonic flow meter and controller was used for measuring the fuel consumption and is made for measuring liquids' volume flow, ranging from 2 to 1500 ml/min with great precision, linearity, and low-pressure drop utilizing ultrasonic wave technology in a small-bore tube. For this specific construction, the pressure rating is 10 bar. Regardless of fluid density, temperature, or viscosity, the measurements of the liquid will be accurate. As a result, conducting calibrations for each fluid is unnecessary, because the instrument can detect the measured liquid's actual speed of sound. Due to these features, the ES-FLOW has many similarities with their Coriolis technology-based instruments. These are very beneficial compared

to other types of flow meters. The ES-FLOW can measure non-conductive liquids like hydrocarbons, demineralized water, and oil-based additives.

3.4.3 Finite element method (FEM)

A useful technique for better understanding the operation of fixed-bed catalytic reactors is the finite element method, which can produce a complex heterogeneous model of the temperature and flow profile across the reactor. Suitable for very viscous flow, FEM offers a broad framework for tackling arbitrary issues. Moreover, FEM is one of the numerical methods used for solving the model equation of fixed-bed reactors [54 – 58], finally, FEM is essential in designing industrial fixed-bed catalytic reactors, In this experiment, the heat and flow profiles via three distinct reactors that were linked to a gasoline engine's exhaust outlet were characterized using FEM. Table 6 lists the engine's operational parameters as well as the flue-gas input parameters that enter the reactor chamber. This experiment was held during the loading of the reactors with 65 grams of the 0.1wt% Pd over spherical Al_2O_3, and it was also held when the reactors were empty. Finally, the simulation and the computer aid design were done using Ansys 2023 R1 software.

The 3D CAD models of the three reactors were made in CAD modeling software and the drawings for production were made from those models. However, for the FEM simulation, these models are not suitable, because we don't want to investigate the chassis rather we are focusing on the information about the gas flow and temperature. Therefore, the first step in the FEM analysis process is the creation of a proper model, starting with the inner space of the reaction chamber as the most important part. For this simulation, we needed 3 empty and 3 loaded models. Those models are the initial models for the simulations. The software is a student version, where the number of elements is limited. After the model preparation, the next step is the mesh generation, afterward we set the boundaries of inlet and outlet conditions. The initial parameters were set as the gas type of the flow in this case CO and of the boundary surfaces in this case steel. After the setting of the initial parameters (type of the gas, temperature, and velocity by the inlet, the behavior of the outlet, etc.) the simulation ran quickly because of the limited number of the elements.

The number of iterations to the solver must be set up before the calculation can begin. The solver process runs automatically, allowing the user to track changes in energy, flow characteristics, and velocities on the computation screen. After the calculation, the result screen allows you to tweak the simulation's visualization and change the range. The range visualization begins with "blue,"

the lowest temperature and velocity, and ends with "red," the maximum temperature and velocity. Visualization of the temperature and velocity profiles can be defined by identifying data on the model, where numbers are added to the corresponding colors, and at the same time the number of contours can be adjusted.

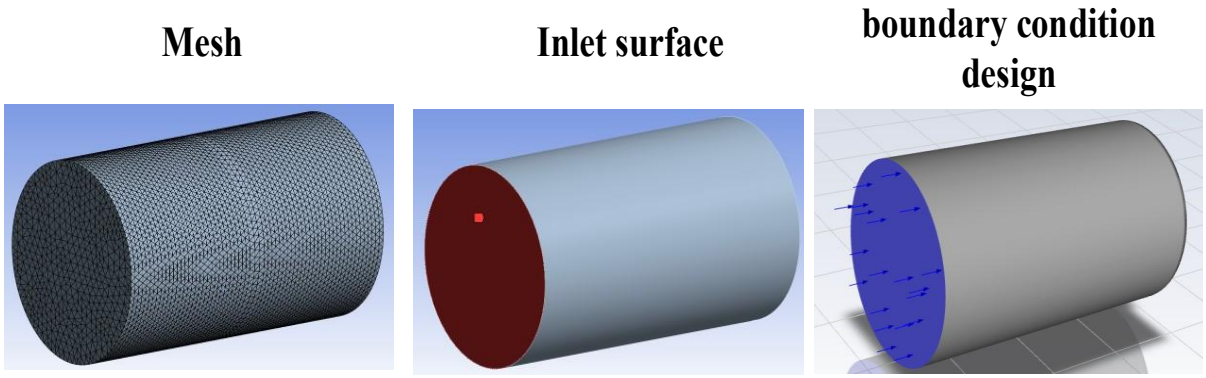

Figure 14. *Representation of the mesh and inlet surface, and the design of boundary conditions.*

3.5 Data analysis and calculations

During this Ph.D. work, we had a weekly meeting with our supervisor Dr. Sápi Andras, and the research group in the Science department as well as regular meetings with Dr. Farkas Ferenc and Dr. Peter Istvan, in the engineering department to discuss the advances in the flue gas conversion project and modifying the approaches to this project, data were gathered using EasyEmission software for the data coming from the testo gas analyzer, also AVL software gathered the data coming from the AVL gas analyzer, which were in xlsx and CSV form respectively, moreover, Microsoft Excel was used to analyze data and measure the averages, OriginPro software was used to draw the graphs, and Ansys software was used to simulate the FEM of heat and flow.

4. Result and Discussion

This chapter will discuss the series of tests, that investigate the performance of five ceramic supports impregnated with 0.1 and 0.2 wt.% palladium (II). Starting with the samples' ability to oxidize CO in a fixed bed reactor, and the evaluation of their effectiveness in converting flue-gas emissions coming from gasoline engines. Also, this chapter will discuss the results of another series of measurements that were held to determine the effect of reaction chamber design on flue-gas conversion. lastly will discuss the results of adding Ni, Cu, and Co promoters to the Pd-loaded Al_2O_3 catalysis and their effect on the catalytic activity and flue gas conversion.

4.1 Support design effect results

Synthesis and characterization of sample results

To begin, the impregnating solution is created by dissolving palladium (II) acetate in acetone solvent for 5 minutes using an ultrasonic sonication bath. The precise amount of dissolved palladium (II) salt was proportional to the mass of the ceramic support, yielding a sample containing 0.1 wt.% Pd and 0.2 wt.% Pd for 125 g of ceramic support. When the solution was ready to use, a dropper was used to impregnate the ceramic support. Finally, it was dried in an 80 °C oven for 1 hour, and the process was repeated until the ceramic sample had absorbed the entire solution. The resulting catalyst was then treated first in an oxidation furnace with air at 400 °C for 4 hours, and then in a reduction furnace with an H-Ar mixture at 750 °C for 12 hours, with a temperature ramping of 5 °C/min for the first 2.5 hours, then 9.5 hours at 750 °C, and finally cooling inside the furnace at room temperature.

Sample preparation results

First the sample's physical properties

To properly assess the differences in sample geometry, we must first know the majority of their physical characteristics, such as characteristic length and Void fraction (or vacancy %) We may calculate these values by solving the following equations and inserting the necessary values based on the shape geometry:

$$\text{Characteristic length} = \frac{\text{surface area}}{\text{volume}} \quad \text{Eq. 3}$$

$$Void\ fraction = \frac{empty\ tube\ volume}{total\ tube\ volume} \quad \text{Eq. 4}$$

Table 7. *Basic properties of the ceramic samples.*

	Surface area to volume ratio for a 400-500mg of catalyst (mm^{-1})	**Void fraction**
Cylindrical/no holes 0.1wt% Pd	0.8	0.969
Cylindrical/one hole 0.1wt% Pd	0.88	0.971
Cylindrical/4 holes 0.1wt% Pd	1.16	0.979
Pellets 1/8" 0.1wt% Pd	6.75	0.972
Spherical 0.1wt% Pd	10.4	0.984

After the five batches of catalyst were prepared, we were left with 65 grams of each batch, Figure 7 represents a picture of an individual support unit after the preparation, The diverse shapes of catalyst samples shown in the figure play a crucial role in investigating the effect of catalyst geometry on flue-gas conversion efficiency. Each shape offers unique characteristics as discussed in the physical properties, that can influence the catalytic process in different ways

The variety of shapes allows for a comprehensive study of how catalyst geometry influences flue-gas conversion:

1. **Surface Area to Volume Ratio**: Different shapes offer varying ratios, which directly impact the number of accessible active sites for the catalytic reaction.

2. **Mass Transfer**: The shape affects the diffusion of reactants and products to and from the catalyst surface. Shapes with higher external surface area may exhibit enhanced mass transfer characteristics.

3. **Heat Transfer**: Catalyst shape influences homogenous heat distribution and dissipation.
4. **Pressure Drop**: In fixed-bed reactors, the catalyst shape significantly affects the pressure drop across the bed. Shapes like pellets and spheres aim to optimize bed packing and reduce pressure drop.
5. **Coking Resistance**: Shapes that promote better gas circulation such as multi-hole cylinders show improved resistance to coking.

Flue-gas conversion results

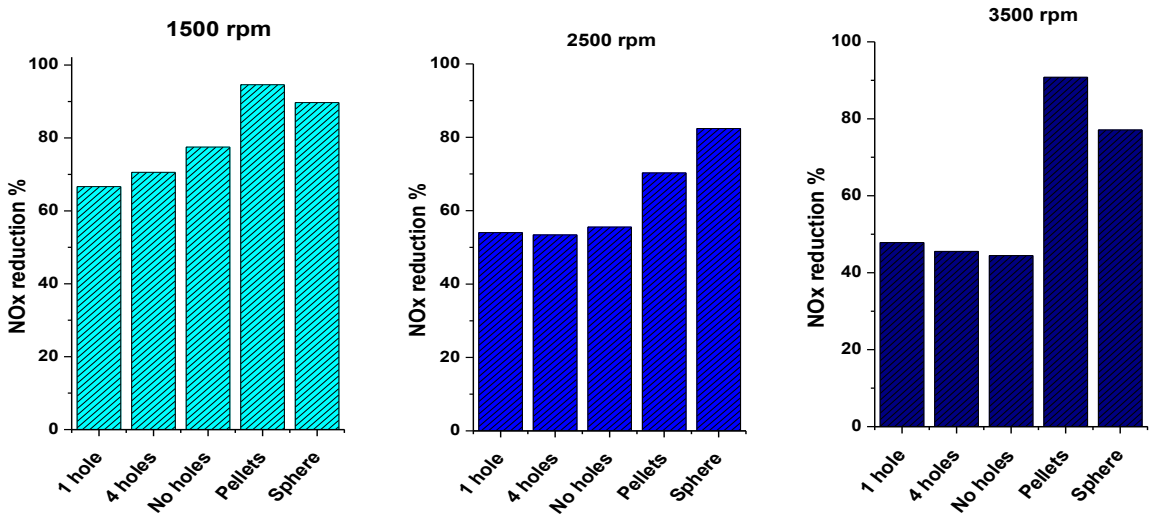

Figure 15. *Performance of the five ceramic samples in reducing NO_x at three different engine speed points (1500 rpm, 2500 rpm, and 3500 rpm).*

All samples demonstrated excellent catalytic activity in reducing NO_x as shown in Figure 15, with both pellets and spheres samples outperforming as expected based on their activity in the fixed-bed reactor.

Moving forward, pellets and spheres maintained their preferred performance at higher flow, speed, and temperature at 2500 rpm and 3500 rpm, as illustrated in Figure 15 / 2500 and 3500 rpm the performance of the other three cylindrical samples had a good conversion at low speeds reaching around 80% conversion for the no-hole sample at best and around 70% conversion for

the 1-hole sample, However, the increased speed of the engine seemed to decrease the performance of these samples, unlike the spherical and pellets.

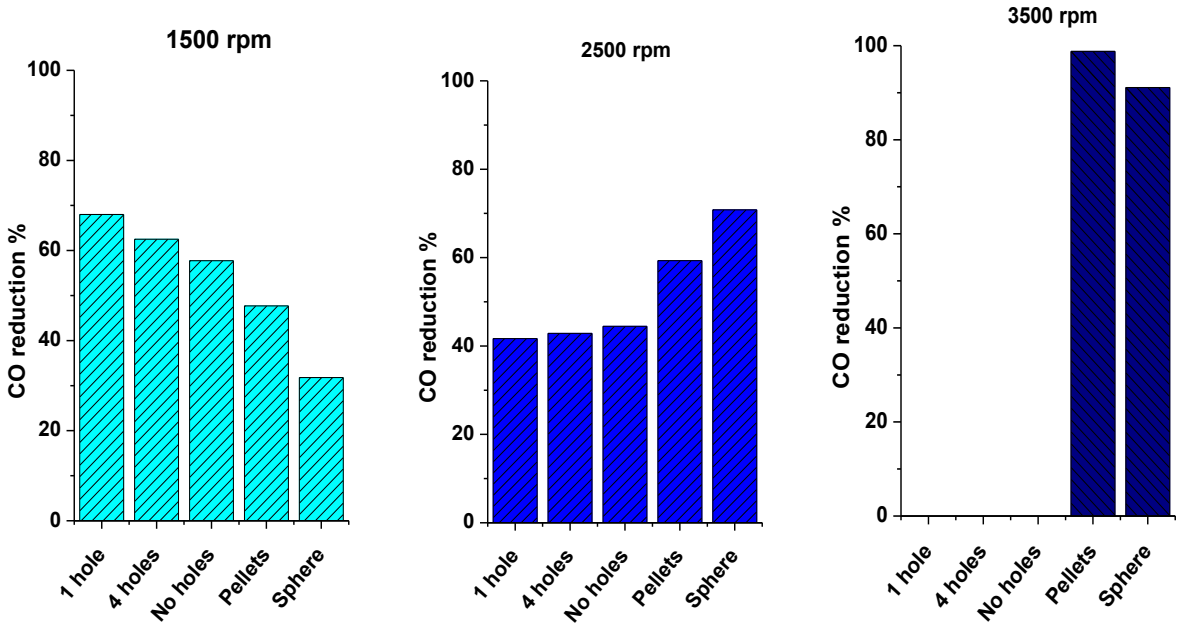

Figure 16. *Performance of the five ceramic samples in reducing CO at three different engine speed points (1500 rpm, 2500 rpm, and 3500 rpm).*

Figure 16, illustrates CO reduction using five distinct samples. The cylindrical samples performed somewhat better at low flow speeds, possibly due to their higher void percentage at this mass, which allows more time for the flue gas to pass through the catalyst and increases the contact surface area. However, the pellets and spheres samples regained the lead in catalytic activity at 2500 rpm and 3500 rpm, when the flow, speed, and temperature of the flue gas rose, as seen in Figure 15/ 2500 and 3500 rpm. One explanation for this performance presented by the pellets and spheres samples is their amorphous nature and high BET surface area, moreover, their activity in the fixed bed reactor is also corresponding to their performance in the catalytic converter. As for the overall performance comparison, it's very much dependent on the application. On the one hand, the pellet-shaped catalyst showed the best conversion of NO_x and CO at 1500 rpm and 3500 rpm, so it's a favorable option for applications in which engines run more at these speeds. On the other hand, the results suggest that the spherical catalyst will have higher activity in applications where engines run more around 2500 rpm, and finally, if the engine is constantly changing.

Fixed-bed reactor results

The experiments were carried out using a fixed bed connected to a gas chromatograph, to imitate the lean and rich conditions occurring inside an internal combustion engine, which generally refers to the ratio of air and fuel in the combustion chamber. The experiments were held under two different conditions: (a) The first condition represented an oxygen-rich scenario in which O2 gas flow was 2.5 times greater than CO flow, whereas (b) the second condition represented an oxygen-deficient example in which CO gas flow was 2.5 times larger than O2 flow.

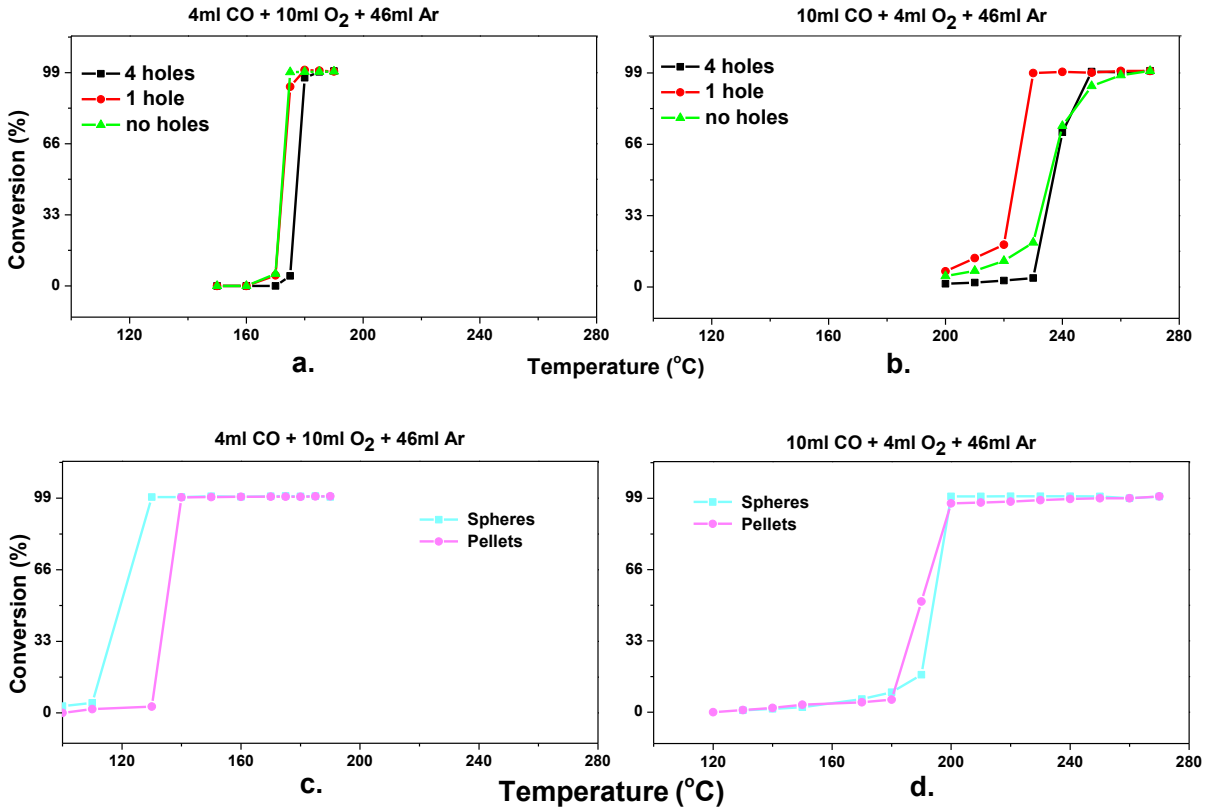

Figure 17. *CO conversion as a function of temperature for five different shapes of ceramic samples, where all samples contain 0.1wt% Pd. Fig a. and b. showing the performance of no holes, one hole, and four holes samples at low temperature and high temperature respectively. Fig. c. and d. show the performance of spheres and pellet samples at low and high temperatures respectively.*

Figure 17/a. shows that the three alpha-alumina catalysts performed similarly under O2-rich conditions, with all samples achieving complete oxidation at 175-178 ºC, Figure 17/b shows that

the one-hole catalyst performs marginally better than the four-hole and no-hole catalysts due to its two-fold larger diameter. The larger the diameter of the hole, the more diffusion occurs through the catalyst rather than increasing the contact surface area. Changing the environment to lean reduced catalyst activity, with one hole completing complete oxidation at approximately 230 ºC and the rest at 250 ºC; this decrease in activity is owing to the low O2 concentration required to oxidize CO. Figure 17/c shows the conversion of gamma-alumina for both pellets and spheres, which begins at lower temperatures and reaches complete oxidation significantly faster than alpha-alumina. This performance is likely due to their amorphous structure and orders of magnitude larger BET surface area, as well as the similar void fraction values, making this assumption more likely. Figure 17/d shows a much-improved performance of the pellets and spheres under lean circumstances, with all samples achieving complete oxidation at 190 ºC. The performance of our samples differed significantly from that reviewed in the literature compared counterparts, with significantly higher activity both at the beginning of conversion and at the end of oxidation; additionally, even at low O_2 concentrations, both alpha-alumina and gamma-alumina performed better.

XRD results

Figure 18 shows the XRD patterns of Pd/ceramic support at 10 to 90 2θ. The ceramic support was mostly composed of hexagonal α-Aluminum oxide (α- Al_2O_3) for cylindrical shapes and cubic γ-Aluminum Oxide (γ- Al_2O_3) for pellets and spheres. All samples included 0.1wt% Pd. The XRD data show that the peaks of the first three samples (a.) correspond to alpha-alumina and are crystalline, but the next two samples (b.) are gamma-alumina and are more amorphous.

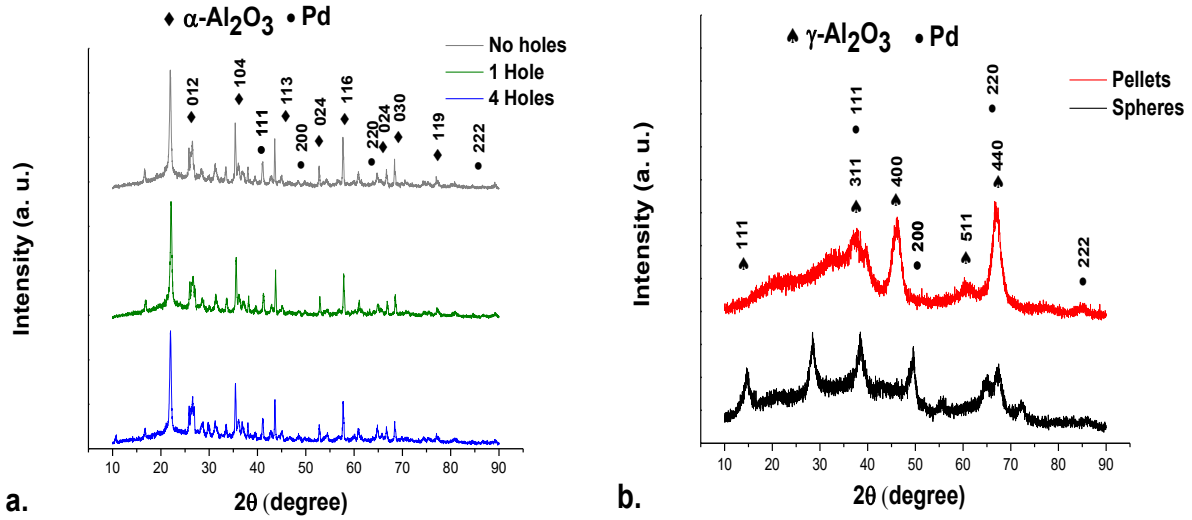

Figure 18. *XRD patterns of the ceramic support powders containing 0.1wt% Pd, where fig. a shows the peaks of alpha Aluminum oxide as well as Pd peaks, and fig. b represents the peaks of gamma Aluminum oxide and Pd.*

Typical α-Al_2O_3 peaks can be seen on the left side XRD figure at 25 (012); 35 (104); 44 (113); 53 (024); 57 (116); 66 (024); 68 (030) and 77 (119) 2θ degrees, which correspond to corundum.

Characteristic γ-Al_2O_3 peaks can be observed on the right side XRD figure at 15 (111); 37 (311); 46 (400); 60 (511) and 67 (440) 2θ degrees.

Pd peaks can be seen on both XRD figures at 40 (111); 47 (200); 68 (220) and 86 (222) 2θ degrees.

TEM results

This characterization was performed to determine the pellets sample's ability to resist coke formation, revealing the direction of the pellets sample's ability to function consistently throughout time. The experiment was conducted at 1500 rpm and 1 N.m, where emissions are normally high. The experiment was repeated three times for one hour each, and the catalyst mass utilized was 63 g. Figure 19 depicts TEM pictures of the sample before and after performing in the catalytic converter, which reveals no symptoms of coke formation.

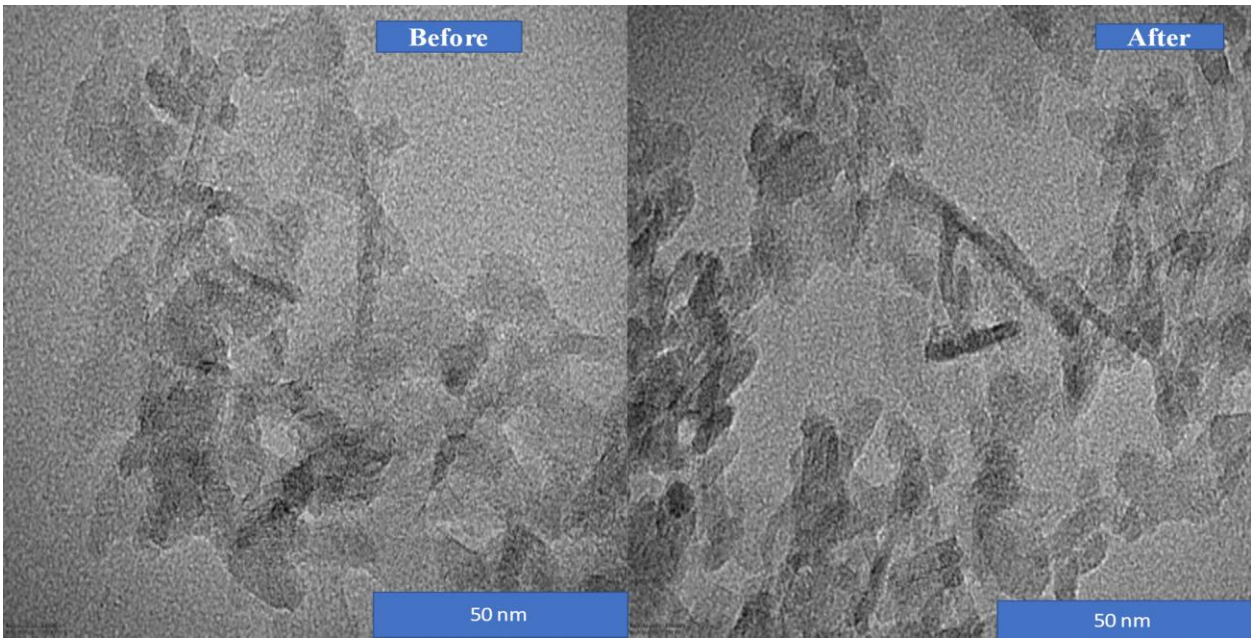

Figure 19. *TEM image of pellet sample before and after performing inside a catalytic converter for three hours*

The nanostructure appears somewhat amorphous before testing the sample, and after performing at the RDE setup the nanostructure is much more crystallin due to activation through CO reduction. This TEM comparison provides valuable visual evidence of no cock formation on the sample impacting its performance in flue-gas conversion and longevity. The enhanced definition and apparent growth of nanostructures in the "After" image suggest a transformation that could potentially improve the material's catalytic properties.

4.2 Reaction chamber design effect results

Sample preparation results

The prepared samples for this project are the catalysis samples shown in Figure 20 below and the three reaction chambers discussed earlier in section 3.3 flue gas conversion, Moreover, Figure 12 in that section shows the three reactors.

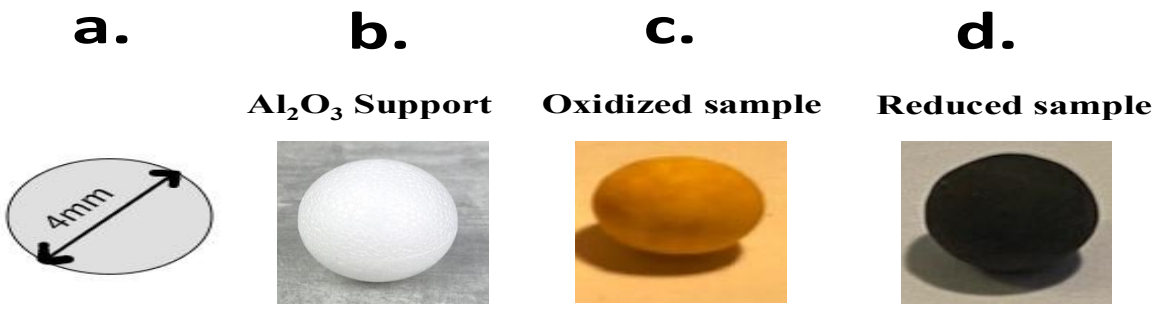

Figure 20. a. *a schematic representation of the spherical support,* ***b.*** *Al_2O_3 support before noble metal loading,* ***c.*** *the Pd/ Al_2O_3 catalyst after oxidation, and* ***d.*** *the Pd/ Al_2O_3 catalyst after reduction*

Flue-gas conversion results

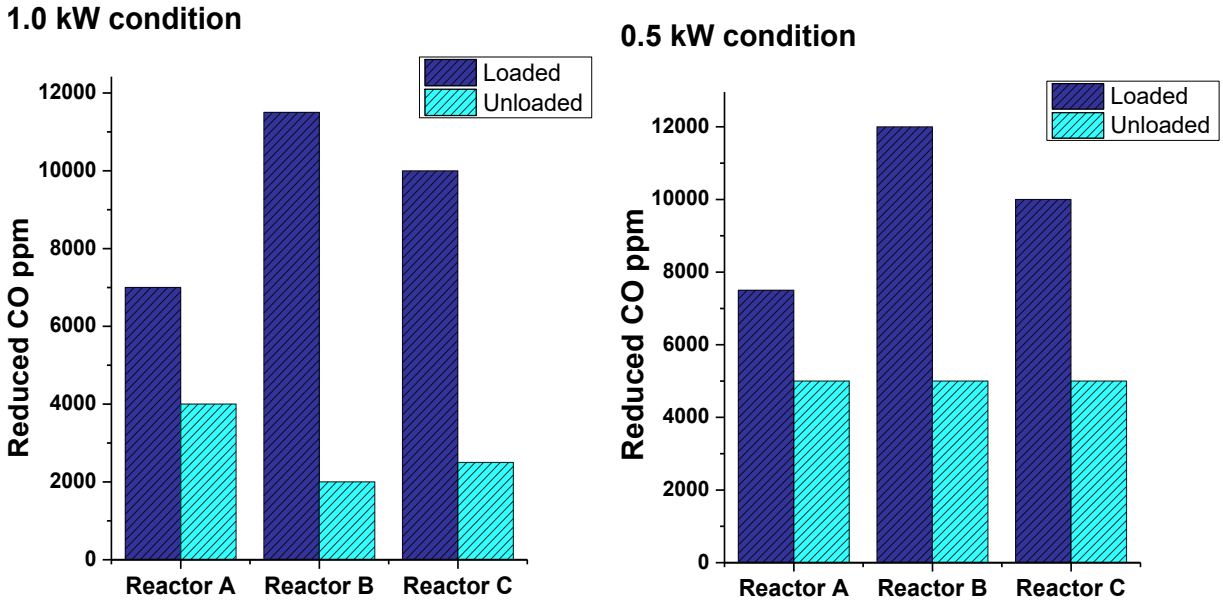

Figure 21. *The amounts of reduced CO ppm across the three reactors, while loaded and unloaded with 65 grams of Pd/Al_2O_3 catalyst at 1.0 and 0.5 kW conditions*

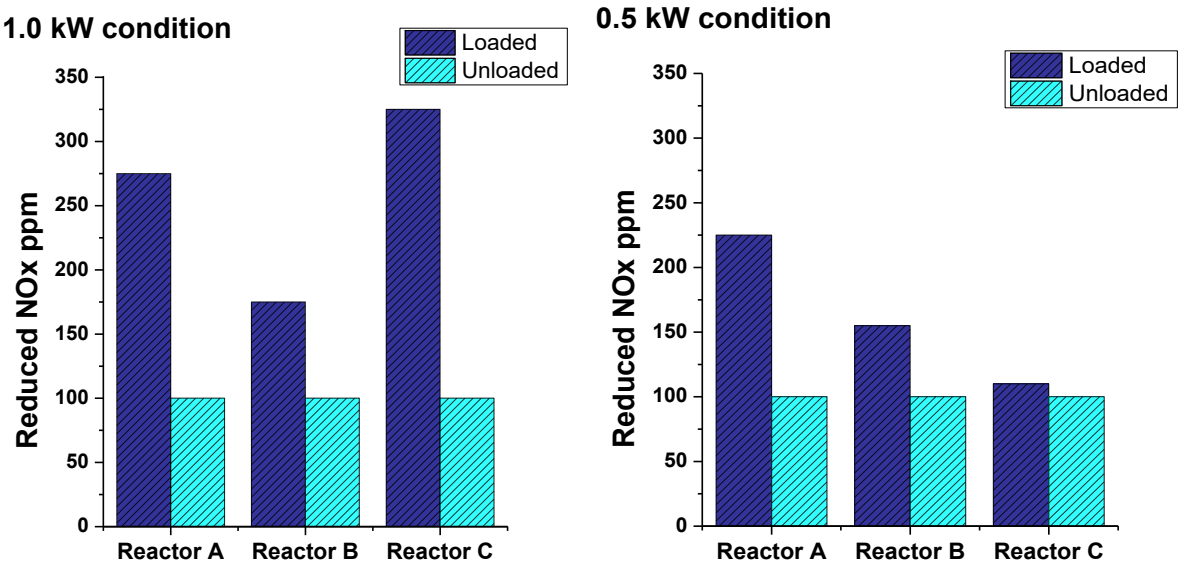

Figure 22. *The amount of reduced NO_x ppm in the three reactors while loaded and unloaded with 65 grams of PD/ Al_2O_3 during the 1.0 and 0.5 kW conditions.*

To achieve a fair comparison between reactors' performance, results are represented by showing the number of reduced flue gas particles per power unit produced by the engine. The CO reduction results for the three reactors at the 0.5 and 1.0 kW conditions, while unloaded, showed almost identical behavior, with all reactors converting 5000 ppm of CO at the 0.5 kW condition and an average of 2500 ppm of CO at the 1.0 kW condition. This type of conversion occurs naturally as some CO ppm oxidizes due to high temperatures. The catalyst loading, on the other hand, had a significant impact on the reduction, with increases of 50%, 140%, and 100% for Reactors A, B, and C at the 0.5 kW operating condition, and 57%, 475%, and 300% at the 1.0 kW operating condition. Figure 21 shows that the design change in Reactor B led to a five-fold increase in conversion, while the design change in Reactor C increased the reduction by three times. As for the NO reduction results, the reactor design and the addition of the catalyst had a significant impact on their amounts, where the relative reduction of NO ppm's from unloaded to loaded increased by 120%, 28.5%, and 7% for Reactors A, B, and C respectively at the 0.5 kW condition, as for the 1.0 kW condition the results were 175%, 75%, and 225%.

Table 8. *conversion increase percentage for CO and NO_x ppm at 1.0 and 0.5 kW operating conditions*

0.5 Kw	CO conversion increase	NO conversion increase
Reactor A	50%	120%
Reactor B	140%	28.5%
Reactor C	100%	7%

1.0 Kw	CO conversion increase	NO conversion increase
Reactor A	57%	175%
Reactor B	475%	75%
Reactor C	300%	225%

XRD results

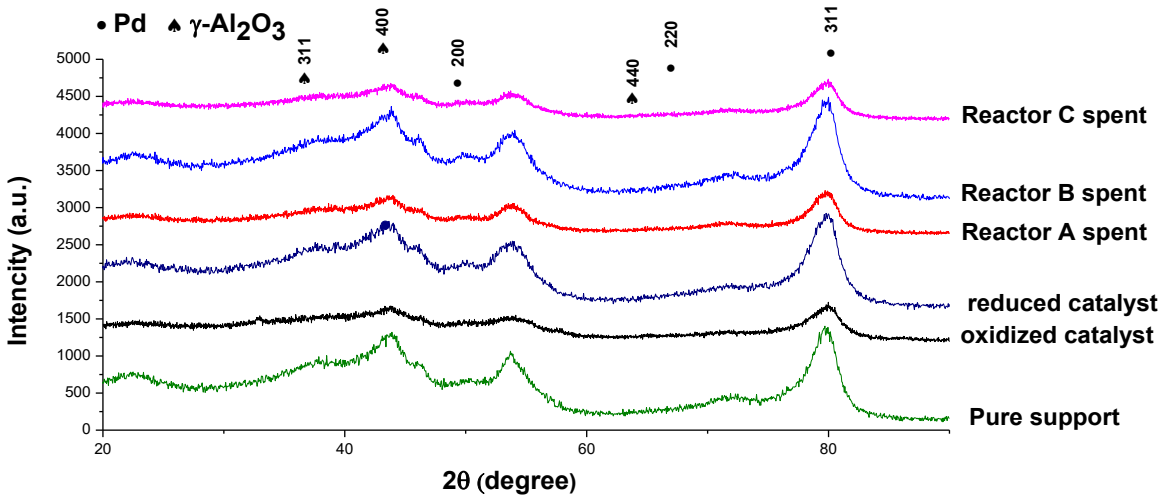

Figure 23. *X-ray diffraction patterns of self-prepared 0.1wt %pd over Aluminum Oxide support oxidized at 450 °C for 4 h (fixed temp, no heat rate) and reduced in H-Ar mixture at 700 °C for 12 h (heating rate of 5 °C/min), including a spent sample in Reactor A, B, and C.*

The Pd/Al_2O_3 sample XRD patterns were obtained in the range of 20 to 90 2θ, where the ceramic support chemical composition mainly showed ϒ-Aluminum Oxide (ϒ-Al_2O_3) and Pd, Figure 23. The samples exhibit major diffraction peaks at 2h values of 45.9 related to alumina. The reduced

sample showed the main peaks of ϒ-Al2O3 with the appearance of Pd and PdO dispersed at the alumina surface, and the spent samples showed some enhancement in crystallinity by increasing the peaks, that is particularly true for reactor B spent which could be due to the heating in the reaction champers. Also, the new phase that appeared at reactor B showed Pd alloy.

BET and XRF results

The physical adsorption test indicates a decrease in the surface area of the three spent catalysts compared to the fresh sample, as expected because the sample inside the catalytic converter is bonded to the poisoning of the flue gas, resulting in the obstruction of active sites. [24] revealed that the deactivation processes of Pd-based three-way catalysts include Pd sintering and loss of the metal-support interface. It was reported that poisoning impacts active sites by decreasing their catalytic activity. For example, in the case of Pd-based catalysts in NO-CO reactions, CO acts as a poison for Pd, reducing catalytic activity [104]. However, this does not preclude the catalyst from being active; Chen et al. reported that the rate constant for the surface reaction was independent of the extent of poisoning, implying that poisoning did not affect the activity of the remaining active sites.

Table 9. *The elemental composition and the BET surface area of the spent sample of the three reactors.*

	Al (%)	**Pd (ppm)**	**BET (m^2/g)**
Reactor A spent	24.9	302	165.8
Reactor B spent	22	315	179.2
Reactor C spent	23.6	243	182
Fresh catalyst sample	27	920	224
Al_2O_3 support	28	0	326

It is worth mentioning that the rate of surface area decline was completely linked with the results of FEM coming in the next chapter since the BET surface area has an inverse relationship with temperature. Francesca et al. observed that temperature influences BET surface area by causing

textural changes in the material. Specifically, as the temperature rises, the surface area of the material reduces due to sintering, resulting in a loss in surface area [60]. Reactor A had the highest heat profile, followed by reactor B and, finally, reactor C, which supported the rate of BET surface area decline.

TGA results

Carbon, the largest component of flue gas emissions traveling through the catalyst, could account for the majority of the weight lost in each sample. The data from Figure 24 below, show that sample A had the lowest weight loss (9.2% of the whole mass), followed by sample B, which had a weight loss of roughly 9.8% of the total mass, and lastly, the sample from reactor C had the largest weight loss (11.2% of the total mass). The results can be simply interpreted as follows: reactors A and B are well-designed for low carbon attraction on the ceramic support surface.

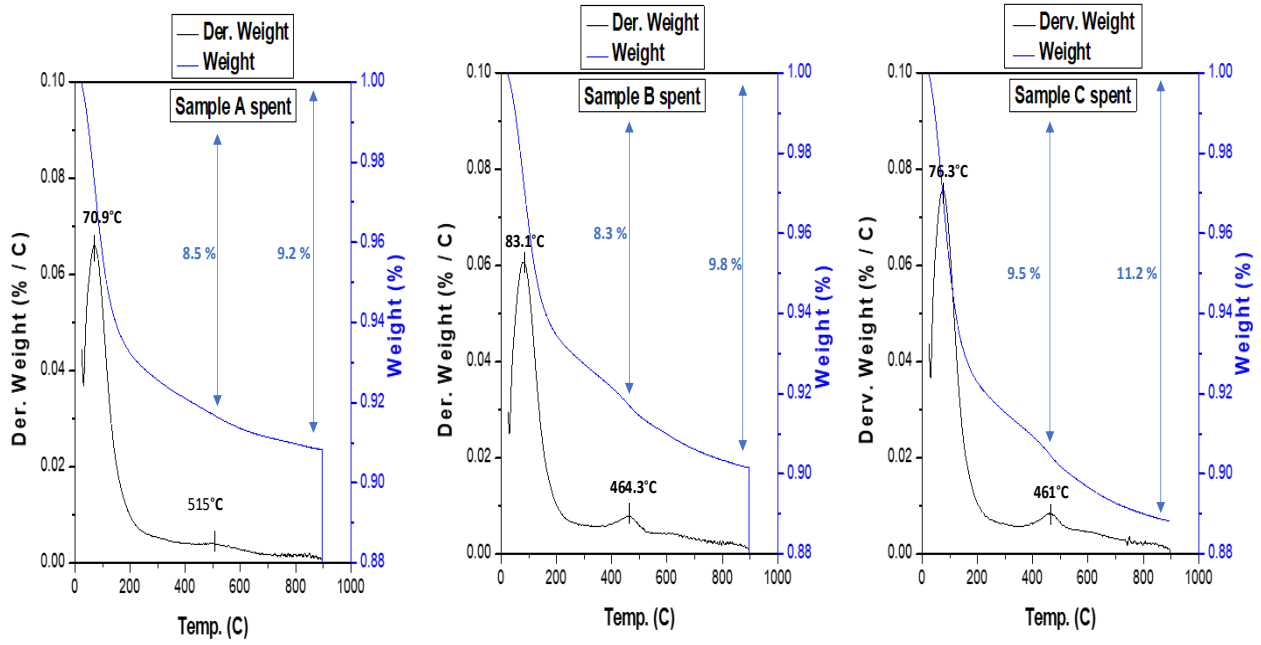

Figure 24. *The thermogravimetric analysis of the spent samples coming from reactors A, B, and C*

FEM results

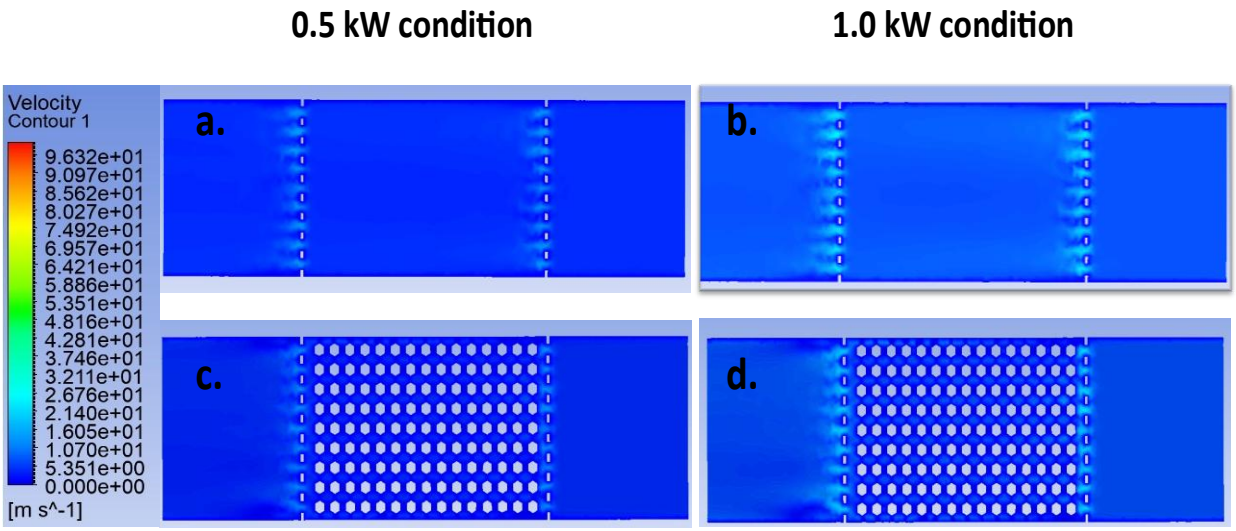

Figure 25. *Reactor A flow analysis where a. and b. show the reactor flow analysis while unloaded under the 0.5 and 1.0 kW operating conditions, on the other hand c. and d. represent the flow analysis while loaded with 65 grams of the catalyst under the same conditions.*

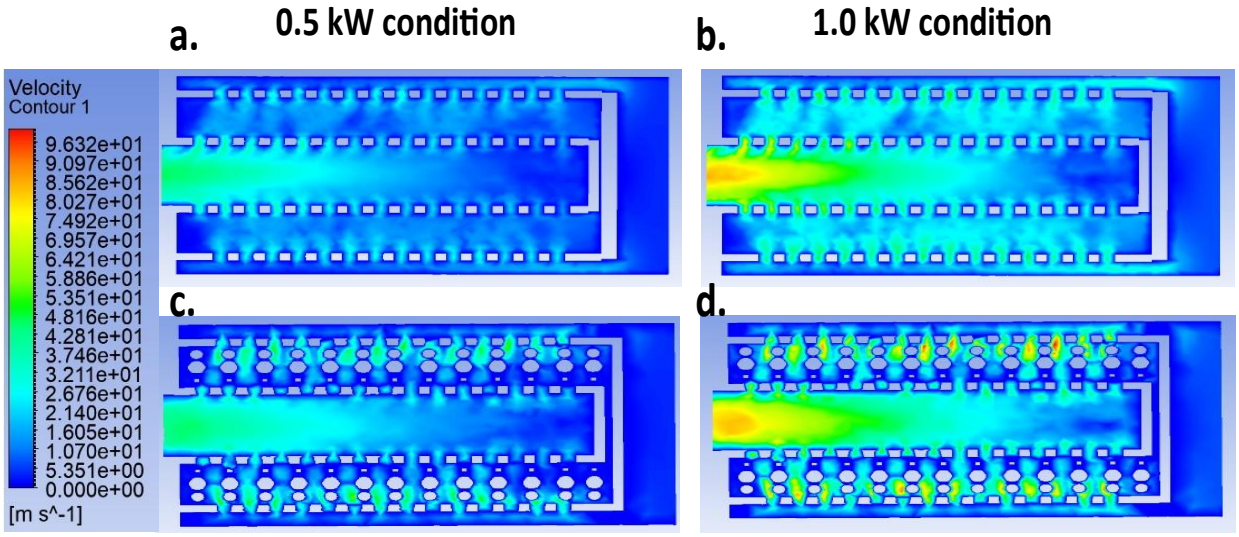

Figure 26. *Reactor B flow analysis where a. and b. show the reactor flow analysis while unloaded under the 0.5 and 1.0 kW operating conditions, on the other hand c. and d. represent the flow analysis while loaded with 65 grams of the catalyst under the same conditions.*

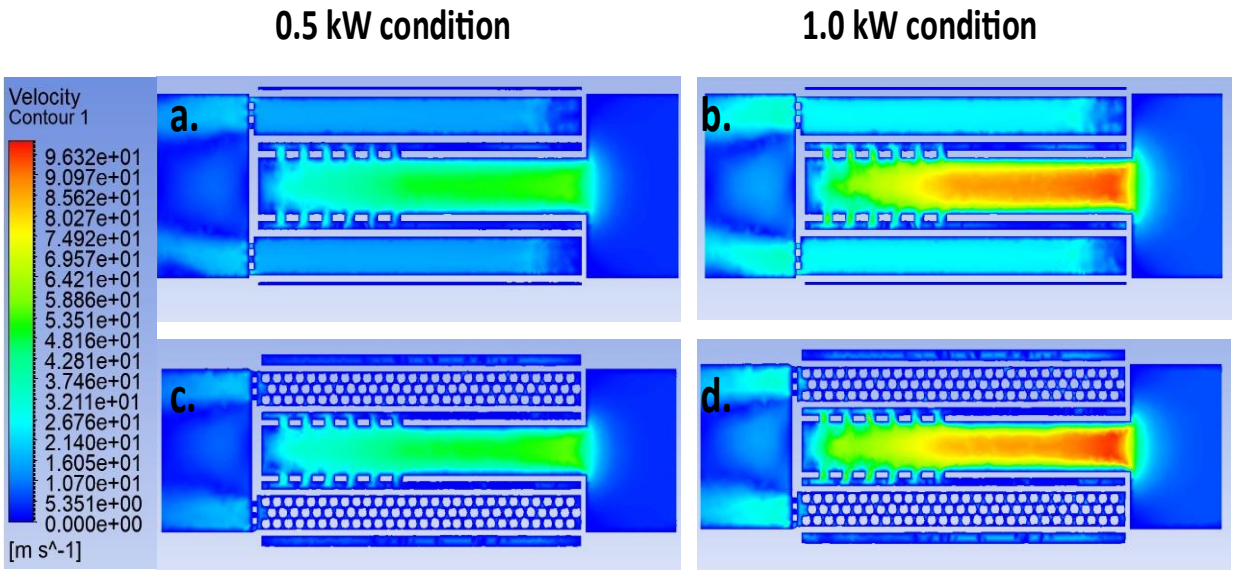

Figure 27. *Reactor C flow analysis where a. and b. show the reactor flow analysis while unloaded under the 0.5 and 1.0 kW operating conditions, on the other hand c. and d. represent the flow analysis while loaded with 65 grams of the catalyst under the same conditions.*

First: Flow profile simulation results. Reactor A, while unloaded at 0.5 kW condition parameters (3,7 m/s 500C), behaved like an empty pipe without any resistance. At the 1.0 kW conditions settings (6,7 m/s, 580C), the behavior of a pipe remained the same, but with larger values as the speed climbed from 7m/s to 15m/s. When loaded at 0.5 kW, the material's resistance reduced the velocity at the pipe's end. The 1.0 kW condition exhibited the same characteristics as the 0.5 kW condition but with greater peak values see Figure 25.

The flow in Reactor B is remarkably comparable to Reactor A, with the exception that it increases velocity throughout the length of the central pipe, another observation of the loaded Reactor B showed that the velocity of the flow decreases as it moves to the outside of the loaded chamber see Figure 27. Finally, reactor C had the highest velocity of the three reactors, with the maximum speed in the central collector/diffuser pipe at around 90m/s and remaining relatively fast in the six tubes while empty; however, once loaded, the flow speed reduced to less than 10m/s, allowing for more contact time with the catalyst see Figure 27.

Second: Heat profile simulation results.

Reactor A **w**hile unloaded at 0.5 kW condition the temperature profile was uniform along the length of the pipe. And at the 1.0 kW condition parameters the behavior stayed the same but with higher values where temperature increased from 760k to 830k. Once it was loaded at 0.5 kW condition the resistance of the material caused a reduced temp. at the catalyst location, and the 1.0 kW condition showed the same tendencies as the 0.5 kW condition but with higher peak values see Figure 28.

Reactor B **w**hile unloaded at 0.5 and 1.0 kW operating conditions had a similar behavior to Reactor A while they were unloaded, where the heat profile was homogenous on the whole reactor. However, the loaded conditions changed the behavior of the heat profile to a non-homogenous see Figure 29.

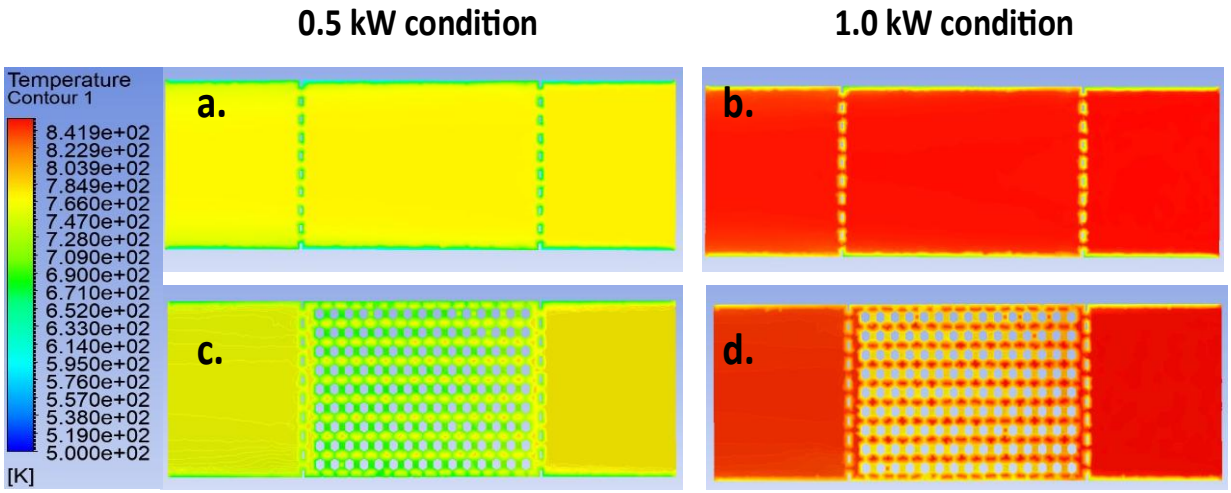

Figure 28. *Reactor A heat profile, where a. and b. show the reactor temp. analysis while unloaded under the 0.5 and 1.0 kW operating conditions, and where c. and d. f represent reactor A temp. analysis while loaded with 65 grams of catalyst under the same conditions.*

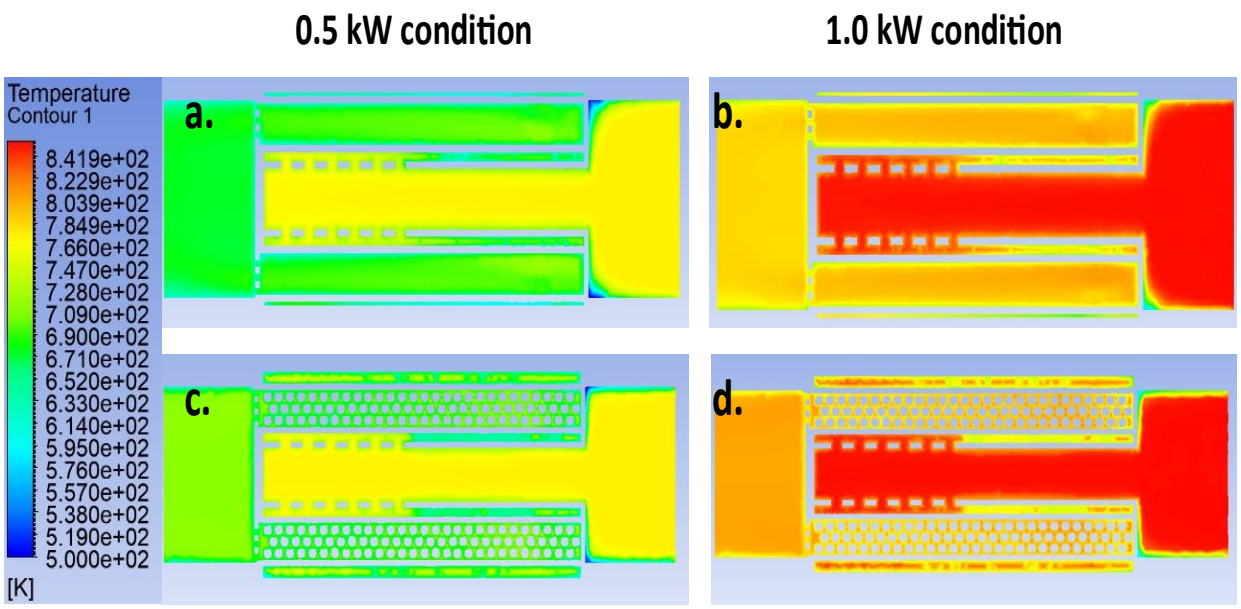

Figure 29. *Reactor B heat profile, where a. and b. show the reactor temp—analysis while unloaded under the 0.5 and 1.0 kW operating conditions, and where c. and d. f represent reactor B temp. analysis while loaded with 65 grams of catalyst under the same conditions.*

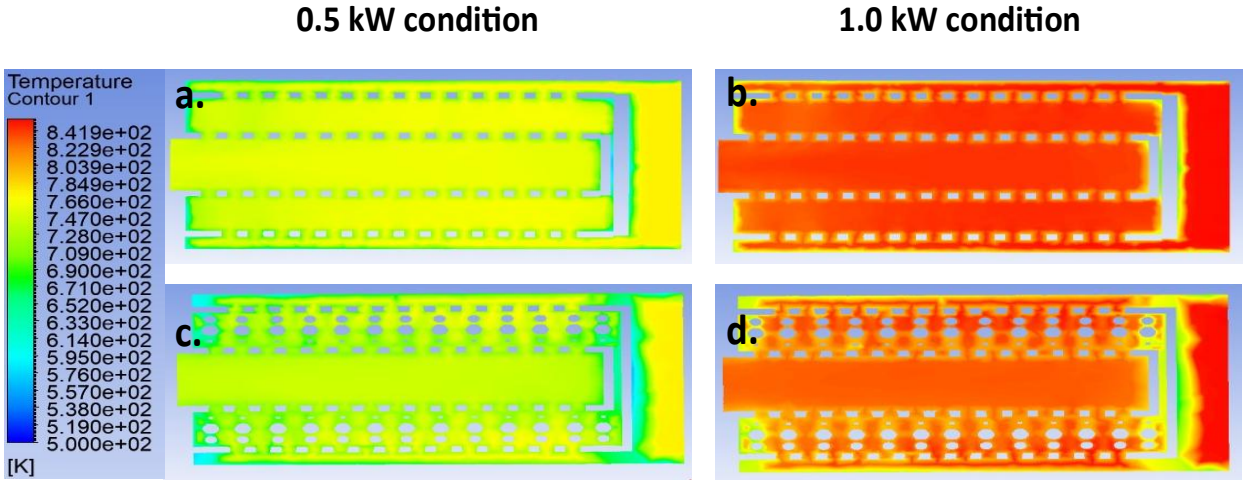

Figure 30. *Reactor C heat profile, where a. and b. show the reactor temp—analysis while unloaded under the 0.5 and 1.0 kW operating conditions, and where c. and d. f represent reactor C temp. analysis while loaded with 65 grams of catalyst under the same conditions.*

Lastly, as for the temperature profile of Reactor C, the distribution of heat was at its maximum at the central collector/diffuser pipe and reduced in the 6 tubes, that was true for both operating conditions and loading conditions see Figure 30.

The Reynolds number (Re) in Ansys cannot be defined automatically; instead, it must be manually calculated using Ansys data and the Re-proforma. When ReD < 2300, laminar flow happens, and when ReD > 2900, turbulent flow happens. Characteristic lengths and velocities can be obtained from the flow simulations and the reactors' 2D drawings, respectively. In general, the loaded reactor simulation reveals only a static state due to the dynamic movement of the particles. The system's randomness makes it impossible to duplicate the particles' actual movement. We can't get accurate and true information from this stationary situation. However, the overall data show that loaded reactors have higher resistance and lower pressure at their outlets.

$$Re = \frac{(r*v*d)}{m} \qquad \text{Eq. 5}$$

r = fluid density (kg/m^3)

v = fluid velocity (m/s)

d = characteristic length (m)

m = dynamic viscosity (kg/m*s)

Reactor A: The velocity of the gas varies from 1-10 m/s in all cases. The simulation shows that the Reynolds number varies a lot depending from the velocity of the gas and the temperature of the reactor. The flow slows down near the obstacles (packing), while also here, the temperature is shown to be lower. This is reflected by the Reynolds number drop together with the temperature and gas velocity. This yields the Reynolds number to drop in the laminar region.

Reactor B: In this reactor great variance of temperature and flow speed was observed (from 1-90 m/s, Figure 11). The simulation showed that he Re number can drop easily in the laminar flow range near the obstacles, causing thermal layering, thus further contributing to the non-isothermal flow conditions. Due to the extreme variations of the Re number, the flow conditions near the catalyst particles are chaotic, meaning that this reactor cannot be simulated and evaluated considering its own functional parameters, thus only empiric approaches could yield acceptable results.

Reactor C: This reactor is the only one in which the flow speed and temperature values constrained the Reynolds number in the laminar zone, thus thermal layering is an issue here, as demonstrated in the figures above. While flow speed is high when entering the system, it slows down when passing into the catalyst-containing chambers, to a maximum of 10 m/s. This means that the flow conditions are stable, compared to the other reactors, thus the crucial task is to induce higher convection in the system to further increase the reactor efficacy.

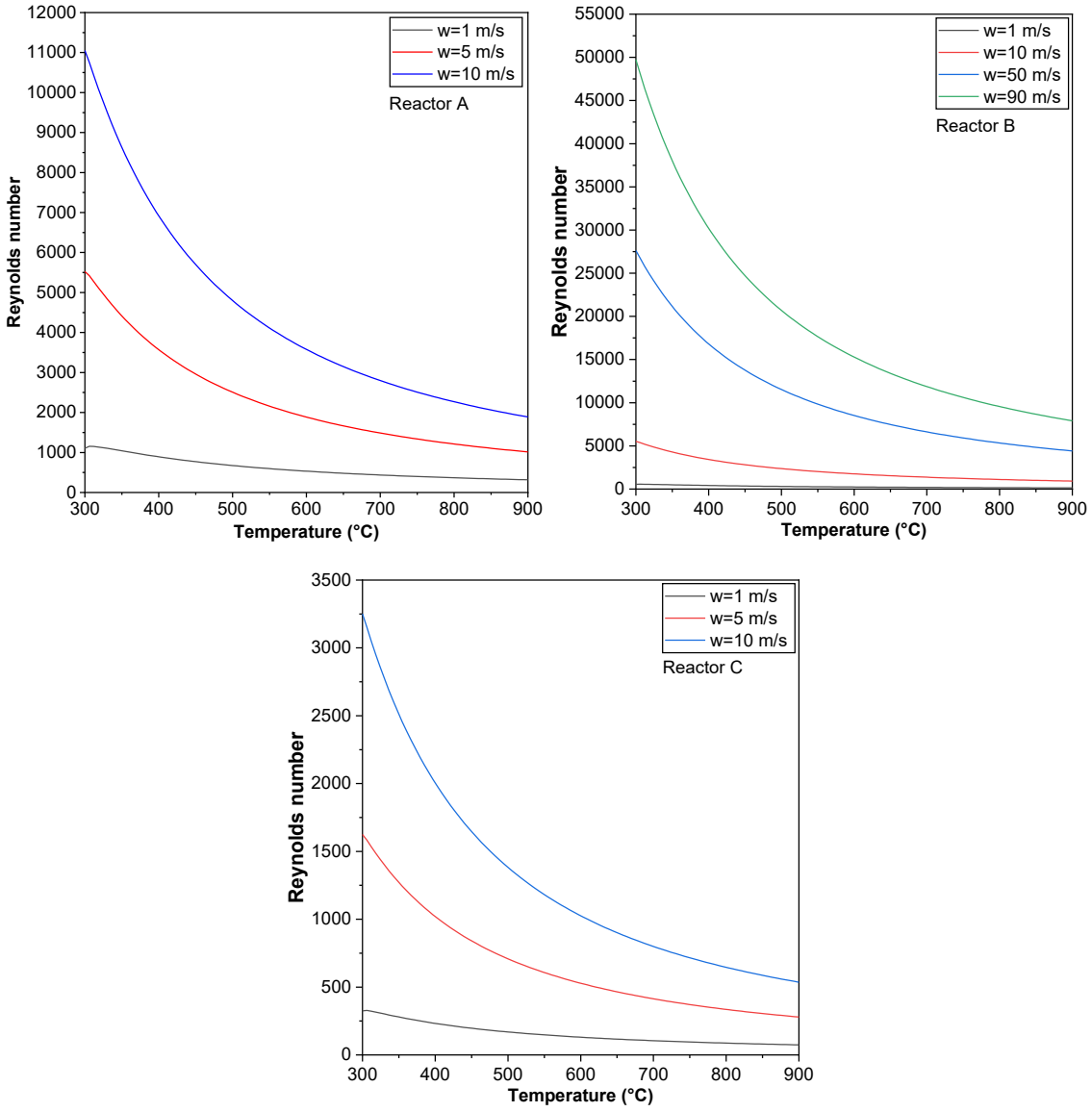

Figure 31. *The variance of the Re number in function of the temperature and specific flow-speed, considering the buoyancy effects caused by non-isothermal flow.*

It should be noted that despite the drastic Re number drop, the investigated reactor systems should not show any high-pressure drop values. However, due to the flow specifics discussed here, the mass transfer near the catalyst particles may drop drastically. Hence, the obtained performances of the reactors discussed can be even higher if the flow of the gas is further optimized.

4.3 Promoter addition effect results

Sample preparation results

The list of resulting samples that were prepared during this experiment is listed in Table 10 below.

Table 10. *The Cu, Ni, and Co samples over Al_2O_3 and 0.1wt% Pd fixed loading.*

	100 grams of Al_2O_3 pellets support			
Copper	1wt% Cu	1wt% Cu + 0.1wt% Pd	2wt% Cu + 0.1wt% Pd	5wt% Cu + 0.1wt% Pd
Nickel	1wt% Ni	1wt% Ni + 0.1wt% Pd	2wt% Ni + 0.1wt% Pd	5wt% Ni + 0.1wt% Pd
Cobalt	1wt% Co	1wt% Co + 0.1wt% Pd	2wt% Co + 0.1wt% Pd	5wt% CO + 0.1wt% Pd

a. **b.** **c.** **d.**

Figure 32. *Pictures of the prepared catalysts where **a.** shows Aluminum Oxide support without loadings, **b.** shows a Ni/Pd sample, **c.** shows a Co/Pd sample, and **d.** shows a Cu/Pd sample.*

As mentioned earlier in section 3.1, all catalyst samples were prepared using the wet impregnation method to form a wash-coat covering the ceramic support, the total number of prepared catalyst

batches was 12 batches each weighing 100 grams, and the loading combinations of these samples were listed in table 10 above see Figure 32.

The samples moving forward are referred to by their short name listed in Table 11 below:

Table 11. *The short name of the 12 promoters' catalysis samples.*

catalyst	Short name
0.1wt% Pd	Pd
1wt% Cu	1% Cu
1wt% Ni	1% Ni
1wt% Co	1% Co
1wt% Cu + 0.1wt% Pd	1% Cu/Pd
1wt% Ni + 0.1wt% Pd	1% Ni/Pd
1wt% Co + 0.1wt% Pd	1% Co/Pd
2wt% Cu + 0.1wt% Pd	2% Cu/Pd
2wt% Ni + 0.1wt% Pd	2% Ni/Pd
2wt% Co + 0.1wt% Pd	2% Co/Pd
5wt% Cu + 0.1wt% Pd	5% Cu/Pd
5wt% Ni + 0.1wt% Pd	5% Ni/Pd
5wt% CO + 0.1wt% Pd	5% Co/Pd

Flue-gas conversion results

Figure 33 below represents the conversion of CO over the prepared 12 samples compared with pure Pd catalyst, and the results are as follows: The results of Cu samples show a slight promotion of the catalytic activity toward CO, 1% Cu/Pd catalyst was able to promote CO conversion by 5%, whereas 2% Cu/Pd increased the conversion by 7% compared to Pd catalyst. However, the continuous addition of Cu reduced the CO conversion, particularly at 5% Cu/Pd where the conversion started dropping. Ni samples showed a unique behavior while converting CO, and although all Ni loading points were able to promote the catalytic activity of the catalyst, increased loading of Ni started dipping the catalyst activity and that is apparent at 5% Ni/Pd catalyst. Lastly,

the Co/Pd samples were the highlight of this experiment as the conversion of CO kept on increasing with the increase of Co loading. The highest loading of Co was 5% for the sake of consistency of the experiment. Table 12 below summarizes the increase in CO conversion at the two different operating conditions for all the prepared catalysts, where pro. refers to the used promoter.

Table 12. *The percentages of increased performance of CO conversion compared to the Pd sample.*

	Cu		**Ni**		**Co**	
	1.0 kW	0.5 kW	1.0 kW	0.5 kW	1.0 kW	0.5 kW
1% pro./Pd	**+5%**	**+20%**	**+15%**	**+10%**	**+2%**	**+8%**
2% pro./Pd	**+7%**	**+22%**	**+17%**	**+12%**	**+20%**	**+30%**
5% pro./Pd	**-4%**	**-**	**+5%**	**+11%**	**+27%**	**+38%**

To provide a practical economic comparison of the catalysts, the "money spent per 100 ppm CO reduced" was calculated. This metric normalizes the cost of the catalyst against its observed performance. The calculation was based on the total cost of the precious metals and promoters (using market prices at the time of purchase) for each 100 g catalyst batch. This total cost was then divided by the amount of CO (in ppm) converted during the RDE tests, and the result was normalized to a standard of 100 ppm for clear comparison. This approach allows for a direct evaluation of cost-effectiveness, where a lower value indicates a more economically efficient catalyst.

Figures 33 below present a compelling economic perspective on various palladium-based catalysts, at 0.5kW and 1.0 kW operating conditions, we observe significant variations in the money spent per 100 ppm CO reduction across different catalyst compositions. However, the 5%Co/Pd catalyst emerges as the standout performer, achieving the highest conversion rates (55% and 93%) while also being the most cost-effective option. Moreover, the overall money spent per 100 ppm reduction at 0.5 kW operating condition is generally lower compared to the 1.0 kW scenario, Lastly, Catalysts like 1%Ni/Pd, 2%Cu/Pd, and 2%Co/Pd present moderate costs and conversion rates, offering a second to best alternative option.

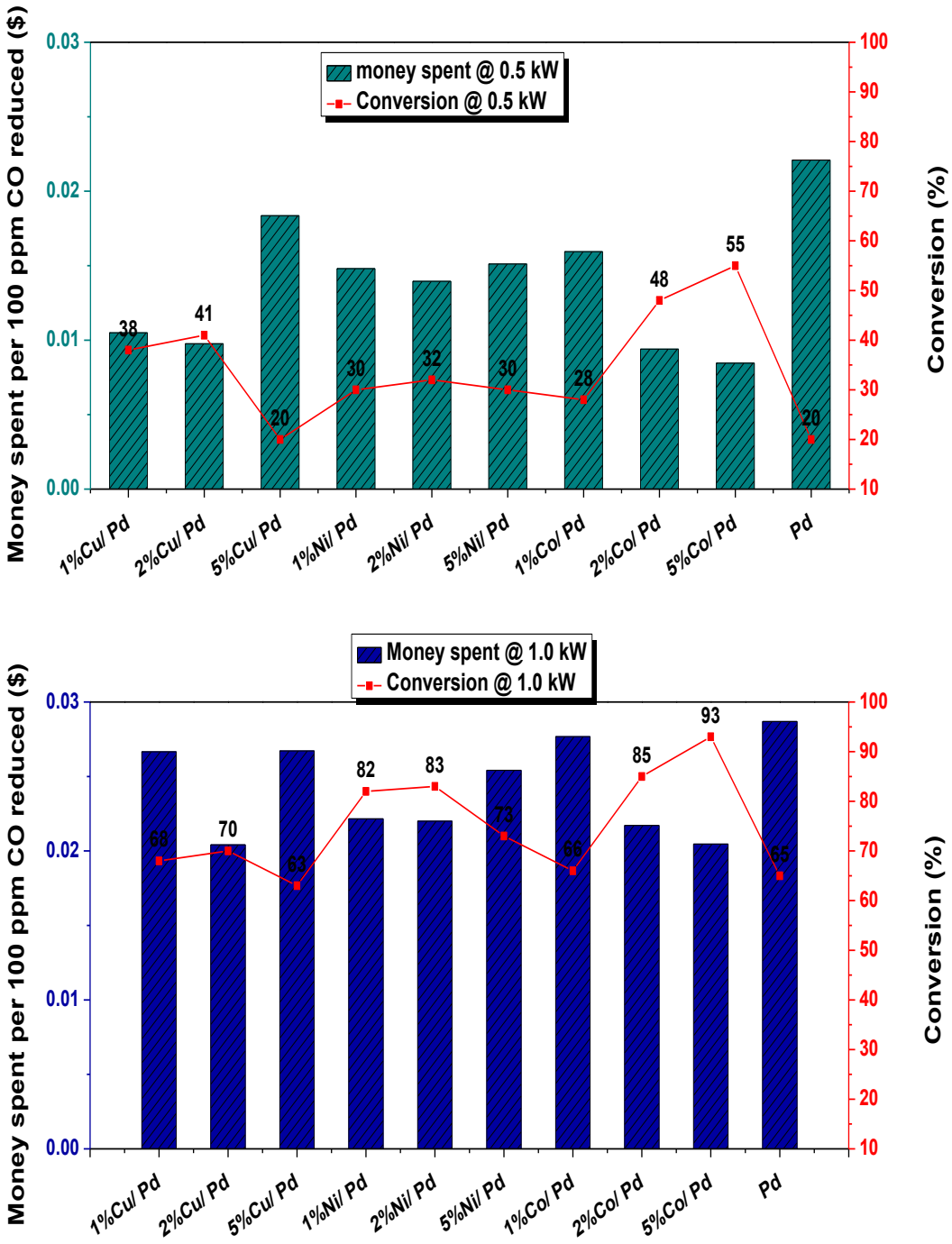

Figure 33. *CO conversion and conversion cost results over Cobalt, Copper, and Nickle samples (1%, 2%, and 5%) compared with CO conversion over Pd catalyst samples without promoter addition, at 0.5 and 1.0 kW engine power output operating conditions.*

As for NO_x conversion in summary, the conversion rates and conversion costs of the different samples are compared to the benchmark conversion of the Pd catalyst which are 73% and 0.71$ at the 0.5 kW operating conditions and 28% and 0.49$ at 1.0 kW. Results suggest that for all metal types, adding Pd generally improves NO_x conversion, especially at higher power. However, the 0.5 kW setting consistently outperforms the 1.0 kW setting across all catalyst types and that is due to the low amounts of NO_x produced at this operating condition which averages around 380 ppm compared to 1400 ppm at 1.0 kW operating condition.

Table 13. *The percentages of the reduced cost of CO conversion compared to the Pd sample.*

	Cu		**Ni**		**Co**	
	1.0 kW	0.5 kW	1.0 kW	0.5 kW	1.0 kW	0.5 kW
1% pro./Pd	**7.1%**	**52.4%**	**22.8%**	**33%**	**3.6%**	**27.9%**
2% pro./Pd	**28%**	**55%**	**23.3%**	**36.9%**	**24.3%**	**57.5%**
5% pro./Pd	**6.9%**	**16.9%**	**11.5%**	**31.6%**	**28.8%**	**61.7%**

The best-performing catalysts at 0.5 kW are 5% Co/Pd, 2% Cu/Pd, and 1% Ni/Pd, whereas at 1.0 kW, the Ni-based catalysts seem to maintain higher conversion rates compared to Co and Cu. Starting with Cobalt-based catalysts, Generally, the 0.5 kW operating condition yields higher NO_x conversion than 1.0 kW, and the 5% Co/Pd catalyst shows the highest conversion at 0.5 kW, reaching about 80%.

The Copper-based catalysts showed the same trend of higher conversion at 0.5 kW, where 2% Cu/Pd shows the best performance at 0.5 kW, with over 80% conversion, similar to Co adding Pd to Cu significantly improves performance, especially at higher power.

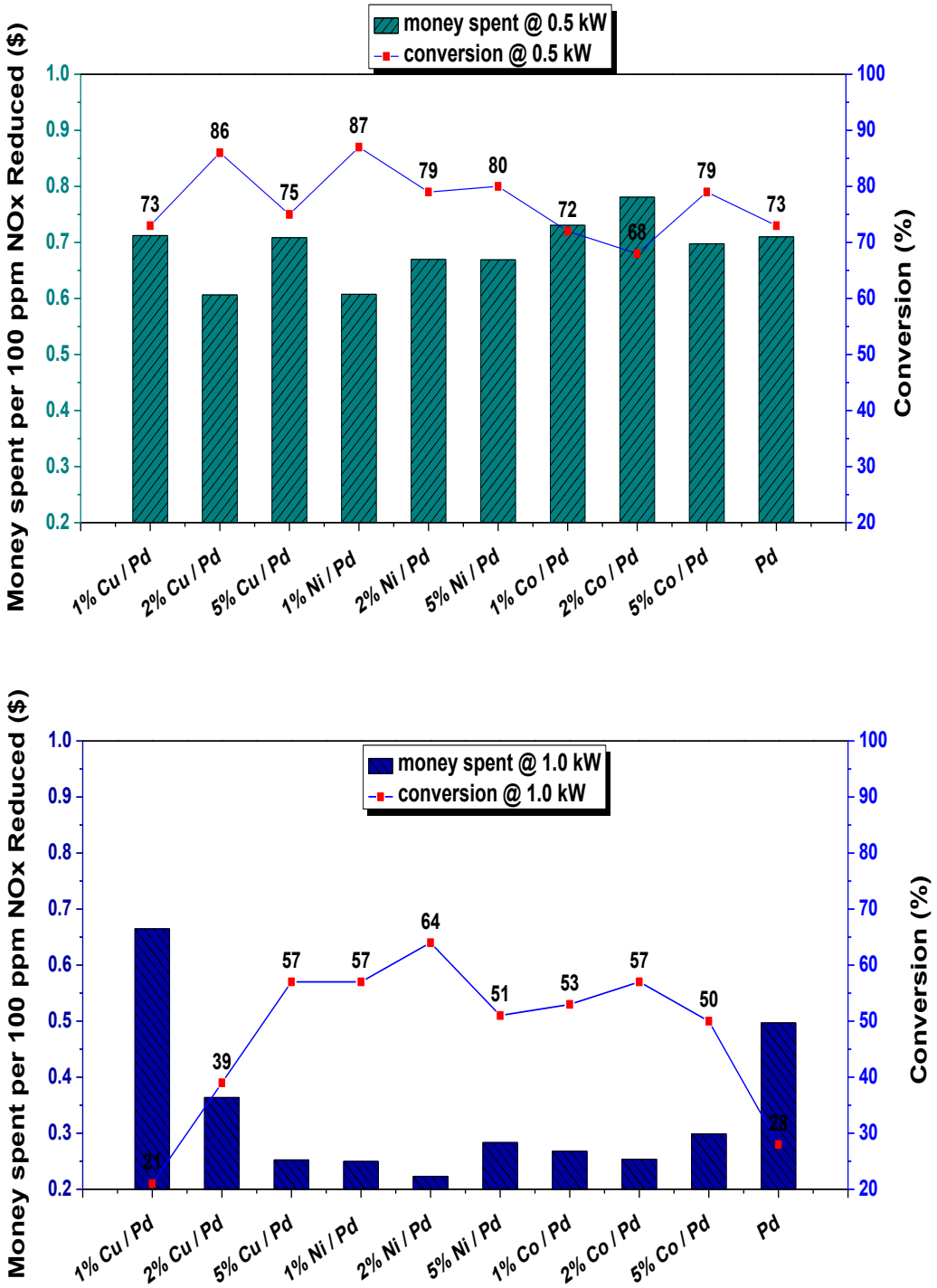

Figure 34. *NO_x conversion and conversion cost results over Cobalt, Copper, and Nickle samples (1%, 2%, and 5%) compared with NO_x conversion over Pd catalyst samples without promoter addition, at 0.5 and 1.0 kW engine power output operating conditions.*

Lastly, for Nickel-based catalysts, the 0.5 kW vs 1.0 kW trend persists as 1% Ni/Pd shows the highest conversion at 0.5 kW, slightly above 80%. However, Ni-based catalysts seem to maintain relatively high conversion at 1.0 kW compared to Co and Cu.

These data suggest that the addition of palladium generally enhances performance, while lower power settings seem to favor higher conversion rates. Moreover, the specific metal and its concentration also play crucial roles in determining the catalyst's effectiveness for NO_x conversion. Table 14 below compares the performance of the samples to a baseline palladium catalyst. The percentages indicate how much each catalyst's performance increased or reduced relative to the Pd sample at two operating conditions 1.0 kW and 0.5 kW.

Overall, these graphs provide valuable insights into the performance of different catalyst compositions for NO_x reduction, and although the use of different noble metals such as Pt would certainly decrease the NO_x production, however, this goes against the purpose of the article which is to explore the synergy between Pd and different metals in catalytic converters, meaning that there is a room for improvement in the performance of these catalysts.

Table 14. *The percentages of increased/reduced performance compared to the Pd sample*

	Cu		**Ni**		**Co**	
	1.0 kW	0.5 kW	1.0 kW	0.5 kW	1.0 kW	0.5 kW
1% pro./Pd	**-7%**	**0**	**+29%**	**+14%**	**+25%**	**-1%**
2% pro./Pd	**+11%**	**+13%**	**+36%**	**+6%**	**+29%**	**-5%**
5% pro./Pd	**+29%**	**+2%**	**+23%**	**+7%**	**+22%**	**+6%**

As for the cost-effectiveness of the samples, results show at 1.0 kW, there's a wide range in cost-effectiveness. Some catalysts (like 5% Cu/Pd) offer high conversion rates at relatively low costs, while others (like pure Pd) are expensive with moderate performance. At 0.5 kW, the cost spread is narrower, but significant differences remain. 5-Co/Pd stands out as highly cost-effective, offering the highest conversion rate at a moderate cost. It was also evident that changing operating conditions from 1.0 kW to 0.5 kW significantly decreases the money spent per 100 ppm NO_x reduced for all catalysts (by roughly a factor of 20-30), however, this cost reduction comes at the expense of lower conversion rates for most catalysts.

We can also deduct from the results that pure Pd sample is relatively expensive and offers moderate performance at both power levels, whereas, doped catalysts, especially at 5% doping levels, generally outperform pure Pd in both cost-effectiveness and conversion rates.

So, the general conclusion of the financial analysis indicates that first, for high conversion requirements, operating at 1.0 kW with 5% Cu/Pd catalyst appears to offer the best balance of cost and performance. As For more cost-sensitive applications, operating at 0.5 kW with 5-Co/Pd catalyst provides excellent cost-effectiveness while maintaining good conversion rates. Pure Pd catalysts are generally not recommended due to their high cost and moderate performance. Doped catalysts offer superior value.

Table 15 below provides a comparison of the cost reduction/increase for reducing NO_x particles compared with palladium catalyst. The percentages indicate how much each catalyst increased or reduced the cost of conversion relative to the Pd sample at two operating conditions 1.0 kW and 0.5 kW.

Table 15. *The percentages of the increased/reduced cost of NO_x conversion compared to the Pd sample.*

	Cu		**Ni**		**Co**	
	1.0 kW	0.5 kW	1.0 kW	0.5 kW	1.0 kW	0.5 kW
1% pro./Pd	**+33.7%**	**+0.3%**	**-49.7%**	**-14.4%**	**-46%**	**+3%**
2% pro./Pd	**-27%**	**-14.6%**	**-55%**	**-5.7%**	**-49%**	**+10%**
5% pro./Pd	**-49%**	**-0.2%**	**-43%**	**-5.8%**	**-40%**	**-1.7%**

XRD results

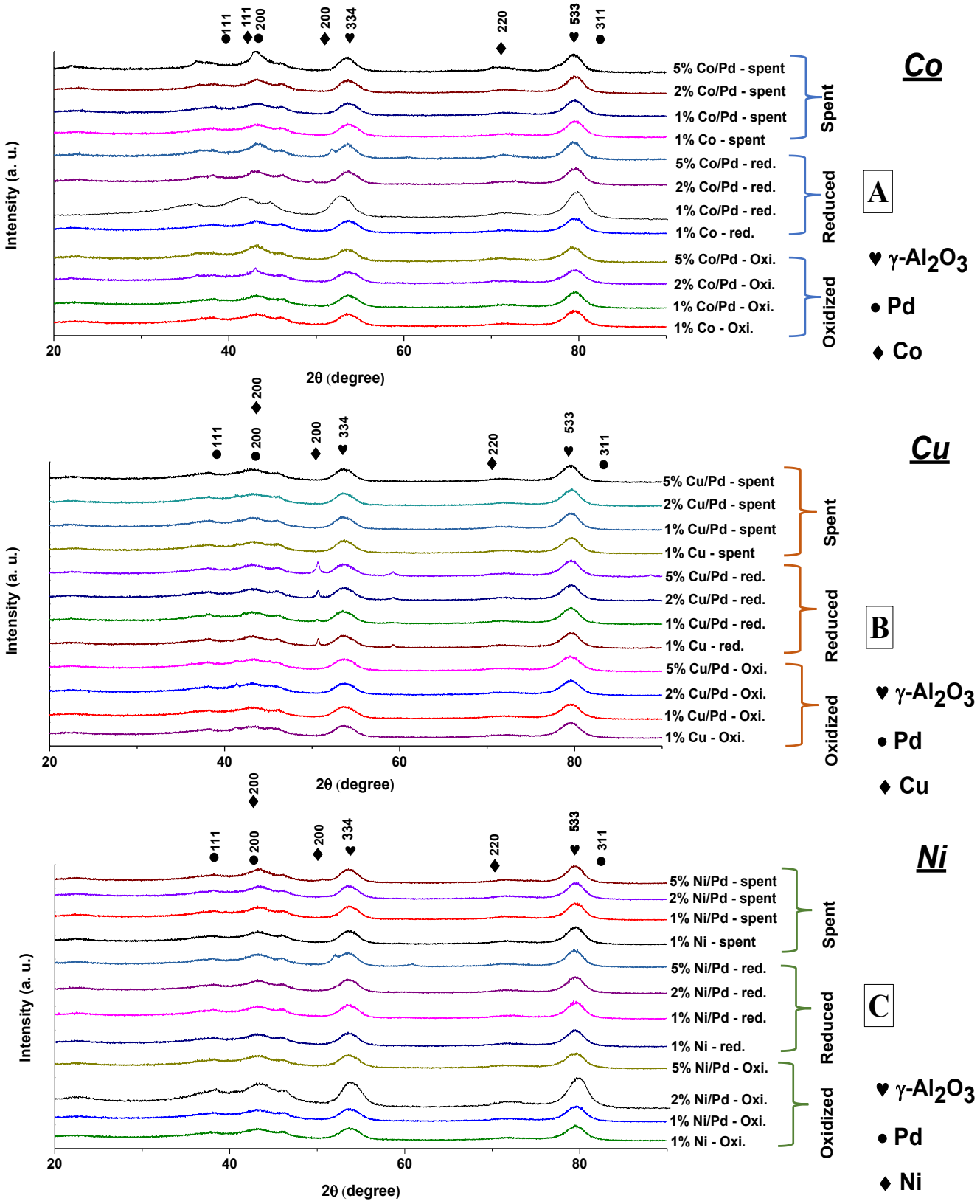
Co
111
111
200
200
334
220
533
311
5% Co/Pd - spent
2% Co/Pd - spent
1% Co/Pd - spent
1% Co - spent
5% Co/Pd - red.
2% Co/Pd - red.
1% Co/Pd - red.
1% Co - red.
5% Co/Pd - Oxi.
2% Co/Pd - Oxi.
1% Co/Pd - Oxi.
1% Co - Oxi.
Spent
Reduced
Oxidized
A
Intensity (a. u.)
2θ (degree)
20
40
60
80
♥ γ-Al2O3
● Pd
♦ Co
Cu
200
111
200
200
334
220
533
311
5% Cu/Pd - spent
2% Cu/Pd - spent
1% Cu/Pd - spent
1% Cu - spent
5% Cu/Pd - red.
2% Cu/Pd - red.
1% Cu/Pd - red.
1% Cu - red.
5% Cu/Pd - Oxi.
2% Cu/Pd - Oxi.
1% Cu/Pd - Oxi.
1% Cu - Oxi.
Spent
Reduced
Oxidized
B
Intensity (a. u.)
2θ (degree)
20
40
60
80
♥ γ-Al2O3
● Pd
♦ Cu
Ni
200
111
200
200
334
220
533
311
5% Ni/Pd - spent
2% Ni/Pd - spent
1% Ni/Pd - spent
1% Ni - spent
5% Ni/Pd - red.
2% Ni/Pd - red.
1% Ni/Pd - red.
1% Ni - red.
5% Ni/Pd - Oxi.
2% Ni/Pd - Oxi.
1% Ni/Pd - Oxi.
1% Ni - Oxi.
Spent
Reduced
Oxidized
C
Intensity (a. u.)
2θ (degree)
20
40
60
80
♥ γ-Al2O3
● Pd
♦ Ni

Figure 35. *X-ray diffraction patterns of self-prepared **A.** Co/Pd catalyst, **B.** Cu/Pd catalyst, and **C.** Ni/Pd catalyst, all wet impregnated over pelletized Al_2O_3 support at 3 different points oxidized at 450 °C for 4 h (fixed temp, no heat rate), reduced in H-Ar mixture at 700 °C for 12 h (heating rate of 5 °C/min), and spent in RDE setup.*

The crystallographic structure and phase purity of the prepared materials were determined through XRD pattern and recorded with 2θ in the range of 4-85 o with type X-Pert Pro MPD, Cu-Kα: λ = 1.54 Å Figure 35 displays characteristic diffraction peaks corresponding to the ~ **22.12°**: Close to the (110) °, **38.12°**: Matches with the (222) **46.27**: Near the (400), **53.64°**: Matches closely with the (334), **71.86°**: Near the (308) and **79.61°**: Close to the (533) plane have appeared. These values correspond exactly to the International Center of Diffraction Data ICDD database pattern gamma-alumina JCPDS reference no. 00-010-0425 (gamma-Al_2O_3). [77, 78]. These peaks provide clear identification of the crystallin Alumina phase. The Cu and Cu/Pd wet impregnated to Alumina support clear peaks appeared for 1%Cu/Pd, 2% Cu/Pd, and 5% Cu/Pd. Also, the Co and Co/Pd wet impregnated to Alumina support, clear peaks appeared for 1%Co/Pd, 2% Co/Pd, 5% Co/Pd, and Ni and Ni/Pd wet impregnated to Alumina support, clear peaks appear Cu, Co, and Ni promoted Pd at the Alumina support through wet impregnation Figure 35 retains the phase structure with enhanced dispersion. This introduction of the mentioned elements doesn't induce phase changes., only at higher doping levels, showing no new secondary phases [79]. Particle size increases with higher Cu, Co, and Ni loading. The Primary crystallite sizes were calculated using the Scherrer formula in Table 16.

Table 16. *Cu, Co, Ni, and Pd loaded Al_2O_3 particle size.*

Sample	Primary particle Size (nm)
0.1% Pd	45.12
1% Cu	45.22
1% Cu/Pd	45.46
2% Cu/Pd	45.70
5% Cu/Pd	46.20

1% Co	45.21
1% Co/Pd	45.36
2% Co/Pd	35.65
5% Co/Pd	46.18
1% Ni	45.21
1% Ni/Pd	45.33
2% Ni/Pd	45.60
5% Ni/Pd	46.17

Generally, all three systems show similar peak positions, indicating that Pd dominates the crystal structure, peak intensities generally increase with metal loading (1% to 5%), the oxidized samples consistently show less pronounced peaks across all systems, and finally the "spent" catalysts often show sharper peaks, which could indicate particle growth during use.

4.4 Combined effort

In summary, three major projects were carried out in an effort to develop an effective system that can convert flue gas emissions. Each project focused on a different aspect of the fundamentals of flue gas conversion, and since the system consists of a catalyst and a reaction chamber that work together as a unit, the main projects were as follows: the first project examined the impact of the geometric and compositional features of supports on flue gas conversion; the second project examined the role of reaction chamber design in flue gas reduction; and the third project examined the interaction between metals and noble metals to determine the appropriate metals and their loading percentages over ceramic support for the optimal flue gas conversion result. Every single project eventually delivered on its set goals, and new experiments were conducted to test the validity of our findings.

For the combined effort experiment we utilized the best-performing sample of each project meaning from the support design effect project we chose the pelletized Al_2O_3 sample as our primary catalyst support, and from the reaction chamber design effect project we chose Reactor C (the six-way reactor) as our primary reaction chamber, and finally from the promoter addition effect project we chose the 5wt.% Co + 0.1 wt. % Pd combination loading as our primary wash

coat of the support see Figure 36, afterward an extensive flue gas conversion experiment was held under RDE setup at three conditions 1500 rpm, 2500 rpm, and 3500 rpm.

Figure 36. *The utilized samples in the combined effort project including 1. The pelletized Al_2O_3 support, 2. Reactor C, and 3. The 5wt. % Co + 0.1wt. % Pd combination loading.*

Table 17 below summarizes the Flue gas conversion at three different operating conditions; The data represents the average results of three independent experiments. Moreover, it's worth mentioning that the conversion process was consistent and stable which is a heavily encountered issue.

Table 17. *The CO conversion percentages in the combined effort experiment.*

	5 wt.% Co + 0.1 wt.% Pd		
CO Conversion	1500 rpm	2500 rpm	3500 rpm
	90%	**94%**	**96%**

The results showed that through innovative engineering and chemical approaches the treated flue gas emissions caused by internal combustion engines were near-zero.

5. Conclusion:

The purpose of this dissertation is to increase the knowledge on new approaches for flue gas treatment, this has been achieved by the use of Cu, Co and Ni modified Pd catalysts, also by introducing a new concept of catalytic converters that addresses the disadvantages of the industrial ones rendered in high cost, flow path blockage, and restorability. It was concluded that utilizing the introduced approach has the ability to negate these disadvantages as well as provide a superior conversion rate of CO and No_x. The results are concluded as follows:

First, the geometric features of the five ceramic supports inspired a reliable and easy-to-install solution for the reduction of the emissions produced by gasoline engines, where a fabricated catalytic converter chamber and an adequate amount of catalyst are enough to decrease pollution drastically. This case can also be profiled to suit engines according to their features. We have shown that by wet impregnation method, we were able to wash-coat our samples with 0.1 and 0.2 wt.% Palladium (II)-acetate, and the carried-out tests indicated that Pd supported Aluminum-oxide catalysts are promising for efficient CO oxidation and selective oxidation of flue gas components. The exact property or set of properties that gave the spherical and the pellet-shaped catalysts their edge over their counterparts can’t be defined by our experiments, however, the fixed bed reactor measurements strongly suggested that amorphous structure and the order of magnitude larger BET surface area were the only significant variables hence the better performance is most likely regards to them.

Secondly, we established that reaction chamber design can influence a significant performance increase, or in other words, we can say that we attempted to prove that if the design of the reaction chamber is the only controlled variable then the performance increase or decrease is attributed to the design regardless of the

uncontrolled variables that appeared due to the nature of the test and machine concluding to the strong suggestion of the six-way reactor as a beneficial concept for improving the performance of catalytic converters and as an adequate solution for the upcoming restriction on flue gas emissions.

Thirdly, the addition of promoters generally improved both the performance and cost-effectiveness of the Pd catalyst for flue gas conversion as all the samples demonstrated the ability to promote the catalytic activity of the Pd catalyst although in different percentages. Notably, the 5wt% Co + 0.1wt% Pd sample showed the highest conversion of the overall emissions at an average of 93%, which translates to a 38% increase while being the most cost-effective sample with a 61.7% decrease in conversion cost compared to pure Pd catalyst. The observed enhanced performance between palladium and transition metal promoters, particularly cobalt offers promising avenues for developing more efficient and cost-effective catalytic converters.

And finally, by combining all introduced methods as in using 70 grams of 5wt% Co – 0.1wt% Pd \ Al_2O_3 catalyst where the support is pelletized γ-Aluminum Oxide inside a six-way chamber we were able to convert 98% of the flue gas emissions produced by gasoline engine.

References:

1. Al-Aqtash, O.; Farkas, F.; Sápi, A.; Szenti, I.; Boldizsár, T.; Ábrahámné, K.B.; Kónya, Z. Differently Shaped Al2O3-Based Pd Catalysts Loaded Catalytic Converter for Novel Non-Road Mobile Machinery Exhaust Systems. *React. Kinet. Mech. Catal.* **2023**, *136*, 149–161.
2. Asif, M. Conversion in Chemical Reactors Using Hollow Cylindrical Catalyst Pellet. *Int. J. Chem. Environ. Eng* **2012**, *6*, 368–373.
3. Oh, S.H.; Cavendish, J.C.; Hegedus, L.L. Mathematical Modeling of Catalytic Converter Lightoff: Single-pellet Studies. *AIChE J.* **1980**, *26*, 935–943, doi:10.1002/aic.690260608.
4. Kalvin, R.; Taweekun, J.; Maliwan, K.; Ali, H.M. Fabrication of Catalytic Converter with Different Materials and Comparison with Existing Materials in Addition to Analysis of Turbine Installed at the Exhaust of 4 Stroke SI Engine. *Sustain.* **2021**, *13*, doi:10.3390/su131810470.
5. Al-Aqtash, O.; Sápi, A.; Farkas, F.; Basheer, H.S.; Kukovecz, Á.; Kónya, Z. Enhanced Performance and Cost-Effectiveness of Pd-Based Catalysts with Cu, Ni, and Co Promoters for CO and NOx Conversion in Flue Gas Emission. *Atmos. Pollut. Res.* **2025**, 102579.
6. Burr, M.L.; Karani, G.; Davies, B.; Holmes, B.A.; Williams, K.L. Effects on Respiratory Health of a Reduction in Air Pollution from Vehicle Exhaust Emissions. *Occup. Environ. Med.* **2004**, *61*, 212–218.
7. Kagawa, J. Health Effects of Diesel Exhaust Emissions—a Mixture of Air Pollutants of Worldwide Concern. *Toxicology* **2002**, *181–182*, 349–353, doi:10.1016/s0300-483x(02)00461-4.
8. Quam, V.G.M.; Rocklöv, J.; Quam, M.B.M.; Lucas, R.A.I. Assessing Greenhouse Gas Emissions and Health Co-Benefits: A Structured Review of Lifestyle-Related Climate Change Mitigation Strategies. *Int. J. Environ. Res. Public Health* **2017**, *14*, 468, doi:10.3390/ijerph14050468.
9. Guerra, G.; Lemma, A.; Lerda, D.; Martines, C.; Salvi, G.; Tamponi, M. Benzene Emissions from Motor Vehicle Traffic in the Urban Area of Milan: Hypothesis of Health Impact Assessment. *Atmos. Environ.* **1995**, *29*, 3559–3569.
10. Lončarević, Š.; Ilinčić, P.; Šagi, G.; Lulić, Z. Problems and Directions in Creating a National Non-Road Mobile Machinery Emission Inventory: A Critical Review. *Sustainability* **2022**, *14*.
11. Mellios, G.; Kastori, M.; Zierock, K.H. Technical Support for the Review Obligations under Regulation (EU) 2016/1628 (NRMM). *Draft Final Report. Hg. v. Eur. Kommission. Draft Final Report. Brüssel. Online verfügbar unter https//circabc. Eur. eu/sd/a/4415ad0e-7946-4fa9-a432-d4c700c6915d/190503_NRMM_final_v3. pdf, zuletzt geprüft am* **2019**, *23*, 2021.

12. Notter, B.; Wüthrich, P.; Heldstab, J. An Emissions Inventory for Non-Road Mobile Machinery (NRMM) in Switzerland. *J. Earth Sci. Geotech. Eng* **2016**, *6*, 273–292.

13. Helms, H.; Heidt, C. *Erarbeitung Eines Konzepts Zur Minderung Der Umweltbelastung Aus NRMM (Non Road Mobile Machinery) Unter Berücksichtigung Aktueller Emissionsfaktoren Und Emissionsverminderungs- Optionen Für Den Bestand*; ifeu-Institut für Energie-u. Umweltforschung, 2014; Vol. 1;.

14. Helms, H.; Jamet, M.; Heidt, C. *Renewable Fuel Alternatives for Mobile Machinery*; Institut für Energie-und Umweltforschung: Heidelberg, 2017;

15. Winther, M. *Danish Emission Inventories for Road Transport and Other Mobile Sources. Inventories until the Year 2013.*; 2015;

16. Tiseo, I. Global CO2 Emissions by Sector 2023. *Statista* 2024.

17. IEA Global Industrial CO2 Emissions in the Sustainable Development Scenario, 2019-2070 2022.

18. Heywood, J.B. Combustion Engine Fundamentals. *1ª Edição. Estados Unidos* **1988**, *25*, 1117–1128.

19. Vodička, J. *Vehicle Type-Approval and Emission Regulation in the EU: Environmental Perspective*; Masarykova univerzita, 2024; ISBN 8028005128.

20. Gomes, S.R.; Bion, N.; Blanchard, G.; Rousseau, S.; Duprez, D.; Epron, F. Study of the Main Reactions Involved in Reforming of Exhaust Gas Recirculation (REGR) in Gasoline Engines. *RSC Adv.* **2011**, *1*, 109–116.

21. Della Torre, A.; Montenegro, G.; Onorati, A.; Paltrinieri, S.; Rulli, F.; Rossi, V. Calibration of the Oxygen Storage Reactions for the Modeling of an Automotive Three-Way Catalyst. *Ind. Eng. Chem. Res.* **2021**, *60*, 6653–6661.

22. Schmitz, P.J.; Otto, K.; de Vries, J.E. An X-Ray Photoelectron Spectroscopy Investigation of Palladium in Automotive Catalysts: Binding Energies and Reduction Characteristics. *Appl. Catal. A Gen.* **1992**, *92*, 59–72.

23. Datye, A.K.; Bravo, J.; Nelson, T.R.; Atanasova, P.; Lyubovsky, M.; Pfefferle, L. Catalyst Microstructure and Methane Oxidation Reactivity during the Pd↔ PdO Transformation on Alumina Supports. *Appl. Catal. A Gen.* **2000**, *198*, 179–196.

24. Wang, J.; Chen, H.; Hu, Z.; Yao, M.; Li, Y. A Review on the Pd-Based Three-Way Catalyst. *Catal. Rev.* **2015**, *57*, 79–144.

25. Bourges, P.; Lunati, S.; Mabilon, G. N2O and NO2 Formation during NO Reduction on Precious Metal Catalysts. In *Catalysis and Automotive Pollution Control IV*; Kruse, N., Frennet, A., Bastin, J.-M., Eds.; Studies in Surface Science and Catalysis; Elsevier, 1998; Vol. 116, pp. 213–222.

26. Després, J.; Elsener, M.; Koebel, M.; Kröcher, O.; Schnyder, B.; Wokaun, A. Catalytic Oxidation of Nitrogen Monoxide Over Pt/SiO2. *Appl. Catal. B Environ.* **2004**, *50*, 73–82, doi:10.1016/j.apcatb.2003.12.020.

27. Graham, G.; Jen, H.; Ezekoye, O.; Kudla, R.; Chun, W.; Pan, X.; McCabe, R. Effect of Alloy Composition on Dispersion Stability and Catalytic Activity for NO Oxidation over Alumina-Supported Pt–Pd Catalysts. *Catal. Letters* **2007**, *116*, 1–8, doi:10.1007/s10562-007-9124-7.

28. Bandel, W.; Fraidl, G.K.; Kapus, P.E.; Sikinger, H.; Cowland, C.N. *The Turbocharged GDI Engine: Boosted Synergies for High Fuel Economy plus Ultra-Low Emission*; 2006;

29. Arnold, S. Single Sequential Turbocharger: A New Boosting Concept for Ultra-Low Emission Diesel Engines. *SAE Int. J. Engines* **2009**, *1*, 232–239.

30. Kouremenos, D.A.; Hountalas, D.T.; Binder, K.B.; Raab, A.; Schnabel, M.H. Using Advanced Injection Timing and EGR to Improve Di Diesel Engine Efficiency at Acceptable No and Soot Levels. *SAE Tech. Pap.* **2001**, 55–68, doi:10.4271/2001-01-0199.

31. Sharma, N.; Agarwal, A.K. Particulate Emission Reduction by Fuel Injection Timing Optimization in a Gasoline Direct Injection Engine. *J. Energy Resour. Technol.* **2022**, *144*.

32. Chincholkar, S.P.; Suryawanshi, J.G. Gasoline Direct Injection: An Efficient Technology. *Energy Procedia* **2016**, *90*, 666–672.

33. Yao, M.; Zhang, Q.; Liu, H.; Zheng, Z.Q.; Zhang, P.; Lin, Z.; Lin, T.; Shen, J. *Diesel Engine Combustion Control: Medium or Heavy EGR?*; 2010;

34. Abd-Alla, G.H. Using Exhaust Gas Recirculation in Internal Combustion Engines: A Review. *Energy Convers. Manag.* **2002**, *43*, 1027–1042.

35. Wei, H.; Zhu, T.; Shu, G.; Tan, L.; Wang, Y. Gasoline Engine Exhaust Gas Recirculation–a Review. *Appl. Energy* **2012**, *99*, 534–544.

36. Alger, T.; Gingrich, J.; Roberts, C.; Mangold, B. Cooled Exhaust-Gas Recirculation for Fuel Economy and Emissions Improvement in Gasoline Engines. *Int. J. Engine Res.* **2011**, *12*, 252–264.

37. Ladommatos, N.; Abdelhalim, S.; Zhao, H. The Effects of Exhaust Gas Recirculation on Diesel Combustion and Emissions. *Int. J. Engine Res.* **2000**, *1*, 107–126.

38. Schnorbus, T.; Pischinger, S.; Körfer, T.; Lamping, M.; Tomazic, D.; Tatur, M. *Diesel Combustion Control with Closed-Loop Control of the Injection Strategy*; 2008;

39. Schihl, P. Control Strategies for Heavy-Duty Diesel Engine Emissions. *IEEE Instrum. Meas. Mag.* **2001**, *4*, 11–15.

40. Armor, J.N. A History of Industrial Catalysis. *Catal. Today* **2011**, *163*, 3–9.

41. Johnson, T. V Review of Selective Catalytic Reduction (SCR) and Related Technologies for Mobile Applications. In *Urea-SCR Technology for deNOx After Treatment of Diesel Exhausts*; Springer New York: New York, NY, 2014; pp. 3–31.

42. Farrauto, R.J.; Deeba, M.; Alerasool, S. Gasoline Automobile Catalysis and Its Historical Journey to Cleaner Air. *Nat. Catal.* **2019**, *2*, 603–613.

43. Dey, S.; Dhal, G.C. Materials Progress in the Control of CO and CO2 Emission at

Ambient Conditions: An Overview. *Mater. Sci. Energy Technol.* **2019**, *2*, 607–623.

44. Gardner, S.D.; Hoflund, G.B. Catalytic Behavior of Noble Metal/Reducible Oxide Comparison of Catalyst Performance Materials for Low-Temperature CO Oxidation, Comparison of Catalyst Performance. *Am. Chem. Soc.* **1991**, *91*, 2135–2140.

45. Weinstock, B.; Niki, H. Carbon Monoxide Balance in Nature. *Science (80-.).* **1972**, *176*, 290–292.

46. Soliman, N.K. Factors Affecting CO Oxidation Reaction over Nanosized Materials: A Review. *J. Mater. Res. Technol.* **2019**, *8*, 2395–2407.

47. Bi, F.; Zhang, X.; Du, Q.; Yue, K.; Wang, R.; Li, F.; Liu, N.; Huang, Y. Influence of Pretreatment Conditions on Low-Temperature CO Oxidation over Pd Supported UiO-66 Catalysts. *Mol. Catal.* **2021**, *509*, doi:10.1016/j.mcat.2021.111633.

48. Chen, J.; Wang, P.; Wang, L.; Cai, J. Lysine-Assisted Synthesis of Porous Ba-Doped Pd/γ-Al2O3 Hollow Microspheres with Enhanced Catalytic Properties for CO and C3H8 Oxidation. *Mater. Lett.* **2019**, *237*, 57–60.

49. Osaki, T. Factors Controlling Catalytic CO Oxidation Activity on Pd/CeO2-ZrO2-Al2O3 Cryogels. *Mater. Res. Bull.* **2019**, *118*, doi:10.1016/j.materresbull.2019.110498.

50. Kim, H.J.; Lee, J.H.; Lee, M.W.; Seo, Y.; Choung, J.W.; Kim, C.H.; Lee, K.Y. SiO2@Pd@CeO2 Catalyst with Improved Thermal Stability: Effect of Interaction between Pd and CeO2 on Activity for CO Oxidation. *Mol. Catal.* **2020**, *492*, doi:10.1016/j.mcat.2020.111014.

51. Guo, L.; Tian, Y.; Li, J.; Zhao, D.; Yu, X.; Ding, T.; Li, X. Effect of Sn-Rich and Ce-Rich Sn1− XCexO2 Supports of Pd Catalysts on CO Oxidation. *Catal. Today* **2020**, *355*, 358–365.

52. Bi, F.; Zhang, X.; Xiang, S.; Wang, Y. Effect of Pd Loading on ZrO2 Support Resulting from Pyrolysis of UiO-66: Application to CO Oxidation. *J. Colloid Interface Sci.* **2020**, *573*, 11–20.

53. Kingsbury, B.; Stewart, J.; Wu, Z.; Douglas, R.; Li, K. *Advanced Ceramic Substrate with Ordered and Designed Micro-Structure for Applications in Automotive Catalysis*; 2014; Vol. 2014-Octob;

54. Mahyon, N.I.; Li, T.; Martinez-Botas, R.; Wu, Z.; Li, K. A New Hollow Fibre Catalytic Converter Design for Sustainable Automotive Emissions Control. *Catal. Commun.* **2019**, *120*, 86–90.

55. Zhu, Z.; Xu, B. Purification Technologies for NOx Removal from Flue Gas: A Review. *Separations* **2022**, *9*.

56. Gao, F.; Tang, X.; Yi, H.; Zhao, S.; Li, C.; Li, J.; Meng, X. A Review on Selective Catalytic Reduction of NO x by NH3 over Mn–Based Catalysts at Low Temperatures: Catalysts, Mechanisms, Kinetics and DFT Calculations. *Catalysts* **2017**, *7*.

57. Liu, Y.; Zhao, J.; Lee, J.M. Conventional and New Materials for Selective Catalytic

Reduction (SCR) of NOx. *ChemCatChem* **2018**, *10*, 1499–1511.

58. Yun, B.K.; Kim, M.Y. Modeling the Selective Catalytic Reduction of NOx by Ammonia over a Vanadia-Based Catalyst from Heavy Duty Diesel Exhaust Gases. *Appl. Therm. Eng.* **2013**, *50*, 152–158.

59. Despres, J.; Elsener, M.; Koebel, M.; Kröcher, O.; Schnyder, B.; Wokaun, A. Catalytic Oxidation of Nitrogen Monoxide over Pt/SiO2. *Appl. Catal. B Environ.* **2004**, *50*, 73–82.

60. Kim, C.H.; Schmid, M.; Schmieg, S.J.; Tan, J.; Li, W. The Effect of Pt-Pd Ratio on Oxidation Catalysts under Simulated Diesel Exhaust. *SAE 2011 World Congr. Exhib.* **2011**, doi:10.4271/2011-01-1134.

61. Thomas, D.; Vanderschuren, J. Nitrogen Oxides Scrubbing with Alkaline Solutions. *Chem. Eng. Technol. Ind. Chem. Equipment-Process Eng.* **2000**, *23*, 449–455.

62. Valluri, S.; Kawatra, S.K. Simultaneous Removal of CO2, NOx and SOx Using Single Stage Absorption Column. *J. Environ. Sci.* **2021**, *103*, 279–287.

63. Kim, H.J.; Han, B.; Woo, C.G.; Kim, Y.J. NOx Removal Performance of a Wet Reduction Scrubber Combined with Oxidation by an Indirect DBD Plasma for Semiconductor Manufacturing Industries. *IEEE Trans. Ind. Appl.* **2018**, *54*, 6401–6407.

64. Liu, Y.; Pan, J.; Wang, Q. Removal of Hg0 from Containing-SO2/NO Flue Gas by Ultraviolet/H2O2 Process in a Novel Photochemical Reactor. *AIChE J.* **2014**, *60*, 2275–2285.

65. Guo, R.T.; Pan, W.G.; Zhang, X.B.; Ren, J.X.; Jin, Q.; Xu, H.J.; Wu, J. Removal of NO by Using Fenton Reagent Solution in a Lab-Scale Bubbling Reactor. *Fuel* **2011**, *90*, 3295–3298.

66. Vaarkamp, M.; Miller, J.T.; Modica, F.S.; Koningsberger, D.C. On the Relation between Particle Morphology, Structure of the Metal-Support Interface, and Catalytic Properties of Pt/γ-Al2O3. *J. Catal.* **1996**, *163*, 294–305.

67. Ivanova, A.S.; Slavinskaya, E.M.; Gulyaev, R. V; Zaikovskii, V.I.; Stonkus, O.A.; Danilova, I.G.; Boronin, A.I. Metal–Support Interactions in Pt/Al2O3 and Pd/Al2O3 Catalysts for CO Oxidation. *Appl. Catal. B Environ.* **2010**, *97*, 57–71.

68. Lee, J.; Jang, E.J.; Kwak, J.H. Effect of Number and Properties of Specific Sites on Alumina Surfaces for Pt-Al2O3 Catalysts. *Appl. Catal. A Gen.* **2019**, *569*, 8–19.

69. Kritsanaviparkporn, E.; Baena-Moreno, F.M.; Reina, T.R. Catalytic Converters for Vehicle Exhaust: Fundamental Aspects and Technology Overview for Newcomers to the Field. *Chemistry (Easton).* **2021**, *3*, 630–646.

70. Hochgreb, S.; Sher, E. *Handbook of Air Pollution From Internal Combustion Engines*; 1998;

71. Hayes, R.E.; Fadic, A.; Mmbaga, J.; Najafi, A. CFD Modelling of the Automotive Catalytic Converter. *Catal. Today* **2012**, *188*, 94–105.

72. Jansson, J. Vanadia-Based Catalysts for Mobile SCR. In *Urea-SCR Technology for deNOx*

After Treatment of Diesel Exhausts; Springer New York: New York, NY, 2014; pp. 65–96.

73. Twigg, M. V; Richardson, J.T. Theory and Applications of Ceramic Foam Catalysts. *Chem. Eng. Res. Des.* **2002**, *80*, 183–189.

74. Twigg, M. V; Richardson, J.T. Fundamentals and Applications of Structured Ceramic Foam Catalysts. *Ind. Eng. Chem. Res.* **2007**, *46*, 4166–4177.

75. Wu, X.; Fischer, M.; Nolte, A.; Lenßen, P.; Wang, B.; Ohlerth, T.; Simon, U. Perovskite Catalyst for In-Cylinder Coating to Reduce Raw Pollutant Emissions of Internal Combustion Engines. *ACS Omega* **2022**, *7*, 5340–5349.

76. Shaikh, S.K.; Pathan, K.A.; Chaudhary, Z.I.; Khan, S.A. CFD Analysis of an Automobile Catalytic Converter to Obtain Flow Uniformity and to Minimize Pressure Drop across the Monolith. *CFD Lett.* **2020**, *12*, 116–128.

77. Shi, X.; Cao, B.; Liu, J.; Zhang, J.; Du, Y. Rare-Earth-Based Metal–Organic Frameworks as Multifunctional Platforms for Catalytic Conversion. *Small* **2021**, *17*, doi:10.1002/smll.202005371.

78. Choya, A.; Rivas, B.; Gutierrez-Ortiz, J.I.; Lopez-Fonseca, R. Beneficial Effects of Nickel Promoter on the Efficiency of Alumina-Supported Co3O4 Catalysts for Lean Methane Oxidation. *J. Environ. Chem. Eng.* **2022**, *10*, 108816, doi:10.1016/j.jece.2022.108816.

79. Choya, A.; Rivas, B.; González-Velasco, J.; Gutierrez-Ortiz, J.I.; Lopez-Fonseca, R. Optimisation of Bimetallic Co-Ni Supported Catalysts for Oxidation of Methane in Natural Gas Vehicles. *Appl. Catal. B Environ.* **2021**, *284*, 119712, doi:10.1016/j.apcatb.2020.119712.

80. Xiong, J.; Yang, J.; Chi, X.; Wu, K.; Song, L.; Li, T.; Zhao, Y.; Huang, H.; Chen, P.; Wu, J.; et al. Pd-Promoted Co2NiO4 with Lattice Co–O–Ni and Interfacial Pd–O Activation for Highly Efficient Methane Oxidation. *Appl. Catal. B Environ.* **2021**, *292*, doi:10.1016/j.apcatb.2021.120201.

81. Zou, X.; Rui, Z.; Ji, H.-B. Core–Shell NiO@PdO Nanoparticles Supported on Alumina as an Advanced Catalyst for Methane Oxidation. *ACS Catal.* **2017**, *7*, doi:10.1021/acscatal.6b03105.

82. Lin, L.-C.; Kuo, C.-H.; Hsu, Y.-H.; Hsu, L.-C.; Chen, H.-Y.; Chen, J.-L.; Pan, Y.-T. High-Performance Intermetallic PtCo Oxygen Reduction Catalyst Promoted by Molybdenum. *Appl. Catal. B Environ.* **2022**, *317*, 121767, doi:10.1016/j.apcatb.2022.121767.

83. Zhong, L.; Barreau, M.; Caps, V.; Papaefthimiou, V.; Haevecker, M.; Teschner, D.; Baaziz, W.; Borfecchia, E.; Braglia, L.; Zafeiratos, S. Improving the Catalytic Performance of Cobalt for CO Preferential Oxidation by Stabilizing the Active Phase through Vanadium Promotion. *ACS Catal.* **2021**, *11*, 5369–5385, doi:10.1021/acscatal.0c05482.

84. Zhong, L.; Barreau, M.; Chen, D.; Caps, V.; Haevecker, M.; Teschner, D.; Simonne, D.; Borfecchia, E.; Baaziz, W.; Šmíd, B.; et al. Effect of Manganese Promotion on the Activity and Selectivity of Cobalt Catalysts for CO Preferential Oxidation. *Appl. Catal. B*

Environ. **2021**, *297*, 120397, doi:10.1016/j.apcatb.2021.120397.

85. Xing, F.; Jeon, J.; Toyao, T.; Shimizu, K.I.; Furukawa, S. A Cu-Pd Single-Atom Alloy Catalyst for Highly Efficient NO Reduction. *Chem. Sci.* **2019**, *10*, 8292–8298, doi:10.1039/c9sc03172c.

86. Li, R.; Zhu, Y.; Zhang, Z.; Zhang, C.; Fu, G.; Yi, X.; Huang, Q.; Yang, F.; Liang, W.; Zheng, A.; et al. Remarkable Performance of Selective Catalytic Reduction of NOx by Ammonia over Copper-Exchanged SSZ-52 Catalysts. *Appl. Catal. B Environ.* **2021**, *283*, 119641, doi:10.1016/j.apcatb.2020.119641.

87. Yakoumis, I. Copper and Noble Metal Polymetallic Catalysts for Engine Exhaust Gas Treatment 2019.

88. Kim, J.; Kwon, D.W.; Lee, S.; Ha, H.P. Exploration of Surface Properties of Sb-Promoted Copper Vanadate Catalysts for Selective Catalytic Reduction of NOX by NH3. *Appl. Catal. B Environ.* **2018**, *236*, 314–325, doi:https://doi.org/10.1016/j.apcatb.2018.05.024.

89. Salaev, M.; Kulchakovskaya, E.; Vodyankina, O. Bimetallic Ag-Based Catalysts for Low-Temperature SCR: Quo Vadis? *Appl. Catal. A Gen.* **2022**, *644*, 118815, doi:10.1016/j.apcata.2022.118815.

90. Liu, L.; Corma, A. Bimetallic Sites for Catalysis: From Binuclear Metal Sites to Bimetallic Nanoclusters and Nanoparticles. *Chem. Rev.* **2023**, *123*, 4855–4933, doi:10.1021/acs.chemrev.2c00733.

91. Guczi, L.; Boskovic, G.; Kiss, E. Bimetallic Cobalt Based Catalysts. *Catal. Rev. Eng. - CATAL REV-SCI ENG* **2010**, *52*, 133–203, doi:10.1080/01614941003720134.

92. Soto Beobide, A.; Moschovi, A.M.; Mathioudakis, G.N.; Kourtelesis, M.; Lada, Z.G.; Andrikopoulos, K.S.; Sygellou, L.; Dracopoulos, V.; Yakoumis, I.; Voyiatzis, G.A. High Catalytic Efficiency of a Nanosized Copper-Based Catalyst for Automotives: A Physicochemical Characterization. *Molecules* **2022**, *27*, doi:10.3390/molecules27217402.

93. Nazarpoor, Z.; Golden, S.J. U.S. Patent No. 9,427,730 2016.

94. Zhou, Z.; Zeng, H.; Feng, C.; Li, L.; Tang, R.; Li, W.; Huang, Y.; Deng, Y. Engineering an Annular Donor-Acceptor Reaction Chamber with Spontaneous Feedstock Collection for Boosting CO2 Photoreduction. *Energy Environ. Sci.* **2024**, *17*, 5627–5638, doi:10.1039/d4ee01543f.

95. Reichman, R.; Rolston, D.E. Design and Performance of a Dynamic Gas Flux Chamber. *J. Environ. Qual.* **2002**, *31*, 1774–1781, doi:10.2134/jeq2002.1774.

96. Hussain, A.; Riaz, A.; Qyyum, M.A.; Lee, M. Design Trade-Offs in a Column with Side-Reactor Configuration for Improving Selectivity in Multiple Reaction Systems. *Chem. Eng. Process. - Process Intensif.* **2018**, *134*, 86–96, doi:10.1016/j.cep.2018.10.008.

97. Deng, S.; Koch, J.A.; Mueller, M.E.; Law, C.K. Sooting Limits of Nonpremixed N-Heptane, n-Butanol, and Methyl Butanoate Flames: Experimental Determination and Mechanistic Analysis. *Fuel* **2014**, *136*, 122–129.

98. Frost, J.; Hellier, P.; Ladommatos, N. A Systematic Study into the Effect of Lignocellulose-Derived Biofuels on the Combustion and Emissions of Fossil Diesel Blends in a Compression Ignition Engine. *Fuel* **2022**, *313*, doi:10.1016/j.fuel.2021.122663.

99. Cullity, B.D.; Smoluchowski, R. Elements of X-ray Diffraction. *Phys. Today* **1957**, *10*, 50.

100. Williams, D.B.; Carter, C.B. Transmission Electron Microscopy. *Syst. Mater. Anal.* **1978**, *4*, 407.

101. Cowell, M. *X-Ray Fluorescence Spectrometry (XRF)*; Wiley Online Library, 2008; Vol. 152; ISBN 9780470753446.

102. Brunauer, S.; Emmett, P.H.; Teller, E. Adsorption of Gases in Multimolecular Layers. *J. Am. Chem. Soc.* **1938**, *60*, 309–319.

103. Gabbott, P. *Principles and Applications of Thermal Analysis*; Wiley Online Library, 2008; ISBN 9781405131711.

104. Jing, Y.; Cai, Z.; Liu, C.; Toyao, T.; Maeno, Z.; Asakura, H.; Shimizu, K.I. Promotional Effect of La in the Three-Way Catalysis of La-Loaded Al2O3-Supported Pd Catalysts (Pd/La/Al2O3). *ACS Catal.* **2019**, *10*, 1010–1023.

.

Summary

This thesis presents a comprehensive study on innovative engineering and chemical approaches to achieve near-zero flue gas emissions from internal combustion engines. The research addresses critical challenges in emission control technology, focusing on the development of advanced catalytic converters that overcome the limitations of current industrial solutions, such as high cost, flow path blockage, and poor restorability.

The study explores six primary research questions: The impact of support shape on flue gas emission conversion efficiency, including optimal loadings and percentages, The role of support properties in influencing flue gas conversion performance, The effect of reaction chamber shape on catalytic converter efficiency, The mechanisms by which reaction chamber design enhances catalyst performance, The identification of ideal promoters that synergize with noble metals for flue gas conversion, and The influence of different metal loading combinations on ceramic supports on overall catalyst performance.

The research employed a Real Driving Emission (RDE) setup for experimental testing. This system consisted of two main components: A controlled flue-gas emission source, and a gas analyzer, where each sample underwent at least 3 tests per operating condition, the average test duration is 1 hour

The key findings were as follows:

First Geometric Features of Ceramic Supports:

- Five different ceramic supports were investigated
- The study revealed a reliable and easy-to-install solution for gasoline engine emission reduction
- A fabricated catalytic converter chamber with an adequate catalyst amounts significantly reduced pollution
- The system can be profiled to suit various engine features

- Wet impregnation method used to wash-coat samples with 0.1 and 0.2 wt.% Palladium (II)-acetate
- Pd supported Aluminum-oxide catalysts showed promise for efficient CO oxidation and selective oxidation of flue gas components
- Spherical and pellet-shaped catalysts outperformed other geometries
- Amorphous structure and larger BET surface area were identified as significant factors in performance enhancement

Second Reaction Chamber Design:

- Significant performance increases were attributed to the design of the chamber
- Six-way reactor concept proved beneficial for improving overall catalytic converter performance
- The design offers an adequate solution for meeting upcoming flue gas emission restrictions

Third bimetallic Promoters:

- Cheap metals (Ni, Cu, Co) were tested as promoters for noble metals (Pd).
- Cobalt showed exceptional synergy with Pd at 5wt% loading.
- The Co-Pd combination provided high and consistent conversion of CO and NOx

Fourth Optimized System Performance:

Combining all the introduced methods:

- 70 grams of 5wt% Co + 0.1wt% Pd / Al_2O_3 catalyst
- Pelletized γ-Aluminum Oxide support
- Six-way reaction chamber design

We achieved 98% conversion of flue gas emissions.

This work led to several conclusions and implications, starting with the Novel Catalytic Converter Concept that addresses the disadvantages of industrial converters such as high cost, flow path

blockage, and poor restorability eventually concluded to providing superior conversion rates for CO and NOx. The Support Geometry showed that amorphous structure and high BET surface area are crucial for catalyst performance which is the case for spherical and pellet-shaped catalysts that demonstrated superior efficiency. The Reaction Chamber Design demonstrated that the Six-way reactor design significantly improves catalytic converter performance which offers a promising solution for meeting upcoming stringent emission standards. bimetallic catalytic converters explained the use of cheap metals as promoters for noble metals is a revolutionary approach, it can reduce catalytic converter costs while increasing emission conversion performance and we found that cobalt at 5wt% loading shows excellent synergy with 0.1wt% Pd. Lastly, the optimized system that combines all approaches used in this project namely the combination of the optimized catalyst composition, support geometry, and chamber design was able to achieve near-zero emissions, which demonstrates the potential for significant advancements in emission control technology.

Finally, this research opens several avenues for future investigation:

1. Further optimization of catalyst compositions and their loadings
2. Exploration of additional support materials and their geometries
3. Refinement of reaction chamber designs for various engine types
4. Long-term durability and performance studies under diverse operating conditions
5. Economic analysis and scalability assessment for industrial application

In conclusion, this thesis presents a significant advancement in flue gas emission control technology. The innovative approaches developed here offer a promising pathway towards achieving near-zero emissions from internal combustion engines, contributing to global efforts in reducing air pollution and mitigating climate change impacts.

Publication list and conferences

Hungarian Scientific Bibliography (MTMT) identifier: 10080733

List of Publications:

- **Al-Aqtash, O.,** Farkas, F., Sápi, A., Szenti, I., Boldizsár, T., Ábrahámné, K.B., Kukovecz, Á. and Kónya, Z., 2023. Differently shaped Al2O3-based Pd catalysts loaded catalytic converter for novel non-road mobile machinery exhaust systems.

  Reaction Kinetics, Mechanisms and Catalysis, *136*(1), pp.149-161.

  IF = 1.7

  Independent Citations = 2

- **Al-Aqtash, O.,** Sápi, A., Farkas, F., Basheer, H.S., Kukovecz, Á. and Kónya, Z., 2025. Enhanced Performance and Cost-Effectiveness of Pd-Based Catalysts with Cu, Ni, and Co Promoters for CO and NO_x Conversion in Flue Gas Emission.

  Atmospheric Pollution Research, p.102579.

  IF = 3.9

  Independent Citations = 0

- **Al-Aqtash, O.,** Sápi, A., Multi-cylindrical packed catalyst-type reactor for efficient flue gas treatment

  Under review in **Catalysts**

  IF = 4.0

List of Conferences:

- ***14th ECerS Conference for Young Scientists in Ceramics,*** Oral presentation "Ceramics-Based catalyst characterization", Novi Sad – Serbia, October 20-23, 2021

- ***27th International Symposium on Analytical and Environmental Problems,*** Poster presentation "Ceramics-Based Catalyst for Treating Exhaust Gases of SI Engine", Szeged – Hungary, November 22-23, 2021

- **Hungarian Society for Microscopy Conference 2023 "HSM",** Oral presentation "Differently shaped Al_2O_3-based Pd catalysts loaded catalytic converter for novel non-road mobile machinery exhaust systems", Siofok – Hungary, May 1 – 4, 2023

- **12th Virtual Nanotechnology Poster Conference "The International NanoScience Community,** Poster presentation "Differently shaped ceramic-based Pd catalysts for flue gas conversion", Online, 24 April 2023

- **18th Carpathian Basin Conference for Environmental Science,** Poster presentation "Differently shaped Al_2O_3-based Pd catalysts for exhaust systems after treatment" Szeged – Hungary, September 8 – 10, 2023

- **ICOSTEE 2024 - International Conference on Science, Technology, Engineering, and Economy,** Oral presentation "Reactor chamber design effect on flue gas conversion", Szeged – Hungary, 31 May 2024

Acknowledgments

As I conclude this significant chapter of my academic journey, I am filled with gratitude for the numerous individuals who have supported and guided me throughout the process of completing this thesis.

First and foremost, I would like to express my sincere appreciation to my advisor, **Dr. András Sápi**, whose expertise, insight, and patience have been invaluable. Your guidance has not only shaped this thesis but has also profoundly influenced my growth as a researcher. My sincere thanks are also extended to Prof. János Kiss and Dr. Tímea Benkó, whose diligent reviews and constructive feedback were instrumental in the refinement and final polishing of this work.

I would like to acknowledge the **Stipendium Hungaricum Scholarship** for its financial support, which made this research possible. Additionally, I extend my thanks to the Doctoral School of Environmental Science, the Department of Applied and Environmental Chemistry, and the Engineering Faculty for allowing me to pursue my Ph.D. degree at the **University of Szeged**

In memoriam of my beloved father, whose spirit and sacrifice illuminated my academic journey. Though you departed during the first year of my doctoral pursuit, your unwavering belief in my potential and the profound sacrifices you made to nurture my dreams have been my guiding light. This achievement is a testament to your legacy a profound tribute to a man whose love transcended his physical presence, whose ambitions for me became the cornerstone of my success. Your memory is etched in every page of this work, a silent yet powerful inspiration that transformed my scholarly endeavors into a living tribute to your enduring vision.

My heartfelt gratitude goes to my lovely wife, daughter, family, and friends for their unwavering support and understanding throughout this challenging journey.

To my colleagues and fellow researchers thank you for the stimulating discussions, collaborative spirit, and moral support.

This accomplishment would not have been possible without all of you. Thank you.

Dedicated to

My late Father & beloved Family